UNIVERSITY OF NAPLES "FEDERICO II"

Faculty of Mathematics, Physics and Natural Sciences

Ph.D. in Chemistry - XXIII Cycle

2007-2010

SYNTHETIC HEME-PROTEINS IN BIOSENSORS DEVELOPMENT

Candidate: Dr. Paola Ringhieri

Advisors:	Prof. A. Lombardi
	Prof. V. Pavone
Supervisor:	Prof. C. Giancola
Coordinator:	Prof. L. Previtera

Table of contents

SUMMARY

The development of biosensors represents a rapidly growing area at the interface of chemistry, biochemistry, physics and of nanotechnology. A biosensor is an analytical device that relies on a biological recognition element, such as an enzyme, an antibody, a DNA fragment, which communicates with a signal transducer, thus providing a measurable response related to the concentration of an analyte.

The common aim in biosensor development is to produce either discrete or continuous digital electronic signals that are proportional to a single analyte concentration.

The development of most biosensors involves the identification of naturally occurring macromolecules that provide the desired analyte specificity (typically an enzyme or antibody): this macromolecule represents the recognition element of the sensor. Once identified, a suitable signal transduction and detection methodology needs to be developed to transform the biological event, occurring between the recognition element and the specific analyte, in a measurable signal. Currently, electrochemical biosensors, which exploit an electron transfer (ET) event at a solid electrode for the signal transduction, are the larger and most promising biosensor category in terms of ease of construction, costs, versatility, tunability and miniaturization (up to the nanoscale) for in vivo applications.

A key factor for the development of these devices is the strategy for ensuring a fast electrical communication between the biological recognition element and the electrode. The *first-* and *second-generation biosensors* use natural (enzyme products) and artificial (dye molecules) “mediators”, which are freely diffusing molecules that shuttle electrons between the recognition element and the electrode. These systems suffered several drawbacks, especially regarding selectivity, interfering reactions and stability of the system.

A real breakthrough toward the development of electrochemical systems with superior selectivity, stability and durability is represented by the *third generation biosensors*. These devices exploit the unmediated direct electron transfer occurring at interfaces made up of an electrode immobilized redox-active specie, with a current transduction of the biological interaction, resulting in an amperometric detection of the analyte. An attractive feature of systems based on

direct electron transfer is the possibility of modulating the properties of the analytical device using protein modification with genetic or chemical engineering techniques.

Efficient direct electron transfer (DET) reactions have been reported for a restricted number of redox enzymes. The majority of these redox enzymes contain metal sites and particularly heme. The heme electrochemical properties, such as the formal redox potential for the Fe^{2+}/Fe^{3+} couple, can be varied over a wide range of potentials by changing the protein environment. By itself, heme exhibits several catalytic properties, which drastically change when incorporated into a protein environment. This creates wonderful opportunities for heme-proteins, in terms of their electrochemical applications, especially in the field of biosensors. Nevertheless, several studies based on heme-proteins adsorbed or immobilized on various electrodes showed that high-molecular weight enzymes are not amenable to direct electrical communication with the electrode. The heterogeneous ET with the redox-active centre is unfavoured, due to unavailability of efficient ET routes, also due to partial or full protein unfolding/denaturation on the electrodesurface.

Our strategy to overcome the above limitations is the exploitation of artificial low-molecular weight proteins, designed on rational bases, to possess the required activity. In our laboratory, a new class of heme-peptide conjugate, named Mimochromes, have been developed, with the aim of understanding the effects of the peptide chain composition and conformation in modulating the heme redox potential. The main features of these molecules are the covalent structure and the well defined helical conformation of the peptide chains linked to the deuteroporphyrin ring.

The presented work exploits the use of two different class of Mimochromes, the penta-coordinated Fe(III)-Mimochrome VI and the esa-coordinated Fe(III)-Mimochrome IV Lys^3, in biosensor technology. These two artificial molecules were used as bio-recognition elements/signal transducers for biosensing. The aim of this thesis was to develop and optimise catalytic and affinity-based biosensors for the rapid screening of target analytes in complex matrices.

In a first step, the two synthetic heme-protein models were characterized by square wave and cyclic voltammetry, freely diffusing and bound to a gold electrode surface, to analyse their electrochemical behaviour.

An affinity electrochemical immunosensor was developed taking advantage of the ability of Fe(III)-Mimochrome IV Lys^3 to act as a redox tag for the detection of the binding event between electrochemically inactive species. The system realized comprises a gold electrode on which the electron transfer protein, Fe(III)-Mimochrome IV Lys^3, was covalently anchored through the formation of a self-assembled monolayer (SAM) of 11-mercaptoundecanoic acid. This protein is functionalized with a suitable recognition element: in particular, an epitope (corresponding to the aminoacids 98-106) of the human influenza virus hemagglutinin (HA), recognized by an anti-HA monoclonal antibody, was used. The assembled biosensor was characterized with voltammetric techniques and then tested for analyte recognition. The results clearly demonstrated that the binding of the specific analyte to the recognition element affects the redox properties of the metal ion encapsulated into Fe(III)-Mimochrome IV Lys^3. This makes the developed device a future candidate for use in antibody detection, and may have interesting applications in the diagnostic field.

A bio-catalytic electrochemical biosensor was developed by adsorbing, via hydrophobic interactions, Fe(III)-Mimochrome VI on a SAM of 1-decanthiol. Mimochrome VI was developed to engineer into the Mimochrome scaffold a catalytic site, by creating a cavity able to accommodate small molecules and/or substrates. It is an attractive system to be exploited as novel catalyst or as a constituent of hybrid synthetic interfaces in electrochemical sensing devices.

Cyclic voltammetry experiments were performed to study the thermodynamics and kinetics of the electron transfer process for the Fe(III)/Fe(II) couple of the immobilized molecule, and the ability of this construct to electrocatalitically turn over molecular oxygen. This study opens the way to the development of electrocatalytic hybrid Mimochrome-modified electrode surfaces for biosensing in the clinical and pharmaceutical areas.

List of abbreviations

11-MUA	11-mercaptoundecanoic acid
a.m.u.	Atomic mass unit
Ab	Antibody
Abs	Absorbance
Ac	Acetyl
Ag	Antigen
Arg	Arginine
Asn	Asparagine
Asp	Aspartic acid
Au	Gold
Boc	t-Butoxycarbonyl
CD	Circular dichroism
CV	Cyclic voltammetry
CYP	Cytochrome P450
DCC	Dicyclohexylcarbodiimide
DCM	Dichloromethane
DET	Direct electron transfer
DIEA	Diisopropylethylamine
DMF	Dimethylformamide
DNA	Deoxyribonucleic acid
DPIX	Deuteroporphyrin IX
DT	1-decanethiol
E°'	Formal potential

EDC, EDAC	1-ethyl-3-dimethyl (aminopropyl) carbodiimide
EDT	Ethanedithiol
EtOH	Ethanol
Fmoc	9-Fluorenylmethoxycarbonyl
Gln	Glutamine
Glu	Glutamic acid
HA	Hemagglutinin
HA_ep	Hemagglutinin epitope
HATU	N-[(dimethylamino)-1H-1,2,3-triazolo[4,5-b]pyridin-1-ylmethylene]-N-methylmethanaminium hexafluorophosphate N-oxide
HBTU	2-(1H-Benzotriazole-1-yl)-1,1,3,3-tetramethyluronium hexafluorophosphate
His	Histidine
HOBt	N-hydroxybenzotriazole
IgG	Immunoglobulin G
IUPAC	International Union of Pure and Applied Chemistry
LC	Liquid Chromatography
Leu	Leucine
Lys	Lysine
mAb	Monoclonal Antibody
MALDI	Matrix Assisted Laser Desorption Ionization
MALDI-TOF	Matrix Assisted Laser Desorption /Ionization- Time Of Flight
MeOH	Methanol

Mmt	Methoxytrity
MP-11	Microperoxidases
MS	Mass spectrometry
NHS	N-hydroxysuccinimide
NMR	Nuclear magnetic resonance
Pbf	2,2,4,6,7-Pentamethyldihydrobenzofurane-5-sulfonyl
PCR	Polymerase chain reaction
ppm	part per million
QCM	Quartz crystal microbalance
RMD	Restrained molecular dynamics
RNA	Ribonucleic acid
RP-HPLC	Reverse Phase High Pressure Liquid Chromatography
SAM	Self assembled monolayer
SAW	Surface acoustic wave
SCE	Saturated calomel electrode
Ser	Serine
SHE	Standard Hydrogen Electrode
SPPS	Solid Phase Peptide Synthesis
SPR	Surface-plasmon resonance
sulfo-SMCC	Sulfo-Succinimidyl-4-(N-maleimidomethyl)cyclohexane-1-carboxylate
SWV	Square wave voltammetry
t-Bu	tert-Butyl
TFA	Trifluoroacetic acid

TFE	Trifluoroethanol
TLC	Thin Layer Chromatography
Tris	2-Amino-2-hydroxymethyl-propane-1,3-diol
Trt	Trityl
UV-Vis	Ultra Violet/Visible
VMD	Visual Molecular Dynamics
YCC	Yeast Iso-1-cytochrome *c*

Introduction

Chapter 1: Biosensors, general principles

1.1 Biosensors: history and definition

The field of biosensors represents a rapidly expanding research area devoted to the development of devices to determine the concentration analytes in complex samples. The most important step for biosensors development was made by Clark and Lyons in 1962, who created the first enzyme biosensor, as a result of the work with oxygen electrodes by Clark (Clark, 1956). They suggested the possibility of using enzyme-containing membranes to transform glucose into a product that could be detected with an oxygen electrode, for a rapid, simple and accurate detection of glucose. In their work, it was described for the first time how to make an electrochemical sensor after the attachment of an enzyme onto a transducer. In particular, glucose oxidase was attached on the oxygen electrode and by measuring the decrease of oxygen concentration it was possible to determine the concentration of glucose in the sample. Based on Clark's pioneering work (Clark and Lyons, 1962), the first biosensor was commercialized in 1975 by the Yellow Springs Instrument Company (Ohio). It was a glucose analyzer based on the amperometric detection of hydrogen peroxide. The original model of glucose analyzer has been superseded by more advanced devices, but the basic construction of the biosensor has changed little over the years: glucose oxidase is immobilized between two membrane layers. The outer polycarbonate membrane retains the enzyme, allows glucose to pass, but prevents larger molecules from entering, thus reducing interference. The glucose enters the enzyme layer, where it is oxidized, producing hydrogen peroxide. This passes through the cellulose acetate membrane to a platinum electrode where it is measured amperometrically. The second membrane acts as a further size exclusion barrier preventing other potentially interfering (electroactive) compounds from reaching the electrode surface.

Since then, scientists from different and complementary disciplines (chemistry, biochemistry, physics, molecular biology and material science) have contributed to this multidisciplinary field, developing more reliable and robust biosensing devices

(Figure 1.1) for applications in diagnostic, veterinary, agriculture, food quality, environmental analysis, and bioterrorism prevention.

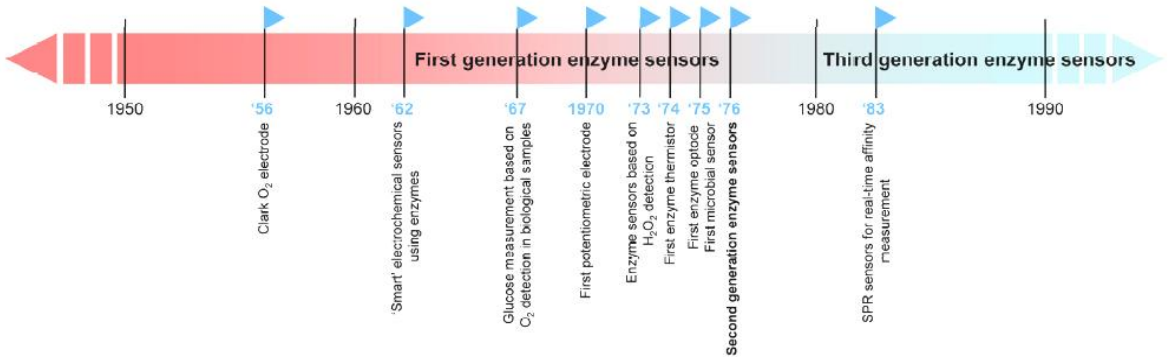

Figure 1.1: *Historical timeline displaying the evolutionary milestones in biosensors development.*

IUPAC defines chemical and biological sensors as in the following: *A chemical sensor is a device that transforms chemical information, ranging from the concentration of a specific sample component to total composition analysis, into an analytically useful signal. Chemical sensors usually contain two basic components connected in series: a chemical (molecular) recognition system (receptor) and a physicochemical transducer. Biosensors are chemical sensors in which the recognition system utilizes a biochemical mechanism (*Thévenot et al., 2001*).*

The biological recognition system translates information, usually an analyte concentration, from the biochemical domaininto a chemical or physical output signal with a defined sensitivity (Figure 1.2). The main purpose of the recognition system is to provide the sensor with a high degree of selectivity for the analyte to be measured *(*Thévenot et al., 2001*).* Biosensing takes advantage of the bio-recognition elements such as whole-cells, cell organelles, tissues, enzymes, antibodies, nucleic acids, proteins and peptides. The fast developments in molecular biology and biomolecular engineering continuously expand the list of possible biological and synthetic bio-recognition elements with great speed.

The biological recognition event needs to be transformed into a measurable signal in conjunction with a physicochemical transduction mechanism. The behavior of both elements, the high specificity of the bio-molecules and the

sensitivity of the transducer mechanism (electrochemical, optical, electrical, piezoelectric, thermal and magnetic) (Collings and Caruso, 1997), make possible to recognize and quantify specific molecules in a complex solution.

The advances in transduction are closely linked to the accelerated technological breakthroughs related to electronics, informatics, data mining, and computer technologies. Signal transduction and data analysis research, oriented to lowering the cost and portability of biosensor analysis, are areas of high activity in electrical and electronic engineering, and analytical chemistry bringing to the construction of more reliable and easy to use biosensors. The coupling between the bio-recognition molecule and the transducer is often a critical step in biosensor development and can be performed by membrane entrapment, physical adsorption, matrix entrapment, or covalent binding among others. It is important to maintain the bio-recognition capacity during such procedures, while at the same time guarantee the robustness and reproducibility of the sensor.

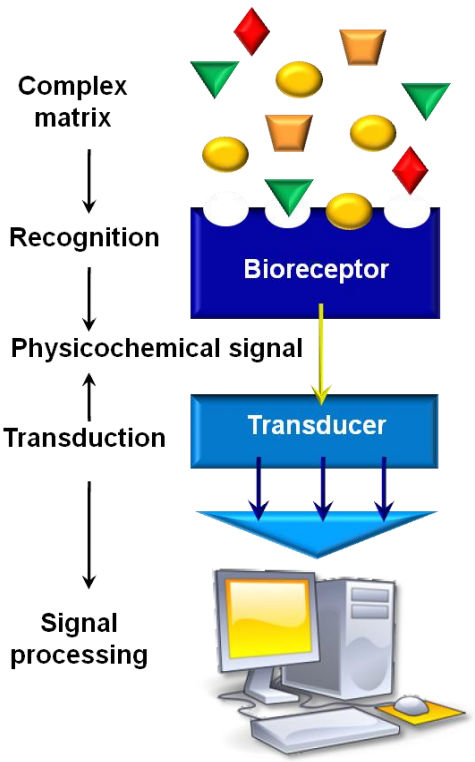

Figure 1.2: *Schematic diagram showing the main components of a biosensor. The bioreceptor binds the analyte. This event is transformed by the transducer, which converts it to an electrical signal. The output from the transducer is amplified, processed and displayed .*

1.2 Biosensors: classification

Biosensors can be classified according to the biological specificity conferring mechanism (recognition element), or to the type of signal transduction or, alternatively, to a combination of the two. They can also be described on the basis of the measurement mode.

1.2.1 Biosensors classification according to the bio-recognition element

Biosensors can be classified according to the type of biological recognition. The interaction of the biological element with a specific analyte can be either “productive” or “non-productive”.

“Productive interaction” is specific to biological catalysis. The biological recognition elements are made up of enzymes or enzymatic cascades.

“Non-productive” recognition is represented by biological affinity interaction, such as antigen-antibody binding, ligand receptor interactions, or DNA-DNA hybridization (Figure 1.3).

Several molecules or whole cells can be used as bio-recognition elements, and the most relevant are discussed below. A particular relevance has been given to enzymatic and immunoaffinity biosensors, since these sensors have been studied during the present project.

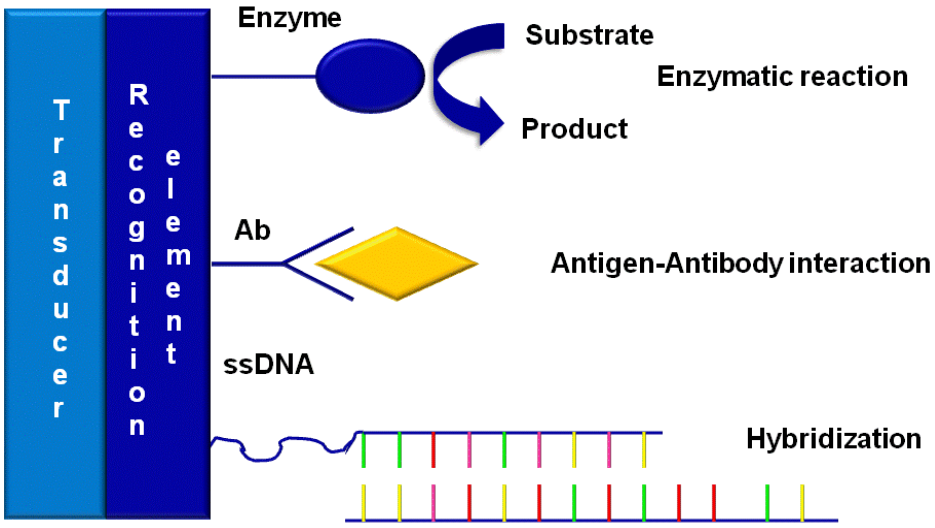

Figure 1.3: *Schematic representation showing the most popular recognition elements.*

a. **DNA biosensors:** They are commonly employed to detect specific sequences of DNA. These biosensors usually employ short synthetic oligodeoxynucleotides for detecting target DNAs with the same length (Palecek, 2002). They can reach high levels of selectivity and affinity based on the hybridization between a DNA target and its complementary probe, which is present either in solution or on a solid support. The system can be used for repeated analysis since the nucleic acid ligands can be

denaturated to reverse binding and then regenerated (Ivnitski et al., 1999). The hybridization event can be detected via electroactive or redox indicators, such as metal coordination complexes or intercalating organic compounds (Peng et al., 2002; Wong et al., 2003; Meric et al., 2002). Besides the electrochemical detection, Surface Plasmon Resonance (SPR) has gained significant popularity in DNA sensing, since measurements can be obtained directly, in few minutes, by measuring the changes in the refractive index of the medium, caused by the binding of the analyte to the sensor surface (Luong et al., 2008). The main disadvantage of this type of biosensor is that DNA has to be extracted from cells or tissue: as a consequence, the sample solution obtained may contain only a small number of molecules; therefore, multiple copies of the sample DNA need to be created for proper analysis. This is achieved by the help of polymerase chain reaction (PCR), providing an additional step in the analysis.

b. **Aptasensors:** Aptamers are oligonucleotides (DNA or RNA) that can bind with high affinity and specificity to a wide range of target molecules, such as drugs, proteins, or other organic and inorganic molecules (Tombelli et al., 2007). Aptamers show a very high affinity towards their targets, with dissociation constants in the micromolar to low picomolar range, comparable to those of some monoclonal antibodies, and sometimes even better (Centi et al, 2009). The high affinity of aptamers towards their target is given by their capability of folding upon binding their target molecule. Aptamers can incorporate small molecules into their nucleic acid structure, otherwise they can be integrated into the structure of larger molecule, such as proteins (Tombelli et al., 2007; O'Sullivan, 2002; Luzi et al, 2003). For the detection of the binding event, electrochemistry offers a large range of techniques, which can be chosen depending on the specific application. Aptamers have also been widely used as bio-recognition elements in optical bioassays, with fluorescence and calorimetry as most popular techniques, and in mass-sensitive biosensors, including evanescent wave-based sensors (e.g., SPR, acoustic wave-based sensors (e.g., quartz crystal microbalance (QCM)) and surface acoustic wave (SAW) devices.

c. **Synthetic peptides biosensors**: New interesting scenarios in the development of affinity biosensors have appeared with the increased understanding of the structure and functions of peptide sequences, in particular as ligand binding molecules. Compared to natural receptors such as antibodies, synthetic receptors, and in particular, synthetic peptides offer many advantages. Peptides are relatively small, stable, and easily obtained through solid phase synthesis (Van den Heuvel et al., 1993). Therefore, peptides and peptide analogues may represent efficient probes in biosensor technology for the detection of specific analytes.

d. **Enzymatic biosensors:** Catalytic biosensors involve a catalytic event in which a substrate is converted into a product. Catalysis occurs at the transducer interface and depletion of the substrate or formation of the product is monitored by a transducer. The most commonly used biological components in catalytic biosensors are enzymes. Enzymes offer several advantages compared to conventional chemical catalysts. These advantages include not only their specificity and selectivity for a particular reaction, but also their discrimination between similar parts of molecules (regiospecificity) and between different isomers (stereospecificity). Enzymes catalyse reactions with a range of reactants (substrates), which may consist of a small number of closely related classes of compounds, a single class of compounds, or even one single compound. In several application, the enzyme stability may represent a problem and the ability to maintain enzyme activity for a long period of time still remains a formidable task to be achieved (Tothill, 2001; D'Orazio, 2003).

e. **Immunosensors:** Biosensors which monitor antigen–antibody interactions are referred to as immunosensors (North, 1985). Either an antigen or antibody is immobilized on a solid-state surface and participates in a biospecific interaction with the other component, allowing detection and quantification of an analyte of interest. The specific interaction is followed by a measuring device (transducer) capable of sensing a change in a physical property resulting from the antigen–antibody interaction. The sensitivity and specificity of an immunosensor are governed by the

specificity and affinity of the antigen–antibody interaction and the noise and selectivity of the transducer. Ideally, an immunosensor would be a reusable device, since the reversibility of the antigen–antibody interaction may allow to regenerate the immobilized component. However, in practice, adequate analytical sensitivity can only be achieved by using antibodies with high affinity (>10^{10} M^{-1}) are used (Hock, 1997). Therefore, a high-affinity constant and a labile immobilized antibody, sensitive to the harsh conditions often required, make regeneration of the surface difficult to realize, limiting practical application of immunosensors to single-use devices (Morgan et al, 1996).

1.2.2 Biosensors according to the transduction method

A variety of transducer methods have been applied in the development of biosensor technology. The most common are reported in Table 1.1 and summarized below:

- **Optical biosensors** are particularly attractive for the applications of direct detection systems (Gerard et al., 2002). They are based on the measurement of the light adsorbed or emitted as a result of a biological and/or chemical reaction. Several optical properties, such as light absorption, fluorescence, bio/chemiluminescence, reflectance, Raman scattering, and refractive index have been exploited as transduction mechanisms for biosensor development (Collings and Caruso, 1997). However, surface plasmon resonance (SPR) has recently been used as the basis for the optical signal transduction in biosensor development (Luong et al., 2008). Even though these biosensors are very sensitive, one of their limitation is that they cannot be used in turbid media.

Table 1.1: *Biosensor transduction systems.*

Types of transducers	Measured properties
Electrochemical	Potentiometric Amperometric Voltametric
Electrical	Surface conductivity Electrolyte conductivity
Optical	Fluorescence Adsorption Reflection
Mass sensitive	Resonance frequency of piezocrystals
Thermal	Heat of reaction Heat of adsorption

- **Piezoelectric biosensors** are considered very useful devices suitable for monitoring bioaffinity interactions in real time without any labeling. The surface of the device, e.g. a quartz crystal, is coupled with a bio-recognition element. When the analyte molecule binds to the specific probe, the mass of the crystal changes. The resulting change in the mass subsequently changes the resonant frequency of the transducer. This frequency change is then measured (Fung and Wong, 2002; Yuan et al., 2002). An example of piezoelectric biosensors are QCM, in which the mass of the crystal increases and the oscillation resonance frequency decreases proportionally upon the binding event. Piezoelectric biosensors offer a real-time output, simplicity of use, wider working pH range, and cost effectiveness. A disadvantage of PZ sensors is the relatively long incubation time, the numerous washing and drying steps, and the problem of regeneration on the crystal surface. This last problem may not be important if small crystals can be manufactured at low cost so that disposable transducers are economically feasible. Possible limitations of this technology include also the lack of specificity, sensitivity and interferences from the liquid media where the analysis takes place (Ivnitski et al., 1999).

- **Calorimetric biosensors** detect substrates on the bases of the heat evolved from the biochemical reactions of the analyte with a suitable biological active substance, such as an enzyme. The most commonly used approach is to attach the substances directly to a thermistor that detects the heat evolved from the biochemical reaction. The majority of the heat evolved in the enzymatic reactions is lost to the surrounding media without being detected. Therefore, the lost heat lowers the sensitivity of the thermal biosensor (Ramanathan and Danielsson, 2001).

- **Electrochemical biosensors** emerge as the most commonly used biosensors, since they are more amenable to miniaturization, have well-suited instrumental sensitivity and can even operate in turbid media. Electrochemical biosensors are mainly used for the detection of hybridized DNA, DNA-binding drugs, glucose concentration, etc. The underlying principle for this class of biosensors is that numerous chemical reactions produce or consume ions or electrons. Therefore, changes in the electrical properties of the analyte can be sensed out and used as measuring parameter.

Electrochemical biosensors can be classified according to the different mechanism of the electronic transport. The so-called *first generation biosensors* are based on the detection of a substrate or a product of a biocatalytic reaction. They work on the direct detection, by an electrode, of the electroactive species that are enzymatically produced or consumed (Dicks et al.,1989). In the most common first generation biosensors that need of a co-substrate in the reaction environment, the enzyme was physically entrapped near the electrode surface. When the electrode was immersed in the sample solution, the enzymatic reaction occurred and the product freely diffused to the electrode surface, generating a signal proportional to its concentration. These systems suffered of several drawbacks, such as the possible interference from electrochemically oxidable compounds in the assay samples and low detection limits due to the slow diffusion of the product to the electrode surface.

The *second generation biosensors* make use of an artificial electron carrier, or mediator, which shuttles the electron involved in the redox process from the active center of the enzyme to the electrode or vice versa (Turner et al.,1989; Pishko et al.,1991; Bartlett et al.,1991; Bourdillon and Majda, 1990). Both mediators and enzymatic substrates must be in the analytical solution. Examples of mediators are low molecular weight redox couple as ferrocene (Yokohama et al., 1989), ferrocene derivatives (Pishko and Katakis, 1990), bipyridil complexes (Betso et al., 1972). Ideally, it is preferable to have a material which communicates directly with a redox enzyme, in order to remove the complexity due to the presence of mediators in the analytical solution. In that case, no cosubstrates (oxygen or mediator) are required and the electrons involved in the process are measured directly at the electrode (DET, direct electron transfer). Enzyme electrodes based on this principle are called *third generation biosensors* (Turner et al.,1989).

The field of third generation biosensors grew a few years ago, when it was found that direct electrochemistry with redox proteins is possible without using a co-substrate (Armstrong and Cox, 1987). The foremost work in this field used mercury electrodes, onto which enzyme adsorption was strong. However, it was observed molecule denaturation. Hence, in order to make the metal electrode compatible with redox enzymes and the biological receptor, surface modification of the bare electrode has been required (Hagen,1989). Nevertheless it has been demonstrated that small redox protein, such as cytochrome *c*, can shuttle electrons directly to bare glassy carbon electrodes (Heller, 1990). For large redox enzyme, such as glucose oxidase, this is difficult to accomplish as they have thick insulating protein shells and their catalytic centers are buried deep inside and protected from the surroundings (Detaxis Du Poet and Miyamoto, 1990). Therefore in these cases they must be immobilized on a compatible modified electrode surface in a way that makes the electron transfer from the catalytic center to the electrode feasible without the occurrence of denaturation (Armstrong, 1988; Boutelle, 1986).

Depending upon the electrochemical property to be measured, electrochemical biosensors can be further classified into conductimetric, potentiometric and amperometric biosensors.

a. ***Conductimetric*** biosensors use noble metal electrodes to measure the changes in conductance/impedance of a solution caused by the biological component. The large applicability of conductimetric detection is due to the observation that almost all enzymatic reactions involve either consumption or a production of charged species, and therefore lead to change in the ionic composition of the enzymatic film. The electric field is generated using a sinusoidal voltage (AC), which helps in minimizing undesirable effects, such as Faradic processes, double layer charging and concentration polarization (Senillou et al., 1999). The primary advantage of this technique is the use of inexpensive, reproducible and disposable sensors. However, in order to obtain a reliable measurement, the ionic species produced must significantly change the total ionic strength of the solution. Therefore, this requirement increases the detection limit to unacceptable levels, and results in potential interferences depending of the ionic strength of the sample.

b. ***Potentiometric*** biosensors measure the potential difference between a working electrode and a reference electrode under conditions of zero current flow (Koncki et al., 2000). The potential generated is directly proportional to the logarithm of the concentration of an ion in an ideal solution. The basis of this type of biosensor is the Nernst equation, which relates the electrode potential (E) to the concentration of the oxidized and reduced species. For the reaction: $aA + ne^- \Leftrightarrow bB$, the Nernst equation can be described as the following,

$$E = \mathrm{E}^\circ + \frac{RT}{nF} \ln\left(\frac{[C_A]^a}{[C_B]^b}\right) \qquad (1.1)$$

where E° is the standard redox potential, R is the gas constant, T is the absolute temperature, F is the Faraday constant, n is the number of exchanged electrons in the reaction, C_A and C_B are the concentration of oxidized and reduced species, respectively. The main advantage of such devices is the wide concentration range for which ions can be detected, generally between 10^{-6} to 10^{-1} mol/l. Their continuous measurement capability is also an interesting possibility for environmental applications. The apparatus is unexpensive, portable, and it is well suited for in situ measurements. The main disadvantage is that the limit of detection for some environmental samples can be high (10^{-5} mol/l or 1 ppm) and the selectivity can be poor.

c. ***Amperometric*** biosensors measure the currents resulting from the electrochemical oxidation or reduction of an electroactive species under a constant potential applied to working electrodes. Amperometric enzyme biosensors form the majority of commercial biosensor devices today available; these biosensors operate at a fixed potential with respect to a reference electrode, while the measured signal is the current generated by the oxidation or reduction of an electroactive species at the surface of a working electrode.

The most important of these is the glucose biosensor, which has been successfully commercialized for blood glucose monitoring in diabetics (Matthews et al., 1987). This signal-transduction mechanism is frequently used for enzymatic and catalytic biosensors. The main advantage of this class of transducer is their low cost; therefore, disposable electrodes often use this technique. The high degree of reproducibility that is possible for these (one time use) electrodes, eliminates the cumbersome requirement for repeated calibration. The type of instrument used for these measurements is also very easy to obtain and can be inexpensive and compact, thus allowing in situ measurements. Limitations of this

signal transduction mechanism include interferences to the response caused by the presence of several electroactive compounds that can generate false current values.

1.3 Coupling between the bio-recognition molecule and the transducer

Since the detection of target molecules and the transduction usually occur at a liquid-solid interface, one key factor in biosensor construction is the development of immobilization technologies for stabilizing biomolecules and tethering them to a solid surface. The usual aim is to produce a thin film of immobilized biologically active material on or near the transducer surface which responds only to the presence of one or a group of materials or substances to be detected. There are a number of requirements that the immobilization technique must satisfy:

- the biological component must retain substantial biological activity when attached to the sensor surface;
- the biological film must remain tightly associated with the sensor surface while retaining its structure and function;
- the immobilized biological film needs to have long-term stability and durability;
- the biological material needs to have a high degree of specificity to a particular biological component.

These conditions must be satisfied for an efficient sensing device.

Further, the immobilization procedure should guarantee that the biological films are assembled by reproducible procedures, and that once formed, these films are adaptable to different environments. In particular, the immobilized films need to be resistant to a wide range of physiological pHs; they must maintain their stability and activity upon changes in the temperature, ionic strength and chemical composition of the solution (Collings and Caruso, 1997). The ability to co-immobilize more than one biologically active component is also desirable in some cases.

Sensitivity is especially important for an efficient biosensor. Biosensor sensitivity depends on both the sensitivity of the detection system and the density of distribution and/or orientation of the biological material near the sensor surface. Therefore, an important aspect of biosensor development, especially for the

affinity based biosensors, is the ability of the immobilization technique used to afford the desired distribution and/or orientation of the biological molecules, once immobilized on the solid surface. Although a high surface density of functional biological molecules is required for a sensitive device, overloading of the surface should be avoided, particularly for affinity-based systems where the biological component is interacting with another biomolecule. While activity generally increases initially with surface loading, high surface loading often leads to biomolecule aggregation with an associated reduction in activity. In these systems, overloading could block or inactivate the active site of the immobilized biomaterial (Collings and Caruso, 1997).

The need of an uniform layering of the biologically active material on the sensor surface, while preserving its structure, has long been recognized as a prerequisite for the production of an optimal biosensor surface. Ideally, the enzyme or protein molecules would be attached to the sensor surface through the same locus, leaving the active site(s) of the biological molecules exposed. It has been suggested that the sensor surface should only react with a single site on the protein, a site which is distant from the active site (Zull et al., 1994).

Numerous biosensors are fraught with problems associated with non-specific binding. Usually, the presence of a specific analyte is to be detected in a 'serum' or in a solution containing many molecular species, and there is interference from other species in the solution. It is common practice to introduce blocking agents (e.g. bovine serum albumin for immunosensing applications) into the system in order to curtail non-specific binding. The non-specific binding must be minimized, in order to obtain unambiguous information on specific biomolecule interactions. It has also been proposed that surfaces with minimal non-specific adsorption of biomolecules should in general be used to attach the biological component through single sites (Zull et al., 1994).

Another important consideration in biomolecule immobilization is that the biological component would not desorb during the use of the biosensor, particularly when the methods of entrapment utilize polymer trapping or membrane barriers to contain the biomolecules.

The available immobilization techniques can be grouped into two categories: direct and indirect binding, that can be further divided into non-covalent and covalent interactions.

1.3.1 Direct binding

Non-covalent interactions. The immobilization by direct, physical adsorption (Figure 1.4 a) is the less complex method, since it involves reversible surface interactions between bioreceptor and support material. The forces involved in the interaction are mostly electrostatic, as ionic and hydrogen bonds, although sometimes hydrophobic interactions become significant. These forces are weak, but sufficiently large in number to enable reasonable binding. This method does not require activation or chemical modification of proteins, and in this way little damage is done to biomolecules. On the other hand, when biomolecules are directly in contact with solid surfaces through adsorption, they can undergo a denaturation process, losing their bio-specific activity (Collings and Caruso, 1997). Another problem of this method is that irregular distributions of randomly oriented protein are commonly observed on the electrode surface. For this reason, biosensors employing adsorbed biomolecules are mostly insensitive and display a large degree of non-specificity.

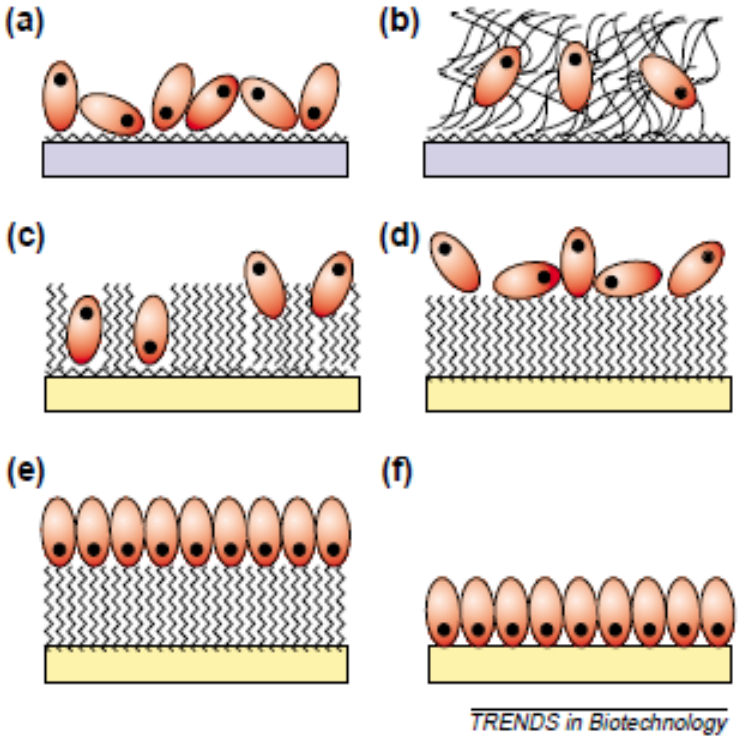

Figure 1.4: *Graphical representation of some methods used to achieve protein immobilization. (a) Physical adsorption; (b) inclusion in polyelectrolytes/conducting polymers; (c) inclusion in self-assembled monolayers (SAMs); (d) non-oriented attachment to SAM; (e) oriented attachment to SAM; (f) direct site-specific attachment to gold.*
(Figure taken from Gilardi and Fantuzzi, 2001.)

Covalent site-specific attachment (Fig 1.4 f). Biomolecules, such as enzymes and proteins, have several functional groups useful for covalent immobilization onto surfaces, such as amino-acid side chains (e.g. amino groups of lysine,

carboxyl groups of aspartate and glutamate, sulfhydryl groups of cysteine), phenolic, thiol and imidazole groups. Covalent coupling between the enzyme or protein and the solid support must occur through functional groups on the biomolecule, which are not required for its biological activity. Suitable functional groups which are available for covalent attachment are also present on some transducer materials (hydroxyl groups on silica). Most surfaces, however, need to be modified in order to introduce a functionality, which may be coupled with the enzyme or protein. Solid supports include glass, titanium dioxide, polysaccharides and polymers (nylon, polymethylmethacrylate), where a bifunctional reagent is reacted with the support giving an activated surface to which enzymes or proteins can then be covalently coupled. Metal surfaces, such as gold and silver, can be modified by reaction with a hydroxyalkanethiol to generate hydroxyl, carboxyl or amino groups, which may react with enzymes or proteins (Collings and Caruso, 1997). Usually, this method leads to the formation of a randomly oriented layer, either on the surface of an electrode or into the cavities formed by the porosity of the matrix.

1.3.2 Indirect binding

The attachment of biomolecules to sensor surfaces can be achieved through indirect binding: the biomolecules are immobilized on the solid surfaces through the formation of self-assembly monolayers (SAM).

Self-assembly is an attractive choice for the immobilisation of probe molecules at surfaces. A self assembled monolayer is a well organized monolayer formed by the attachment of head group of molecules (in case of alkanethiols -SH group) with the surface of a support (Nuzzo et al., 1983). Self-organization is achieved when the alkyl chains align themselves by van der Waals forces and form a compact monolayer (Figure 1.5).

SAMs spontaneously form upon exposure of the substrate to a solution containing the molecules. SAMs have become the focus of intensive investigation as they provide a facile means of defining the chemical composition and structure of a surface (Finklea, 2000). Self-assembled monolayers of thiols, sulphides, cyanides and alkylphosphonates are known to form on different substrates, but most of the work on self-assembled monolayers has focused on SAMs of

alkanethiols. It is possible to find a wide range of terminal functional groups in the adsorbing thiolated molecule without disturbing the self-assembly process or destabilising the SAM. The high affinity of the sulphur head group for a metal substrate and the high strength of the interaction between the two is one of the reasons for the use of SAMs based on alkanethiols in biosensors, as the method is simple and allows for a number of useful attachment chemistries to be realised (Ulman, 1996; Schreiber, 2004; Love et al., 2005). SAMs offer substantial advantages in biosensor development. The ability to pre-design the monolayer on a molecular rational introducing specific interactions between the monolayer and the protein to immobilize should enable tailoring surfaces and acquire them with specific properties and functions. The possibility of achieving an ordered molecular structure oriented specifically and consistently, makes it possible to optimize complexation and protein orientation. Furthermore, the high organization exhibited by the monolayer assures a cooperative and homogeneous behavior of the entire electrode surface. Finally, the molecular dimension of the layer avoids slow diffusion of unwanted electroactive species toward the surface reducing undesired accumulation of species close to the electrode surface (Mandler and Turyan, 1995).

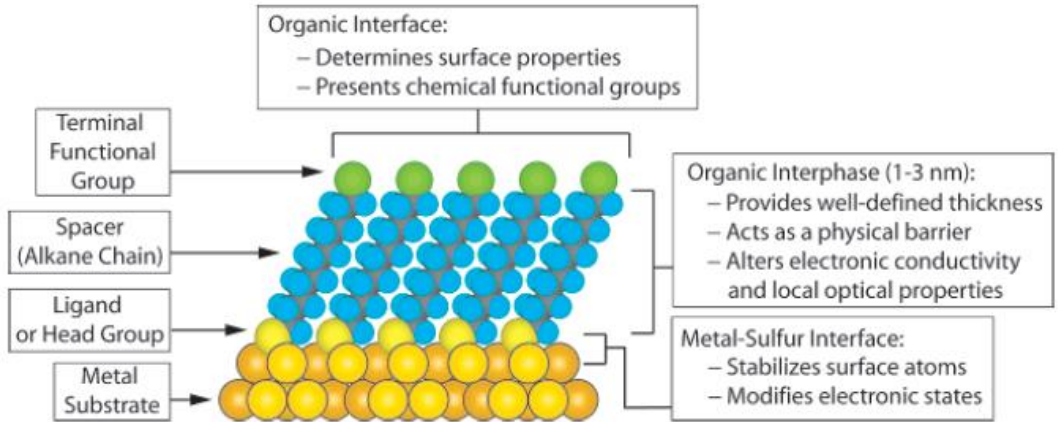

Figure 1.5: *Schematic representation of self-assembled monolayer of alkanethiols on metal substrate (Figure taken from Love et al., 2005).*

SAMs can be used with three different approaches:

Inclusion in SAM (**Fig. 1.4 c**) can be achieved, for example, using alkane-thiol or other thiol-terminated chains immobilized on the surface of a noble metal. The left part of Fig. 1.4 c shows a monolayer of thio-lipids forming a membrane-like structure in which the proteins are immersed in different orientations. The right-hand part of Fig. 1.4 c shows a SAM of alkanethiol chains of different length allowing the formation of depressions on the surface that can accommodate the protein molecules.

The other two approaches involve interaction of the molecules to be immobilized with the exposed terminal functional groups (ω-groups) (Mandler and Turyan, 1995). Functional groups such as $-NH_2$, -OH and -COOH have been widely used. Through the proper selection of the terminal functional group, specific surface/solution interactions (chemical covalent, electrostatic, or hydrophobic) can be exploited to immobilize molecules at the interface.

Non-covalent interactions with SAM. The most common non covalent approach to immobilizing molecules to a SAM coated surface is via electrostatic binding (Gooding and Hibbert, 1999). This simple and gentle method provides the potential for control over the orientation of the immobilized protein molecules depending on the charge distribution of the protein. It can provide even oriented (Fig. 1.4 e) and non-oriented attachment to the SAM (Fig. 1.4 d), depending on the protein structure and aminoacidic composition. Therefore this method has been used to investigate direct electron transfer between enzymes (Li et al., 1997) or redox proteins (Tarlow and Bowden, 1991) more frequently than for the development of sensors directly. The major drawback of electrostatic binding is that the strength of the bond is dependent on the solution conditions. Changes in ionic strength and pH can cause the protein to be lost from the surface of the SAM (Hodak et al., 1997).

Covalent attachment to SAMs has the greatest potential for the development of commercial sensors due to the stability of the resultant bond (Gooding and Hibbert, 1999). A popular, and highly versatile, method for covalently attaching proteins to SAMs is by using carbodiimide coupling which couples amines to carboxylic acids. If proteins to immobilize have several reactive groups, this interaction is not site-specific, it results in a *non-oriented attachment to SAM* (Fig.

1.4 d). *Oriented attachment to SAM* (Fig. 1.4 e) can be achieved with the same strategy, but here, the reactive function of the SAM can interact specifically, with a unique site on the protein surface. This unique site, if not naturally present in the protein sequence, can be made either by chemical modification of an existing surface residue or by a genetic engineering approach.

Gold is the most widely used substrate for alkanethiols based SAMs. The first reports of SAMs formed on gold substrates were highly focused on the preparation of atomically flat, well-defined, gold surfaces. Using these surfaces some very important characteristics alkanethiols SAMs have been extracted. Gold is a noble metal that can be handled in air without the formation of an oxide surface layer, and can survive harsh chemical treatments such as those used to remove organic contaminants during cleaning. Gold electrodes may be composed of bulk gold, either polycrystalline or single crystal, or thin films deposited on various substrates.

Finally, an alternative method for the non-covalent immobilization of biological molecules is *encapsulation in polyelectrolytes or conducting polymers* (Fig 1.4 b). In this case, the proteins are trapped either in a polyelectrolyte or in a conducting polymer that is directly adsorbed or linked to the surface. This results in a non-oriented multilayer film.

Chapter 2: Heme-proteins and biosensors development

2.1 Heme-proteins, structures and functions

Hemes are prosthetic groups widely used in nature. Heme-containing proteins include molecules with distinct activities, ranging from electron transfer, catalysis, oxygen transport and storage, ligand binding, signal transduction, and control of gene expression. This functional diversity is strictly related to the versatility of the heme group and to the protein scaffolds, that create different heme environments. Because of these reasons, heme-proteins have been the focus of a great deal of work over the last century. In addition to their distinct functions, heme-proteins feature a fascinating range of different folding architectures. The phylogenetic

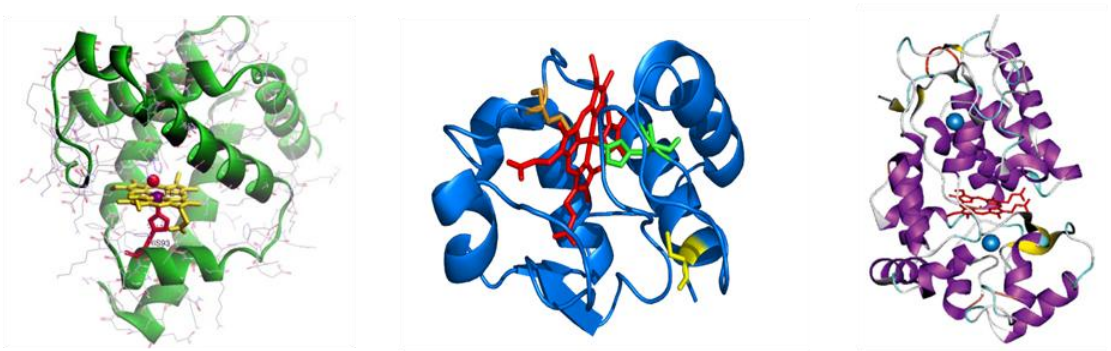

(a) **(b)** **(c)**

Figure 2.1: *Three natural heme-proteins: Myoglobin (a), Cytochrome c (b) (Figure taken from Bortolotti et al., 2006) and Horseradish Preoxidase (c).*

widespread occurrence of hemes originates from the use of porphyrins in photosynthesis and cellular respiration for energy transduction reactions, supporting the proton motive force (PMF) (Paoli et al., 2002). Oxygen transport and storage by hemoglobin and myoglobin account for the ubiquitous presence of heme throughout vertebrates and invertebrates.

How different proteins are able to fine-tune the environment of the heme cofactor, thus producing such different chemistries, is becoming increasingly clear through the study of natural and artificial model systems.

High-resolution X-ray crystallographic data as well NMR analysis available for an increasing number of heme-proteins, have deeply contributed to understanding their reactivity and structural and electronic properties at the molecular level (Bertini and Luchinat, 1999; Perutz et al., 1998; Peterson and Graham, 1998;

Loew and Harris, 2000; Li and Poulos, 1994; Wong, 1998; Smith and Veitch, 1998; Banci, 1997; Sono et al., 1996; Barke, and Ferguson, 1999; Poulos et al., 1999; Michel et al., 1998; Lederer, 1994). It is now well ascertained that the protein matrix, which surrounds the heme active site, controls the intrinsic reactivity of the prosthetic group, selecting one reaction as the only or predominant one.

However the inherent complexity of natural heme proteins continues to obscure the full description of the factors governing the heme properties.

Therefore, a large number of artificial model systems are being developed in an attempt to (i) provide further insights for structure-activity relationships, (ii) understand the minimal requirements for function, (iii) reproduce the properties of the parent natural proteins in smaller molecules, and (iv) most importantly construct new, tailor-made molecules useful for biomedical, pharmaceutical, biological, and environmental applications.

2.1.2 Heme structure: properties of the porphyrin macrocycle

The basic structure of natural heme protein is a tetrapyrrole macrocycle called porphyrin. The porphyrin (shown in figure 2.2) consists of four pyrrole-like five-membered units, A, B, C and D, which are linked by four methine bridges, 5, 10, 15, 20 (meso positions). The porphyrin macrocycle is an aromatic system

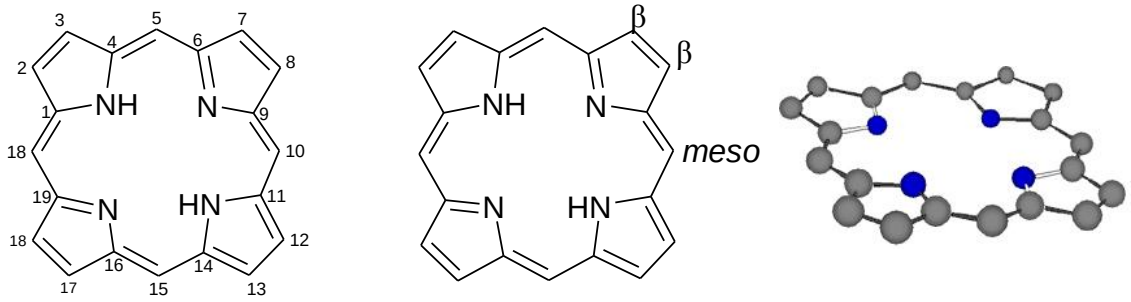

Figure 2.2: *Basic structure of the porphyrin macrocycle: numbering, functionalization sites and planarity.*

containing 22 π electrons, but only 18 of them are involved in a delocalization pathway. Porphyrin obeys Huckel's rule of aromaticity (4n + 2 π electrons, n = 4) and is shown by X ray crystallography to be planar. The aromatic character of porphyrins can also be seen by NMR spectroscopy. Due to the anisotropic effect from the porphyrin ring current, the NMR signals for the deshielded meso protons appear at low field (8 to 10 ppm), whereas the signals for the shielded protons (on the inner nitrogen atoms) appear at very high field (-2 to -4 ppm).

The identity of porphyrin in natural heme proteins is distinguished by its peripheral β-pyrrolic substituents, as shown in Figure 2.3. The most common heme tetrapyrrole macrocycle is *heme b* or iron(II) protoporphyrin IX, whose structure was synthetically demonstrated by Hans Fischer (Fischer and Zeile, 1929). The term “heme” specifically refers to the ferrous complex of protoporphyrin IX, with the ferric-hydroxy and ferric-chloride complexes to as hematin and hemin, respectively.

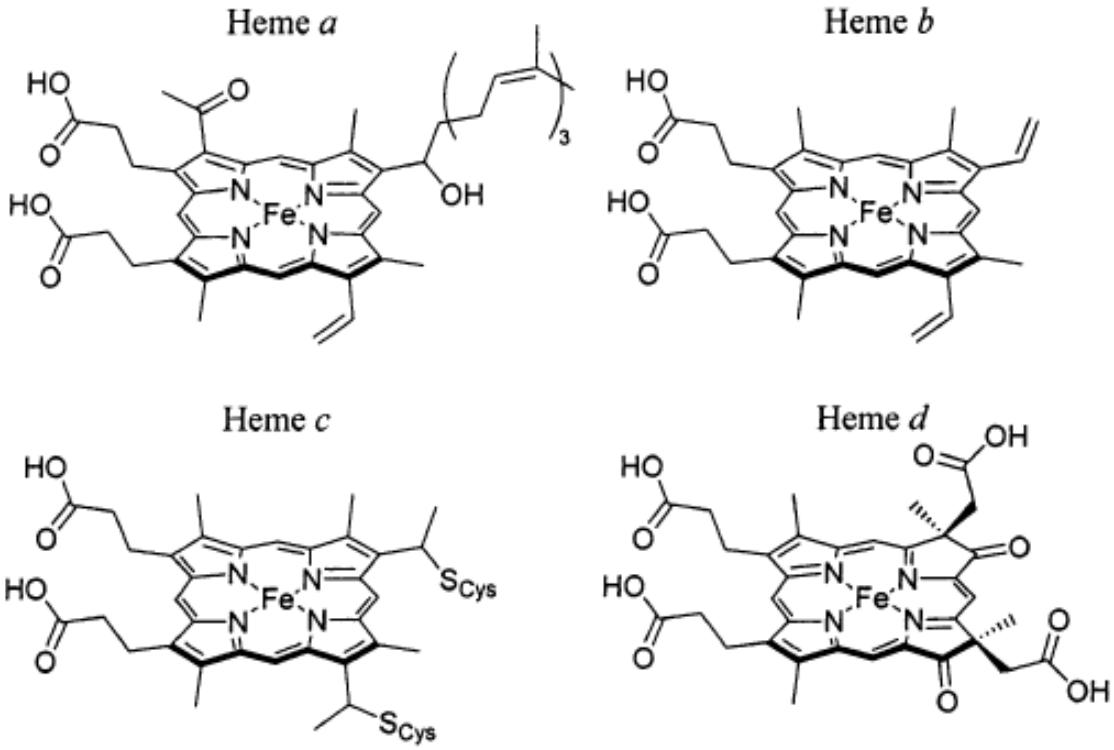

Figure 2.3: *: Chemical structures of commonly occurring natural hemes a, b, c, and d. (Figure taken from Reedy and Gibney, 2004).*

Heme b, also called protoheme, has methyl groups at positions 1, 3, 5, and 8, vinyl groups at positions 2 and 4, and propionates at positions 6 and 7 on the macrocycle. All the porphyrins are synthesized in vivo as the free base forms before incorporation of the iron(II) by the enzyme ferrocheletase (Sellers et al., 2001; Wu et al., 2001). Additionally, *heme b* serves as the structure from which *hemes a* and *c* are biosynthetically derived (O’Brian and Thony-Meyer, 2002; Mogi et al., 1994; Brown et al., 2002). Aside from b-type cytochromes, heme b is also found in globins, cytochromes P-450, and heme-sensor proteins. Protein scaffolds bind hemes via the combination of the axial coordination positions available on

iron, hydrophobic interactions with the heme macrocycle, and polar interactions with the propionic acids (Hargrove and Olson, 1996; Hargrove et al., 1996; Breslow and Koehler, 1965; Breslow et al., 1967).

Heme c is structurally similar to *heme b* except that thioether bonds to cysteine residues replace one or both the vinyl groups and covalently link the heme macrocycle directly to the protein scaffold (Moore and Pettigrew, 1990). The covalent attachment of heme to the protein is effected by the enzyme heme lyase (Drygas et al, 1989), but in vitro chemical synthesis has also been used to form the thioether bonds in b-type cytochrome and c-type cytochrome scaffolds (Sano and Tanaka, 1964; Barker et al., 1996; Tomlinson and Ferguson, 2000; Arnesano et al., 2000). Cytochromes c typically contain a CXXCH sequence motif from which the two cysteines link to the porphyrin macrocycle and the histidine binds to the encapsulated iron. The presence of the covalently linked heme designates it a c-type heme that includes all cytochromes c as well as cytochrome f (Martinez et al., 1996). *Heme a* is biosynthesized from *heme b* by conversion of the vinyl group at position 2 into a hydroxyethylfarnesyl side chain, yielding *heme o*, followed by subsequent oxidation of the methyl at position 8 to a formyl group (Mogi et al., 1994). These modifications render *heme* both more hydrophobic and more electron-withdrawing, as an equatorial ligand to iron, than *heme b*. *Heme a* is found only in terminal oxidases such as mammalian cytochrome c oxidase. Other less common heme architectures include heme d (Vainshtein et al., 1986), heme (Williams et al., 1997), heme P-460 (Igarashi et al., 1997), siroheme (Crane et al., 1995), and chlorocruoroheme (Lemberg and Falk, 1951).

2.1.3 Coordination properties

It is now well ascertained that the protein matrix, which surrounds the heme active site, controls the intrinsic reactivity of the prosthetic group, selecting one reaction as the only or predominant one. The protein composition and structural organization of the peptide chain dictate the properties of the primary (metal coordination geometry, number, type, and donor properties of the axial ligands) and secondary (local dielectric constant, hydrophobicity, and hydrogen bonding interactions near the active site coordination sphere) coordination shells. Further, the protein directs long-range interactions (Tainer et al., 1992). These factors all contribute to the functional specificity of the heme.

It has been well recognized that the primary coordination sphere plays important roles in modulating the structure and function of heme proteins, such as

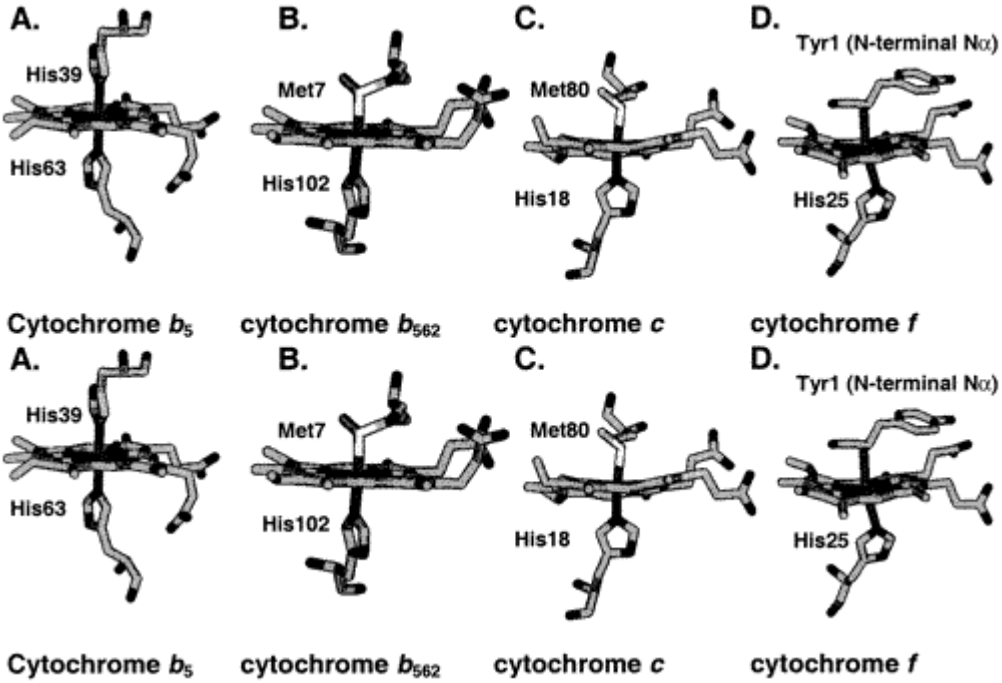

Figure 2.4: *: Cytochromes with different axial ligand coordination.*

redox potentials, electronic structure, spin states, electron-transfer rates, and catalytic properties (Moore and Pettigrew, 1990; Scott and Mauk, 1996; Turano and Lu, 2001; Goodin, 1996; Gross, 1996, Banci et al., 1996; Weiss et al., 1996).

Several amino acids are known to serve as axial or proximal ligands to heme proteins (Moore and Pettigrew,1990; Scott and Mauk, 1996; Turano and Lu, 2001). In cytochromes (cyt), histidine, methionine, lysine, and cysteine are common axial ligands that coordinate the heme. Bis-His and His-Met coordination, found in cyt b5 and cyt c, respectively, are by far the most common ligation states of the cytochromes (Figure 2.4). Other ligation states, such as bis-Met and His-Lys, have also been found. Interesting ligation from the terminal α-amino group of a peptide bond has been observed in cyt f (Figure 2.4) (Martinez et al., 1994).

Heme-based sensors and enzymes are mostly five coordinate with an open site for binding small molecules such as O_2 and CO. In these proteins, histidine is by far the most common axial ligand, with cysteine and tyrosine found in a few classes of heme enzymes such as cyt P450, chloroperoxidase (CPO), and catalase (Figure 2.5). Recently, a new axial ligand, the N-terminal nitrogen of proline, was discovered in the CO sensing heme protein called CooA (Figure 2.5) (Lanzilotta et al., 2000).

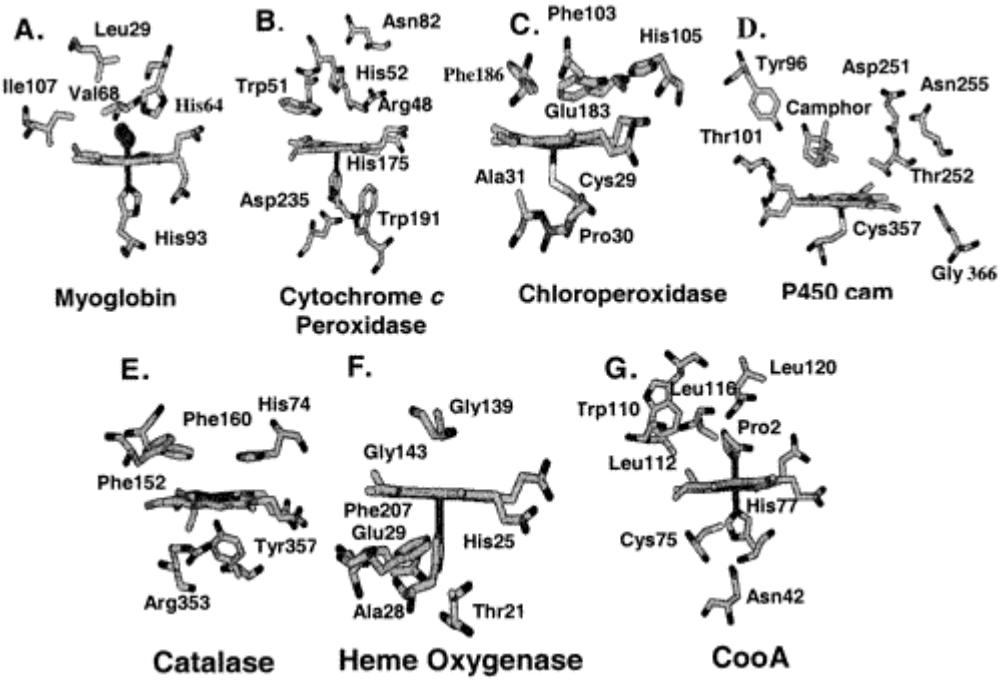

Figure 2.5: *: Heme proteins with one open coordination site.*

While the axial ligands to heme iron establish the basic coordination chemistry, the interaction of amino acids beyond the primary coordination sphere is critical of modulating the chemical properties of the heme, allowing it to perform a variety of biochemical functions. The local protein environment surrounding the heme more finely regulates the heme-protein properties, such as the iron redox potential (Tezcan et al., 1998; Mauk and Moore, 1997; Gunner et al., 1997; Naray-Szabo', 1997; Wuttke and Gray, 1993; Gray and Winkler, 1996). For instance, a large number of positively charged residues around the heme in hemoglobin and myoglobin may favour a low oxidation state for the iron, making it ready to bind dioxygen. On the contrary, the progressive change in the polarity of the surrounding peptide environment, from a negative charge distribution in cytochromes b to a positive one in cytochromes c, determines a gradual increase

in the Fe(III)/Fe(II) redox potential. The resulting stabilization of the matching Fe(II) and Fe(III) states enables cytochromes to mediate the electron transfer.

2.2 Direct electron transfer

Electron transfer reactions of biomolecules are central to the most fundamental processes of life. Respiration, for example, is the stepwise oxidation of an organic substrate through a series of redox reactions involving a chain of electron acceptors, between which electrons are shuttled by electron carriers such as cytochromes, iron-sulphur proteins and flavin nucleotide coenzymes. These molecules also play a similar role in the photo-induced electron transfer chain of the photosynthesis. Consequently, the study of metalloproteins electrochemistry should provide invaluable insights into the dynamic behaviour of the molecules involved in meeting the energy requirements of all living organisms. In particular, direct electrochemistry of metalloproteins and metalloenzymes is a subject of immense interest in recent years, because of its potential application in the study of the redox and electron transfer properties of the biomolecules (Armstrong et al., 1986; Armstrong, 1990).

Efficient direct electron transfer reactions have been reported for a restricted number of redox enzymes. The majority of these redox enzymes contain metal sites and particularly heme. The first reports on a reversible DET between redox proteins and electrodes were published 30 years ago, and showed that cytochrome c (Cyt c) is reversibly oxidized and reduced at tin doped indium oxide (Yeh and Kuwana, 1977) and gold in the presence of 4,4 -bipyridyl (Eddowes and Hill, 1977). At the same time the DET between bare electrodes and enzymes was reported for laccase, peroxidase, and P450-enzymes (CYP-enzymes) (Varfolomeev and Berezin, 1978; Yaropolov et al., 1979; Tarasevich, 1979; Scheller et al., 1977).

The redox potential of the heme moiety varies from high negative value, -450 mV (Davis, 1978) in simple aqueous and non-aqueous solutions, to a very high positive value when embedded inside the protein cavity, e.g. + 260 mV (vs SHE) in cytochrome *c* (Guo and Hill, 1991). Moreover, its electrochemical characteristics, e.g., formal potential ($E^{0'}$) for its redox conversion from Fe^{3+} to Fe^{2+}, can be varied over a wide range of potentials by the protein environment, e.g., from + 260 mV for cytochrome *c* to −270 mV for HRP (Harbury, 1957). By itself, heme exhibits

various catalytic properties, which drastically change when incorporated into a protein environment. This creates wonderful opportunities for the heme-proteins and heme-enzymes in terms of their bioelectrochemical applications, e.g., in biosensors based on direct electron transfer between redox proteins and electrodes (third generation biosensors).

Cytochromes *c* and P450 have been studied as components of bio-catalytic surfaces (Gray et al., 1994; Scott and Mauk, 1995). These proteins have a good stability in a wide range of temperature and pH, and they are able to exchange electrons quite rapidly with solid electrodes (Battistuzzi et al., 1997; Battistuzzi et al., 1999), therefore they have been employed as components of electrocatalytic complexes protein-electrode, active in the reduction of dioxygen and hydrogen peroxide.

Cytochromes P450 constitute a super family of heme enzymes found from bacteria to humans (Nelson et al., 1996). Cytochrome P450 monooxygenases are versatile biocatalysts that introduce oxygen into a variety of substrates, many of them are molecules of pharmaceutical interest. The ability of all P450s to activate the Fe–O–O moiety (universal for all P450s) is determined by the mode by which the heme (here, heme b) is bound to apoprotein. The central atom of the heme macrocycle, i.e., the heme iron, is bound to the protein through the anionic, thiolate sulfur of a cysteine residue. This type of bond gives the heme moiety the ability to mediate the transfer of electron density to the dioxygen bound as the trans (sixth) ligand of the heme iron (Anzenbacher et al., 1989). Hence, this bond also explains why the heme b (the same as in the well-known hemoproteins, hemoglobin and myoglobin) possesses here this unique property characteristic of all P450s, that is the ability to activate the dioxygen for chemical reactions (Anzenbacher and Anzenbacherová, 2001).

Since their discovery and the elucidation of their structure, cytochromes P450 have attracted the interest of scientist for many years, particularly due to their catalytic abilities. Since the late 1970s, attempts were concentrated on the construction and development of electrochemical sensors. Although sensors based on mediated electron transfer have also been constructed, the direct electron transfer approach has attracted most of the interest (Bistolas et al., 2005).

The electrochemistry of CYPs was investigated using a variety of metal electrodes such as Au, Pt and Tin oxide, as well as non-metal electrodes such as glassy carbon (GC), pyrolytic graphite (PG), edge-plane graphite (EPG), and carbon cloth (CC). Although direct electron transfer was observed on bare electrodes, modifying the electrode with an appropriate medium, such as a polymer or a polyelectrolyte, has been very popular in recent years. This was often performed in order to attain native structure and appropriate orientation, with the consequence of increasing electron transfer between the enzyme and the electrode, (Bistolas et al., 2005). Cytochrome P450, efficiently linked to solid electrodes, can provide the opportunity of studying numerous xenobiotics from a biosensoristic point of view (Gilardi and Fantuzzi, 2001). Gilardi and co-workers took advantage of protein engineering to build assemblies with improved electrochemical properties (Gilardi et al., 2002). They used the molecular Lego approach with the bacterial P450 BM3 from Bacillus megaterium (BMP). The heme domain of P450 BM3 was used as a module in the construction of an electrochemically active assembly, fused with a redox modules, flavodoxin from Desulfovibrio vulgaris (FLD) generating the BMP–FLD fusion protein and creating an artificial redox chain (Fantuzzi et al., 2006). In this work it was found that the catalytic activity of BMP was improved by almost 6 times when it was fused to the non-physiological redox partner FLD. Thus, the authors demonstrated that the molecular Lego approach was successful for improving electrochemical and catalytic properties of P450 BMP, suggesting that the same approach could be used for the production of new devices for nanobiotechnoloical applications.

Cytochromes *c* is the most extensively studied molecules at various electrode surfaces, due to their diffusion (they are present virtually in all living systems), stability, and ease of purification (Banci et al., 1999; Gray and Ellis, 1994; Moore and Pettigrew, 1990; Pettigrew and Moore, 1987; Scott and Mauk, 1996). These species are monomeric heme-proteins, in which the heme group(s) is covalently linked to the polypeptide chain through two thioether bonds involving two cysteines and two axial ligands to the iron (His, Met). Cyt *c* are grouped into four subclasses on the basis of their structural properties (Moore and Pettigrew, 1990). The most widely studied species belong to class I, found in both eukaryotes and prokaryotes, which feature a low spin six-coordinate heme iron possessing a His-

Met axial coordination, and to class III, which are multiheme proteins with bis-histidinyl coordination of bacterial origin (Moore and Pettigrew, 1990; Pettigrew and Moore, 1987; Scott and Mauk, 1996). In electrochemical studies, particular emphasis was placed on the redox behaviour of the molecules, the rate dependence of the electron transfer process on pH, and the type of electrode, employing bare metal or modified electrode surface (Hanrahan et al., 1996). Electron transfer from cytochrome *c* to metal electrodes such as platinum, gold, nickel, mercury and p-type silicon has shown to be slow due to adsorption induced denaturation (Tarasevich, 1985; Bowden et al., 1985; Daido and, Akaike, 1993). However, direct and quasi-reversible electrochemistry was observed with the surface modified electrodes of metals, such as platinum (Gui and Kuwana, 1987), gold (Bortolotti et al., 2006; Monari et al., 2008), and glassy carbon (Wang et al., 2002). For example, Sola and co-workers studied the redox behavior of the Yeast Iso-1-cytochrome *c* (YCC), native and mutated, covalently immobilized on unmodified gold electrodes at varying temperature and pH values (Bortolotti et al., 2006). They found that pH induced conformational transition both in the native protein and in its mutants (C102T/N62C). The observed conformers presented differences of 300 mV in the measured E°', due to the detachment of both the axial ligands from the heme iron at low pH. In this acidic condition, the Iso-1-cytochrome *c* was able to catalyze dioxygen reduction. Moreover, the electron transfer rate was slow and strongly influenced by the protein orientation on the electrode surface. The same group achieved the electrochemical characterization of the Met80Ala YCC variant (Casalini et al., 2008), in which the axial heme iron Met ligand was replaced by a non-coordinating Ala residue. This penta-coordinated mutant, covalently bound to a gold electrode surface, was able to electrocatalitically reduce dioxygen between pH 5 and 11. This opens the way to the exploitation of Met80Ala YCC variant for O_2 biosensing.

Despite the tremendous progress made in the development of heme-proteins based biosensors, a major problem in these electrochemical systems lies in the electrical communication between the redox protein and the electrode.

Direct electron transfer can be difficult to achieve, and the electron transfer rates between the majority of redox proteins and electrode surfaces are often

prohibitively slow (Zhang and Li, 2004). This may be due to several reasons, as reported in the following:

- Unfavourable orientation of protein molecules on electrode surface may hinder electron exchange between the electrode and the electroactive centre of the proteins, which is usually deeply buried inside the polypeptide chains, especially in larger proteins.
- The "bad" orientation may increase the distance between the redox centre and the electrode surface, thus limiting the direct electrochemistry of the molecules (Zhang and Li, 2004).
- The monolayer concentration/coverage of the redox protein on the electrode surface decreases as the protein size increased, thus resulting in low electrochemical signals.
- Natural proteins can also denaturate on the electrode surface, blocking the electron exchange (Heller, 1990; Armstrong, 1990).

A strategy to overcome the above limitations is the use of artificial proteins, designed on rational bases to possess the required activity, structural robustness (to prevent denaturation on the electrode surface), and small size (to simplify the electron transfer path to the electrode and increase surface coverage).

For application in biosensor technology, we have employed a particular class of heme-protein models, named Mimochromes.

2.3 Synthetic heme-protein systems: the Mimochromes family

Our laboratory has approached the challenge of constructing heme-protein models using a miniaturization process (Nastri et al., 1998). A miniaturized heme-protein is a peptide-based model which contains a minimum set of constituents necessary for

- an accurate reconstruction of a well-defined structure and
- a fine tuned reproduction of a defined function.

This strategy leads to the development of a class of miniaturized heme-proteins, named mimochromes (Nastri et al., 1997; D'Auria et al., 1997; Lombardi et al., 1998; Nastri et al., 1998; D'Andrea et al., 1999). The schematic structures of mimochromes are reported in Figure 2.6.

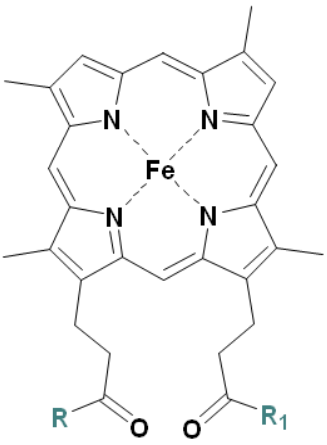

Mimochrome	R, R_1	
I	R=R_1	Ac-L-A-Q-L-H-A-N-K-L-NH_2
II	R=R_1	Ac-D-L-S-D-L-H-S-K-K-L-K-I-T-L-NH_2
IV	R=R_1	Ac-E-S-Q-L-H-S-N-K-R-NH_2
III, V	R	Ac-D-E-H-K-L-H-S-K-K-R-K-I-T-L-NH_2
	R_1	Ac-D-E-H-K-L-Y-S-K-K-R-K-I-T-L-NH_2
VI	R	Ac-D-E-Q-Q-L-H-S-Q-K-R-K-I-T-L-NH_2
	R_1	Ac-D-E-Q-Q-L-S-S-Q-K-R-NH_2

K= Lysine bound to the porphyrin

H= Histidine coordinating the metal center Y=G or S

Figure 2.6: *: Schematic representation of Mimochromes.*

Mimochromes are peptide-porphyrin conjugates, with *pseudo*-C_2 symmetry. They are made up of deuteroporphyrin, covalently linked to two peptides (nine or fourteen residues), via an amide bond between the porphyrin propionyl groups and the side chains of two Lys residues (Nastri et al., 1997; D'Auria et al., 1997; Lombardi et al., 1998; Nastri et al., 1998). The peptide fragments, which face the porphyrin plane, are in α-helical conformation, a common feature of several natural heme-proteins. The α-helix is a well-defined rigid scaffold, which can accommodate several amino acid substitutions without severe structural perturbations; therefore, numerous model compounds, based on helical peptides, have been developed (Moffet and Hecht, 2001; Lombardi et al., 2001). The peptide sandwiched mesoheme (Benson et al., 1995; Arnold et al, 1997; Wang et al., 1997), the disulfide linked α-helices-mono-heme adducts (Sakamoto et al., 1998; Sakamoto et al., 1999; Rosenblatt et al., 2002), the MOP derivatives (Rau and Haehnel, 1998; Rau et al., 1998; Rau et al., 2000), and the heme-maquettes (Robertson et al., 1994; Shifman et al., 1998; Shifman et al., 2000; Gibney and Dutton; 1999) are examples of either covalent or non-covalent artificial heme-peptide conjugates.

The prototype Mimochrome I was designed on the β-chain of human deoxyhemoglobin as template structure. The X-ray structure of deoxyhemoglobin (Perutz et al., 1982) showed that the proximal His^{89} residue is located in the central position of the Leu^{88}-Leu^{96} protein fragment. This protein fragment adopts an helical conformation. It represents a rigid framework both for properly positioning His^{89} in the correct coordination site, and for completely covering one face of the heme. The helix axis is about parallel to the porphyrin plane; hydrophobic residues surround the axial coordinating residue and face the heme directly.

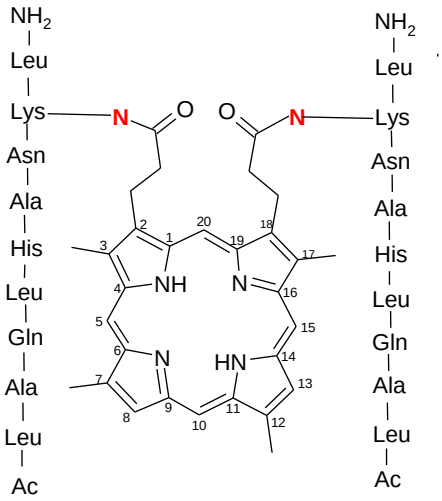

***Figure 2.7**: Formula of Mimochrome I: (3, 7, 12,17-tetramethyl-porphyrin-of N^{ε}_{8}-(Ac-Leu^{1}-Ala^{2}-Gln^{3}-Leu^{4}-His^{5}-Ala^{6}-Asn^{7}-Lys^{8}-Leu^{9}-NH_2)-propionamide).*

All the information derived from the analysis of the natural systems served as starting points for engineering the mimochrome models. As a first step in this direction, we used the Leu^{88}-Leu^{96} fragment as a scaffold for building a nine residue polypeptide sequence able to fold into an α-helical conformation (Nastri et al., 1997; Figure 2.7). The natural sequence was appropriately changed by considering the factors that affect helix stability.

Therefore, Ser^{89} and Cys^{93} were replaced with alanine, which is known to have a high preference for the α-helical conformation. The resulting sequence contained five helix inducing residues, $Leu^{1,4,9}$ and $Ala^{2,6}$. Moreover, Glu^{90} and Asp^{94} were substituted with Gln and Asn respectively, in order to obtain an uncharged compound. N- and C-terminal ends were acetylated and amidated, respectively, to avoid unfavorable end-charge to helix-dipole interactions. The peptide chain was then covalently linked to the porphyrin propionic group through the ε-amino function of Lys^{8}. Molecular modeling showed that changing the side chain conformation of Lys^{95} as found on the β chain of deoxyemoglobin and the conformation of the closest propionyl carboxyl group, the lysine ε-amino group may approach the carboxyl group at bonding distance. Finally, an identical peptide

chain was placed on the other side of the heme by applying a C_2 symmetry operation (Figure 2.8) .

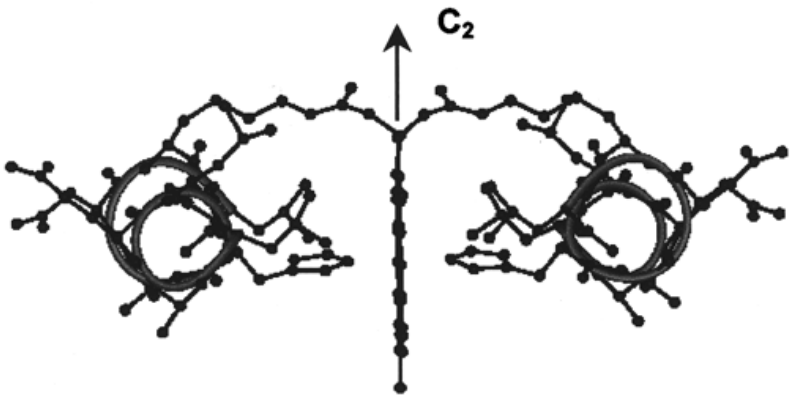

Figure 2.8**:** *Helix-heme-helix sandwich obtained by applying a C_2 symmetry operation.*

The two covalent bridges between the peptide moiety and the porphyrin, together with the coordination of the two His residues, would make the peptide chains able to cover both heme faces. These factors would also serve as a strong local constraint to firmly keep the prosthetic group inside the hydrophobic cavity created by the two peptide chains. Finally, deuteroporphyrin was preferred to the most common protoporphyrin IX to avoid degradation of the sensitive vinyl substituents during the synthesis.

The fully characterization of Mimochrome I iron and cobalt complexes confirmed the design, even though some unexpected features were observed. The iron complex showed quite low solubility in water (in the µm range), in a wide range of experimental conditions (D'Auria et al., 1997; Nastri et al., 1997; Nastri et al., 1998;) Its detailed characterization was henceforth strongly limited. On the opposite, the cobalt complex was soluble in water (up to mM concentration), but two equally abundant isomers were obtained (Figure 2.9).

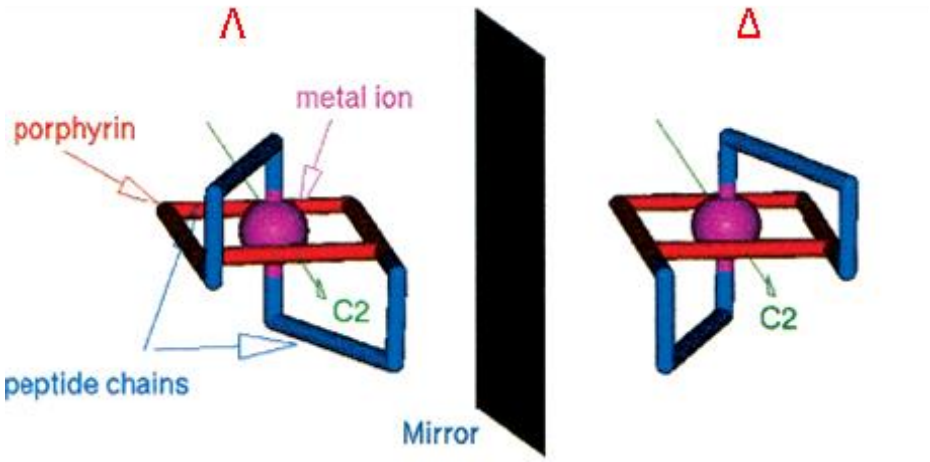

Figure 2.9**:** *Schematic representation of the two possible orientations of the peptide chains around the metal center, which give rise to the two Λ and Δ diastereomers.*

Because of the flexibility of the linker between the peptide and the deuteroporphyrin ring, each peptide chain can be positioned either above or below the porphyrin plane, giving rise to Λ and Δ diastereomers (Lombardi et al., 1998; Figure 2.10). This finding was confirmed by the solution structural characterization (D'Auria et al., 1997). In fact, the NMR structures of the two diamagnetic Co(III) isomers (Figure 2.10), which represent the first example of structure determination of a designed heme-protein models, allowed a definitive identification of the two isomers as the Λ and Δ diastereomers and a straightforward correlation between their structure and spectral properties. As expected, the peptide chains adopt an almost regular α-helical conformation; the helices lie parallel to the porphyrin plane, and they are antiparallel to each other in the Λ isomer and about orthogonal in the Δ isomer (Figure 2.10). The analysis of the three-dimensional structure of the two cobalt isomers was important in understanding the properties of the Fe(II) and Fe(III) complexes, which could not be studied by NMR spectroscopy because of their poor solubility. The remarkably different solubility between the iron and cobalt complexes was tentatively attributed to the simultaneous presence of the two diastereomers, for the iron complex, in fast interconverting equilibrium. During this process both peptide chains might be displaced from the porphyrin plane. The porphyrin ring is thus exposed to the solvent, and aggregation by stacking of the porphyrin ring may occur. Confirmation for this hypothesis came from the CD spectral properties in the Soret region, which are an average of those corresponding to the two separate diastereomers.

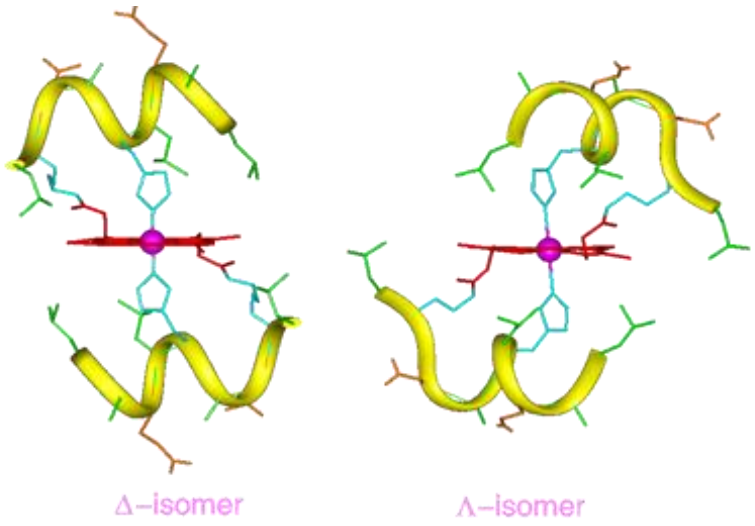

Figure 2.10: *Average molecular structures of Co(III) mimochrome I Δ and Λ isomers, as obtained from NMR experimental data and RMD calculations.*

The unpredicted but experimentally observed Λ and Δ isomers of Co(III)-mimochrome I clarify the concept of diastereomerism that may occur when polypeptides coordinate to metal ions. The use of local *pseudo*-C_2 symmetry is particularly advantageous to construct symmetric molecules with minimized size, because it simplifies the design, reduces the size of the molecules to be synthesized, and may simplify their structural characterization (Lombardi et al., 2000a; b). However, great attention should be paid in the design to overcome the problem of diastereomer formation.

The information derived from Mimochrome I was fruitfully applied for improving the structure by design. Two strategies were used to reduce the peptide flexibility:

- by elongating the peptide chain at the C-termini, with a four residue fragment, modeled in an extended conformation;
- by amino acid substitutions that may provide intra-molecular, inter-chain interactions.

The first strategy was successfully applied, as reported for mimochrome II, where the stabilization of the Λ isomer was achieved (Lombardi et al., 1998). The second strategy led to the design of mimochrome IV, where the lambda isomer was observed as unique species.

2.3.1 Fe(III)-Mimochrome IV and its analogs

Mimochrome IV was designed by using the NMR structures of Co(III)-Mimochrome I Δ and Λ isomers as templates (D'Auria et al., 1997). Mimochrome I contains two leucine residues at both the N- and C-termini. These residues were selected in the initial design of Mimochrome I, because of their high propensity to be accommodated in α-helical conformation (DeGrado et al., 1999). Further, it was expected that hydrophobic interactions, between the leucine side chains and the porphyrin, would drive the helices to lay on the porphyrin. Nevertheless as mentioned previously , the sandwich was stable for the Co(III) derivative, and not for the Fe(III) (Nastri et al., 1997; D'Auria et al., 1997). In order to provide an extra contribution to the stability of the sandwich, beside the metal coordination force, the sequence of Mimochrome I was modified by introducing intra-molecular, inter-helical interactions.

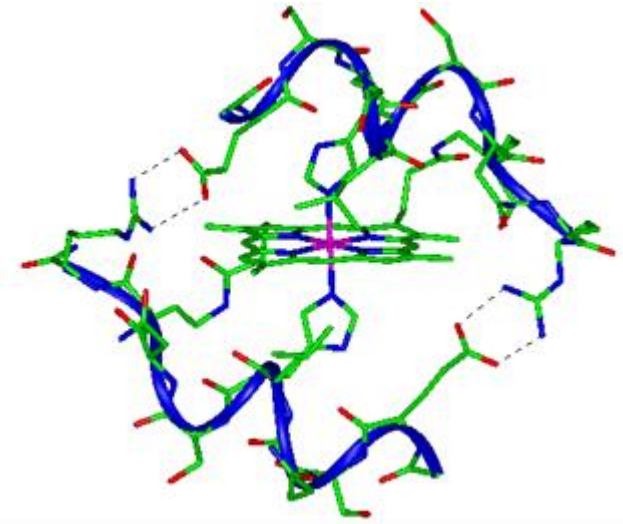

Figure 2.11: *Co(III)-Mimochrome IV average structure as obtained from NMR data and RMD calculations.*

The C_α atoms of Leu^1 of one helix and of Leu^9 of the other helix are about 12 Å apart in both isomers. At this distance, the carboxylate side chain of a Glu residue at position 1 of one peptide chain could ion pair with the guanidine group of an Arg residue at position 9 of the other peptide chain. Thus, Glu^1 and Arg^9, which replace Leu^1 and Leu^9, was inserted to stabilize one of the two possible diastereomers. Further, the solvent exposed Ala^2 and Ala^6 in Mimochrome I, were replaced by Ser residues in Mimochrome IV, in order to further increase the water solubility of the new molecule.

The insertion of Glu and Arg residues at position 1 and 9 of the sequence, respectively, was successful in stabilizing the sandwich structure and in favoring the formation of Λ isomer (Figure 2.11) over the other, both in the Fe(III) and Co(III) complexes. These results were confirmed by NMR data and RMD calculations (Lombardi et al., 2003). The UV-vis pH titration showed the iron *bis*-His coordination is strong enough to bring the His pK_a value around 3.8. The *bis*-

His coordination is even stronger in Co(III) complex, and it occurs at very acidic conditions (pH < 2).

This finding is related to the high preference of cobalt for nitrogen donor ligands, and to the exchange inertness of low-spin Co(III) complexes. These low pK_a values of the axially coordinating His (with values very close to what observed in several myoglobins, hemoglobins and cytochromes in the oxidized and reduced forms) strongly support the designed sandwich structure (Palaniappan and Bocian, 1994; Coletta et al., 1997).

CD spectra in the far UV region confirmed the peptide chain to be predominantly in an α-helical conformation in both the apo and metalated species. The definitive answer of the structural identity of the diastereomer stabilized in Mimochrome IV was obtained by NMR structural characterization of the cobalt complex. The NMR analysis fully confirms the UV-Vis and CD data, both regarding the helical conformation of the peptide chains, and the Λ configuration of the hexacoordinated CoIII ion. The RMD calculations, using the NMR experimental data as conformational restraints, indicated two helical peptide chains, oriented about perpendicularly.

In summary, Mimochrome IV is a simple, structurally defined heme protein model, which provide an excellent opportunity for exploring the subtle mechanisms that control the heme functions. The peptide structure of Mimochrome IV is such that a partially open hydrophobic cage around the imidazole ring is present. Except for the position 20 of the deuteroporphyrin ring, all the other meso positions are covered by the polypeptide chains, which, similarly to the natural systems, may protect the deuteroporphyrin ring from degradation during catalytic cycles.

The amino acid composition of Mimochrome IV was then modified by the substitution of serines, glutamines and asparagines, which point outward from the molecular core, with differently charged residues for modulating the redox potential of the heme. Based on the Mimochrome IV design, two new models were obtained: Mimochrome IV 8Glu and Mimochrome IV 8Lys (G. Del Gatto PhD thesis, 2007; Figure 2.12), that contained respectively eight Glu residues and eight Lys residues.

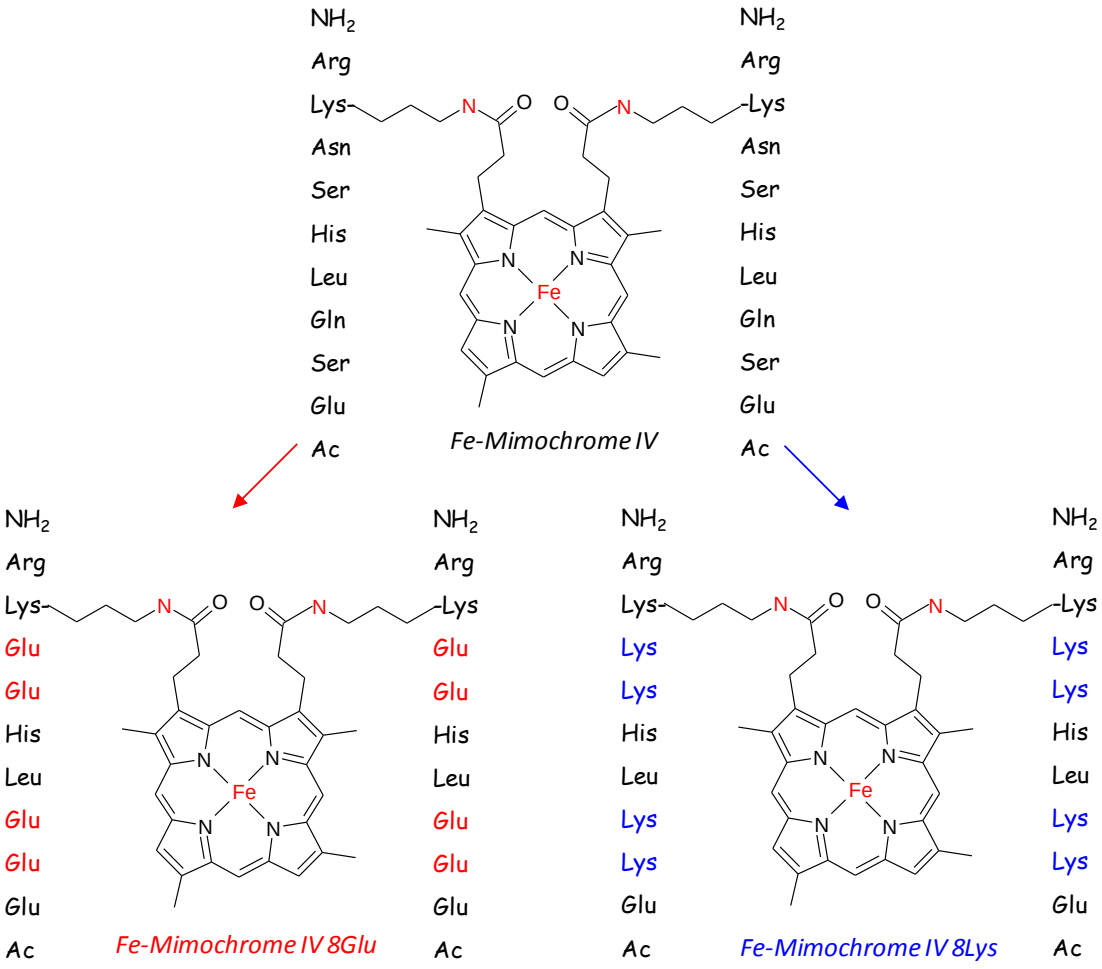

Figure 2.12: *Schematic structures of Mimochrome IV and its differently charged analogs Mimochrome IV 8Glu and Mimochrome IV 8Lys.*

The spectroscopic characterization of the two models, Mimochrome IV 8Lys and Mimochrome IV 8 Glu were performed. The UV-vis spectra of both Fe(III)-Mimochrome IV 8Glu and Fe(III)-Mimochrome IV 8Lys, at pH 7, are typical of octahedral *bis*-His low spin complexes, in good agreement with the spectral features previously observed for Fe(III)-Mimochrome IV. CD measurements in the

UV region indicates the peptides to be in helical conformation, in both complexes at pH 7 (G. Del Gatto PhD thesis, 2007).

The effect of the charge distribution on the redox properties of the metal center has been determined by square wave voltammetry in solution.

The deuteroheme redox potential of Fe-Mimochromes, at pH 7, are the following:

Fe-Mimochrome IV 8Glu: -170 mV vs SHE
Fe-Mimochrome IV: -58 mV vs SHE
Fe-Mimochrome IV 8Lys: -48 mV vs SHE

E°'Fe-Mimohrome IV 8Glu < E°'Fe-Mimochrome IV < E°' Fe-Mimochrome IV 8Lys

The measured redox potential of -170 mV for Fe-Mimochrome IV 8Glu and -48 mV for Fe-Mimochrome IV 8Lys demonstrate that negatively charged residues, as for Fe-Mimochrome IV 8Glu, around the molecular core, stabilize the ferric deuteroheme, while the positively charged residue of Fe-mimochrome IV 8Lys stabilize the ferrous deuteroheme. This hypothesis was further confirmed from the redox potential of the parent Mimochrome IV (-58 mV), that is intermediate between that Fe-Mimochrome IV 8Glu and Fe-Mimochrome IV 8Lys (G. Del Gatto PhD thesis, 2007). The potential values measured are that expected from the electrostatic properties of the heme environment.

Moreover, these redox potential values of Mimochromes are significantly more positive than the reduction potential of bis-imidazole-ligated heme, as Fe(protoporphyrin IX)$(Im)_2$, -235 mV vs SHE, or Fe(mesoporphyrin IX)$(Im)_2$, -285 mV vs SHE. This result would suggest that the sandwich structure of Mimochromes decreases solvent exposure, thus leading to a positive shifts of the reduction potential.

In summary, Fe-Mimochrome IV and the analogs Fe-Mimochrome IV 8Glu and Fe-Mimochrome IV 8Lys are simple, structurally defined deuteroheme protein models, which may provide an excellent opportunity for exploring the subtle mechanisms that control the redox properties of the heme in natural proteins. Additionally, they are able to exchange electrons with solid electrodes, making them suitable for application in biosensor technology.

2.3.2 Fe(III)-Mimochrome VI

Mimochrome VI (Fig. 2.13) is the result of a refinement procedure, which involved several cycles of molecular design, characterization end redesign. In particular, the NMR solution structure of Co(III)-Mimochrome IV (Lombardi et al., 2003) and the model structure of Co(III)-Mimochrome II (Lombardi et al., 1998) were used as starting point. They both are examples of *bis*-His cobalt porphyrin-peptide conjugate. The first is a bis-tetradecapeptide-porphyrin conjugate, and the latter is a bis-nonapeptide-porphyrin conjugate. Both are *pseudo*-C_2 symmetrical systems. the sequences of Mimochrome II and IV were combined to construct an unsymmetrical five-coordinate *mono*-histidine model. The primary structure contains a histidine (His^6) on the tetradecapeptide chain (derived from the sequence of Mimochrome II), as potential axial ligand to the metal (proximal face), and a serine (Ser^6) on the decapeptide chain (derived from the sequence of Mimochrome IV) in order to create a cavity near the metal site (distal face). Some substitutions from the sequences of Mimochrome II and IV were introduced to further stabilize the secondary and tertiary structure. Similarly to other Mimochromes, both peptide chains are covalently linked to the porphyrin propionate through the Lys^9 side chains. In terms of secondary structure, the tetradecapeptide was designed to adopt: a short helical conformation (residues 1-9), a loop $\gamma\alpha_D$ (residues 10-11), and a short β-strand (residues 12-14) that folds back (through the loop) to interact with the helical part; the decapeptide adopts a helical conformation (residues 1-8). The tertiary structure can be described with the characteristic sandwich of the Mimochrome molecules. The two peptide chains embrace the metalloporphyrin; the helical segments are antiparallel to each other and the helix axes are about parallel to the porphyrin plane. Stabilization of the

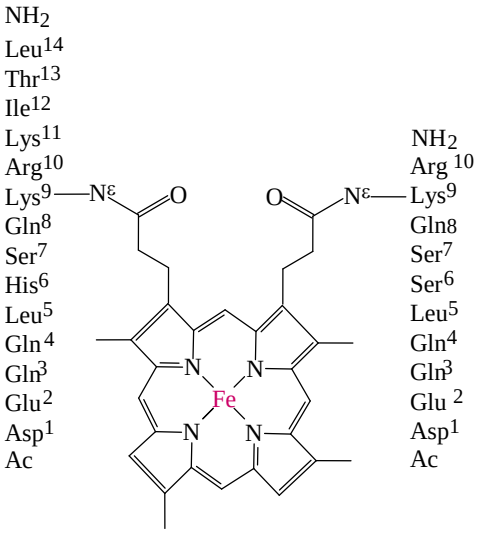

Figure 2.13: *Schematic structure of Mimochrome VI.*

tertiary structure was contributed by inter-chain ion-pairs between the carboxylate side chains of glutammate residue (Glu^2) on the helix and the guanidine groups of arginines (Arg^{10}) on the other helix. The positive Arg^{10} and the negative Glu^2 at the C-terminal and N-terminal ends, respectively, with opposite sign relative to the helix dipole, may also provide stabilization of the secondary structure. Finally, several glutamines ($Gln^{3,4,8}$) and a serine (Ser^7) were introduced in the solvent exposed positions to convey water solubility (Nastri el al., *submitted*). Spectroscopic studies indicate that Fe(III)-Mimochrome VI is able to coordinate small exogenous ligands, such as carbon monoxide and nitric oxide, thus confirming the existence of an easily accessible face of the heme (Nastri el al., *submitted*). Further, Fe(III)-Mimochrome VI catalyzes the oxidation of several substrates by the activation of hydrogen peroxide (Nastri el al., *submitted*). All these results demonstrates that Fe(III)-Mimochrome VI embodies some of the key elements for reproducing the functional properties of heme oxidases, such as peroxidases and cytochrome P450, which catalyze a variety of oxidation reactions by using clean oxidants (H_2O_2 and O_2).

2.4 Aims of the thesis

This work aims at the development of nano-structured devices made up of heme-protein mimetics immobilized on solid electrodes, to be exploited as active constituents of third-generation biosensors, to detect and quantify analytes of clinical and environmental interest.

The first objective is to take advantage of the remarkable properties of the Mimochrome models, in terms of direct electron transfer, molecular recognition and redox catalysis, to obtain layers of synthetic proteins immobilized on electrode surfaces, able to yield quantitative amperometric responses upon interaction with given molecular targets.

In particular, two type of devices for the development of third-generation biosensors will be discussed:

- Affinity biosensors, obtained by coating a gold electrode with one of the Fe(III)-Mimochrome IV analogs, functionalized with a RE, through an appropriate spacer. The heme-protein mimetic acts as redox wire to detect the biological event, such as the recognition between the epitope HA_ep and its specific antibody.

- Biocatalytic biosensor, developed using gold electrodes coated with Fe(III)-Mimochrome VI, able to electrocatalitically reduce molecules of clinical interest, such as dioxygen.

Results and Discussion

Chapter 3: Development of affinity electrochemical biosensors

3.1 Introduction

During the past few years, affinity biosensors have attracted growing attention. In fact, they show numerous advantages over alternative methods, such as high sensitivity, selectivity and robustness (Hock et al., 1997). The extremely high selectivity and affinity of antibody/antigens, receptors and DNA molecules for their corresponding targets have been widely exploited for analytical purposes in various fields (environmental analysis (Suri et al., 2002; Mallat et al., 2001), clinical diagnostics (Luppa et al., 2001) and the food and drink industries (Mello and Kubota, 2002)).

The development of an affinity biosensor involves first the selection of a naturally occurring macromolecule, which provide the desired analyte specificity (typically DNA or antibodies). Subsequently, a suitable signal transduction and detection methodology needs to be adapted to the selected macromolecule (Rogers, 2000). This step in affinity biosensor construction generally requires long development time, since the recognition elements are so different that is impossible to realize a simple, unique detection method (Rogers, 2000).

To overcome this limitation, new approaches are being developed. Protein engineering is used to adapt the signal-transduction properties of the biological molecules to the detector instrumentation and to the transduction chemistry, rather than adapting instruments and chemistry to the unique requirements of each natural molecule. In the present work, we have followed this approach by integrating a small synthetic heme protein, which provides a simple signal-transduction mechanism, between the detector and the bio-recognition element.

3.2 Affinity biosensor based on synthetic peptides

The system developed in the present study is a third generation electrochemical affinity biosensor, based on the artificial heme-protein models named Mimochromes IV. These molecules have been selected as redox tags for the detection of the binding event between electrochemically inactive species.

3.2.1 General structure of the biosensor and working hypothesis

The basic element of the biosensor system proposed (Figure 3.1) is an electrode linked to a signal transducer, which is made up by a miniaturized electron transfer proteins derivatized with a recognition element (RE). The working hypothesis is that upon binding of the RE (antigen, enzyme inhibitor, receptor agonist or antagonist, DNA binding peptides, etc.) to the analyte (antibody, enzyme, receptor, DNA, etc.) the redox potential of the metal ion encapsulated into the electron transfer protein changes. This change is very likely to occur because the charge distribution is affected by the binding. Thus, detection of a target analyte can be performed through measurements of electron transfer protein redox potentials. The innovation offered by such a system relies on the direct integration of the signal-transducer into the recognition element.

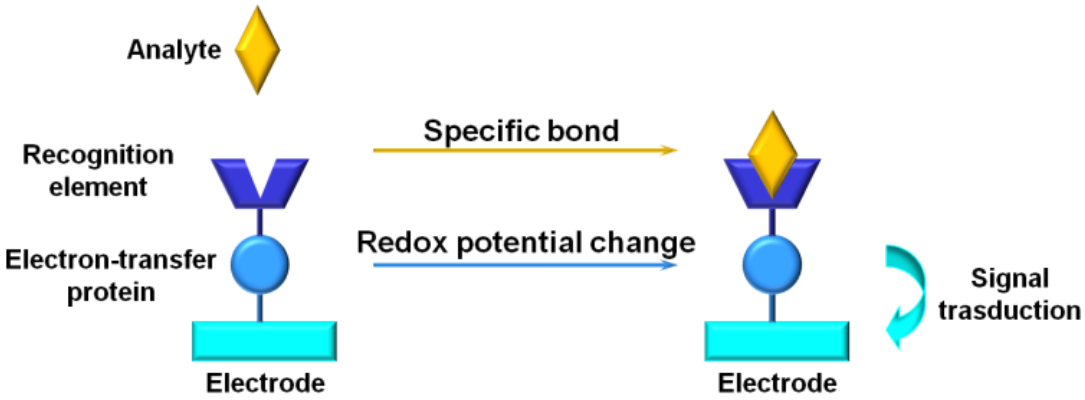

Figure 3.1: *Schematic representation of the proposed affinity electrochemical biosensor.*

The main feature of this system is its versatility: in principles, it could work with every recognition element/analyte pair able to produce a conformational change that can influence the charge distribution around the metal center of the electron transfer molecule.

3.2.2 The electron transfer protein

In an electrochemical biosensing system like the one we have developed, it is of fundamental importance the choice of the electron transfer protein, which must be able to exchange electrons rapidly and directly with the electrode. This can be obtained using small synthetic heme proteins models, the Mimochromes IV analogs. They consist of a heme group linked to two α-helical peptide chains via an amide bond between the porphyrin propionyl groups and the side chains of two

Lys residues. Two His residues axially coordinate the heme-iron (See section 2). Owing to their small size, the heme group is not buried inside the protein scaffold, and they can successfully achieve direct electron transfer with the supporting electrode.

In a previous PhD thesis (G. Del Gatto PhD thesis, 2007), three Mimochrome IV analogs (Mimochrome IV, Mimochrome IV 8 Glu and Mimochrome IV 8 Lys) were synthesized and characterized. All the results demonstrate that these molecules could be useful for electrochemical application. As a consequence, the first step of the present work was to investigate the most suitable procedures to immobilize Mimochrome molecules on the electrode surface, and to functionalize them with a biorecognition element.

The most popular methods to bind a protein on a solid surface or to another protein is the introduction of functional groups on the ε-amino group of the Lys residues side chain. Mimochrome IV and the 8 Glu analogue lack free lysines in their sequence. On the opposite, the 8 Lys analogue possesses too much free lysine to obtain a mono-oriented layer.. Therefore, a new analog was synthesized, starting from the sequence of the parent Mimochrome IV. The Gln^3 in the peptide sequence was substituted with a Lys, in order to have one free lysine residue on each peptide chain. This molecule was named Mimochrome IV Lys^3 and its schematic structure in shown in Figure 3.2.

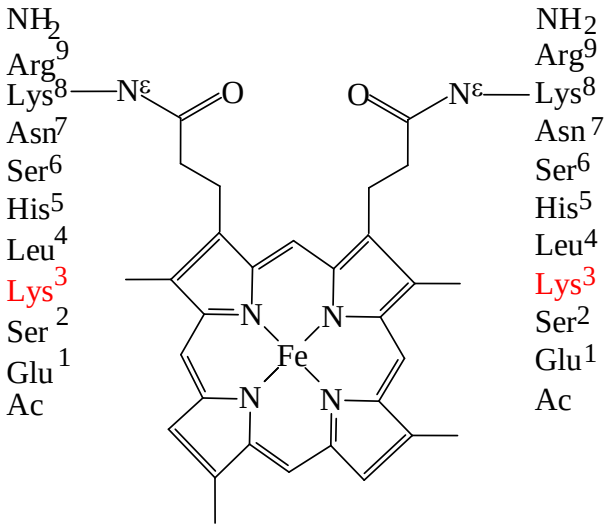

Figure 3.2: *Schematic structure of Mimochrome IV* Lys^3.

3.2.3 Choice of the analyte-recognition element couple

Biosensors, which monitor antigen–antibody interactions, are referred to as immunosensors, and are among the most popular affinity biosensors. This kind of sensors employ either an antigen or antibody immobilized on a solid surface and participates in a biospecific interaction with the other component, allowing

detection and quantification of an analyte of interest. The specific interaction is followed by a measuring device (transducer) capable of sensing a change in a physical property resulting from the antigen–antibody interaction.

Coupling of immunological reactions to amperometric electrodes has been demonstrated as a versatile technique for the measurement of numerous analytes of clinical interest (D'Orazio, 2003; Liu et al., 2008; Liu and Gooding, 2009).

To assay the effectiveness of the hypothesized biosensor system, we decided to test the ability of Fe(III) Mimochrome IV Lys^3 to transduce an antigen-antibody binding event into an electrochemical signal.

To this purpose, we decided to functionalize the heme-protein model with a synthetic peptide corresponding to the 98-106 amino acid sequence (YPYDVPDYA) of the human influenza virus hemagglutinin (HA), known as HA epitope (Kolodziej and Young, 1991). This epitope constitutes the recognition element in the affinity electrochemical biosensor developed, to detect the presence of the specific antibody. This epitope was chosen because of the simplicity of the synthesis and the availability of commercial monoclonal antibodies, with high affinity that can ensure the specificity of binding.

3.2.3.1 A brief description of antibodies (the analyte) and antigens (the RE)

Antibodies are immune system-related proteins, called immunoglobulins. Antibodies can be classified into five classes, IgG, IgM, IgA, IgE and IgD (Figure 3.3). The IgD, IgE and IgG antibody classes are each made up of a single structural unit, whereas IgA antibodies may contain either one or two units. IgM antibodies are pentameric made up of five disulfide-linked structural units (Figure 3.3).

IgG antibodies are further divided into four subclasses (*isotypes*). Immunoglobulin G (IgG) is the most abundant immunoglobulin derivative in serum. This class of antibodies is also the most commonly used in immunochemical assays and sensor applications. The IgG molecule consists of four polypeptide chains, two identical heavy (H) chains and to two identical light (L) chains, joined together to form a Y shaped molecule (Figure 3.4). The identical H-chains are connected via disulfide bridges. Disulfide bonds are also responsible for the connection between the L- and H-chains, referred to as inter-chain disulfide

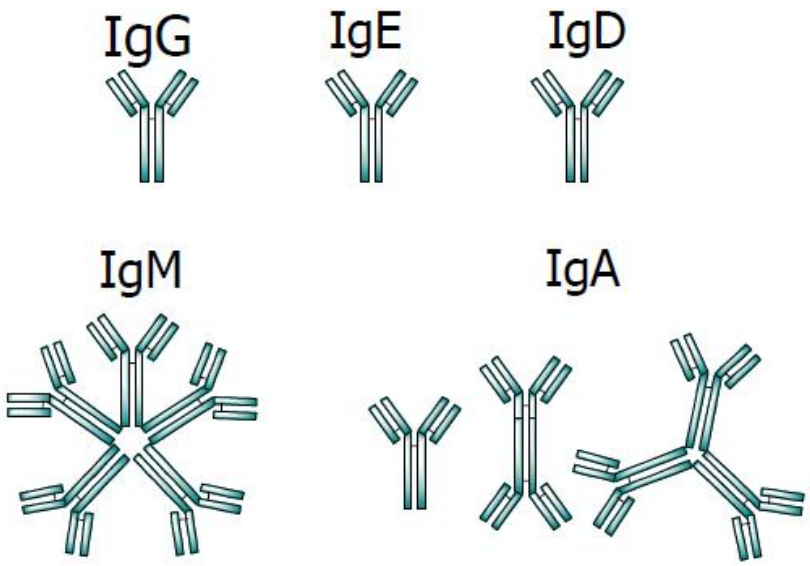

Figure 3.3: *Structures of the different classes of immunoglobulins.*

bridges. Each chain is further divided into regions or domains, consisting of ≈ 110 aminoacid residues. The light chain consists of two domains while the heavy chain is made up of four domains. The N-terminal domain at the tip of the arms of the "Y" on both the light and the heavy chain are known to be variable in their amino acid sequence, and are thus referred to as variable (V_L and V_H) regions. The subdomains of the H-chain are made up of three C regions (C_H1, C_H2, C_H3) and one V region (V_H). The L-chain, on the other hand, consists of one C region (C_L) and one V region (V_L). The base of the Y shaped antibodies is called Fc fragment (fragment that crystallizes) and is formed by the association of the two C_H2 and two C_H3 domains. Each arm of the Y shape is referred to as Fab fragment (fragment containing the antibody binding site) and is formed by the association of C_H1 with C_L and V_H with V_L (Figure 3.4). The binding site (paratope) of the antibodies is located within the V_H and V_L domains, each arm containing one binding site. In the variable regions, amino acid sequences can vary from one antibody to another. Certain regions within the V regions have very high amino acid residue variability. These regions are called hypervariable regions, also known as complementary determining regions (CDRs). Three CDRs are integrated into the L-chain and three into the H-chain resulting in six CDSs for each arm (Roitt et al., 1985; Kaplan et al., 2003).

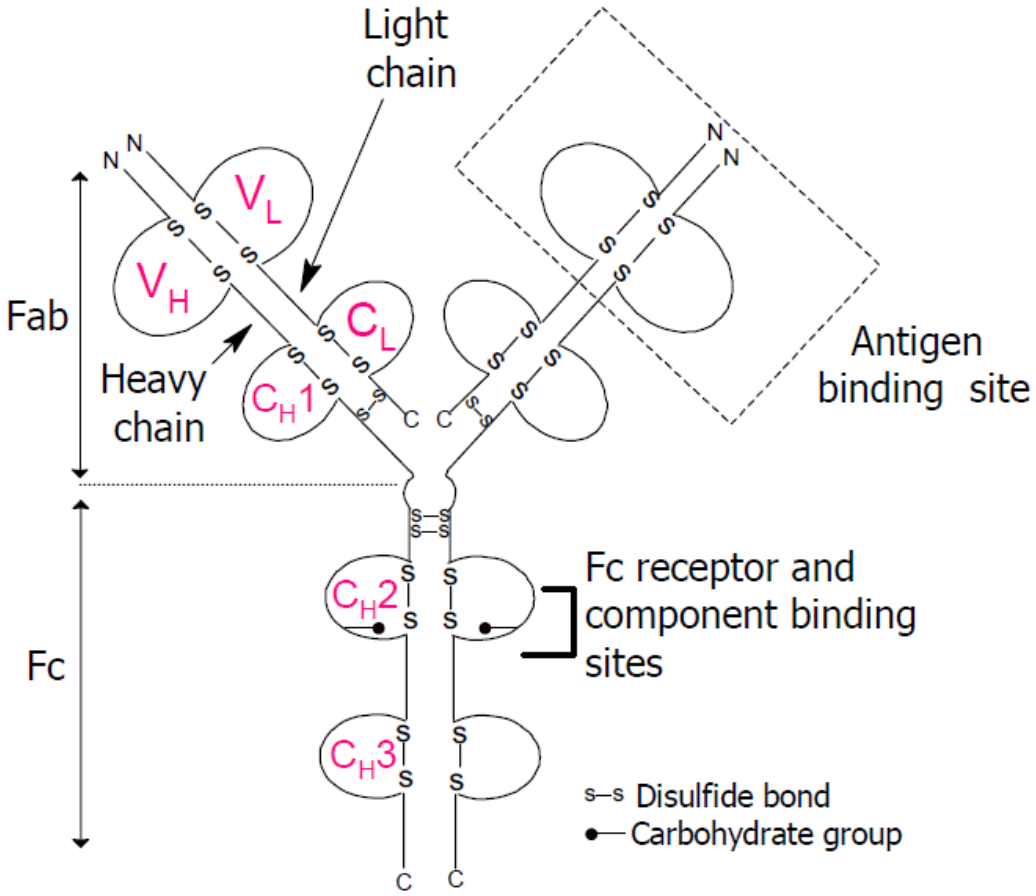

Figure 3.4: *Schematic structure of an antibody.*

An antigen is a molecule that can bind to an antibody. The region of the antigen that binds to an antibody is called epitope or antigenic determinant, where the corresponding part of the antibody is named paratope. Antibody- antigen binding is usually reversible and it is mainly based on non-covalent interactions, such as hydrogen bonds, Van der Waals and electrostatic forces. The nature of the interactions depends on the structure of the antibody, which varies with isotype, and on the structure of the antigen. The antibody can have either one (monovalent) binding interaction with an antigen, or multiple simultaneous (multivalent) interactions (Absolom and Van Oss, 1986).

The affinity is the measure of the strength of the binding of an antigen to an antibody. The reaction between an antibody and an antigen can be described by the following equation (3.1):

$$Ab + Ag \underset{K_d}{\overset{K_a}{\rightleftharpoons}} Ab\text{-}Ag \qquad K_a = \frac{[Ab\text{-}Ag]}{[Ab]\,[Ag]} \qquad \textbf{3.1}$$

Where [Ab] represents the antibody concentration, [Ag] the antigen concentrations and [Ab-Ag] the concentration of the antigen-antibody complex. k_a is the association rate constant and k_d is the dissociation rate constant. Generally, antibodies with association constants K_{ass} of 10^8 M^{-1} are used in immunochemical assays (Davies, 1994).

In this chapter, all the steps that have been followed to construct the affinity electrochemical biosensor are reported.

In particular, the following aspects will be discussed:

- Synthesis of the transducer, Fe(III)-Mimochrome IV Lys^3.
- Synthesis of the recognition element.
- Synthesis of the transducer-recognition element complex.
- Characterization of the transducer by voltammetric techniques:
    a. freely diffusing;
    b. immobilized on a gold electrode surface.
- Characterization of the transducer-recognition element complex covalently bound on a gold electrode by voltammetric techniques.
- Working test of the complete biosensor in the recognition of the analyte.

3.3 Synthesis of the transducer: Fe(III)-Mimochrome IV Lys^3

3.3.1 Peptide synthesis

The nonapeptide (Ac-Glu^1(OtBu)-Ser^2(tBu)-Lys^3(Boc)-Leu^4-His^5(Trt)-Ser^6(tBu)-Asn^7(Trt)-Lys^8(Mmt)-Arg^9(Pbf)-NH_2) was synthesized by the solid-phase method using the Fmoc strategy, using the following protocol:

1) Automatic peptide synthesis, consisting of the following steps:
- Deprotection of the α- Fmoc group
- α-carboxyl group Activation
- Coupling

2) Deprotection of the Lys ε-amino group.
3) Cleavage from the resin.

The most difficult step in the Mimochrome synthesis was the preparation of the nonapeptide fragment, protected at all functional groups, except at the ε-amino function of the Lys^8 residue.

The Sieber amide resin (Figure 3.5) was chosen because it allows the cleavage of the peptide from the resin, while leaving all the protecting groups on the side-chains, as well as on the N-terminal residue, intact.

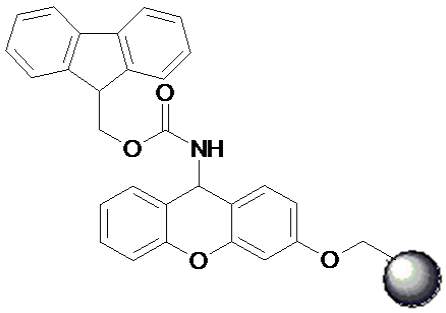

Figure 3.5*: Sieber amide resin.*

Another fundamental point was the choice of the protecting group on N-ε function of the Lys^8, since its cleavage conditions should be different than those used for the other side chain protecting groups. The Mmt protecting group was chosen, since it can be easily removed by repeated treatments with a solution containing 10% acetic acid and 20% trifluoroethanol (TFE) (v/v) in CH_2Cl_2, without affecting the other protecting groups.

The peptide was synthesized on a 0.2 mmol scale, using a 0.16 mmol/g resin substitution. At the end of the synthesis, when the peptide is still linked to the resin, the N-ε Mmt protecting group of the Lys^8 residue was removed with repeated treatments of a solution containing 10% acetic acid and 20% trifluoroethanol (TFE) in CH_2Cl_2. After this step, cleavage of the peptide from the

resin was achieved with a solution 1%TFA in DCM, and the fractions eluted from the resin were checked by TLC and pooled if they contained the desired product. The pooled fractions obtained from the cleavage reaction were evaporated under reduced pressure up to 5% of the volume. Ice-cold water was added to the residue and the mixture was cooled on ice to aid precipitation of the protected peptide. The product was filtered, washed several times with fresh water, and dried under vacuum to give the crude C-terminal peptide amide. The product was analyzed by RP-HPLC (Figure 3.6).

This analysis showed that the desired product was obtained in high purity. It was used in the next reaction without further purification.

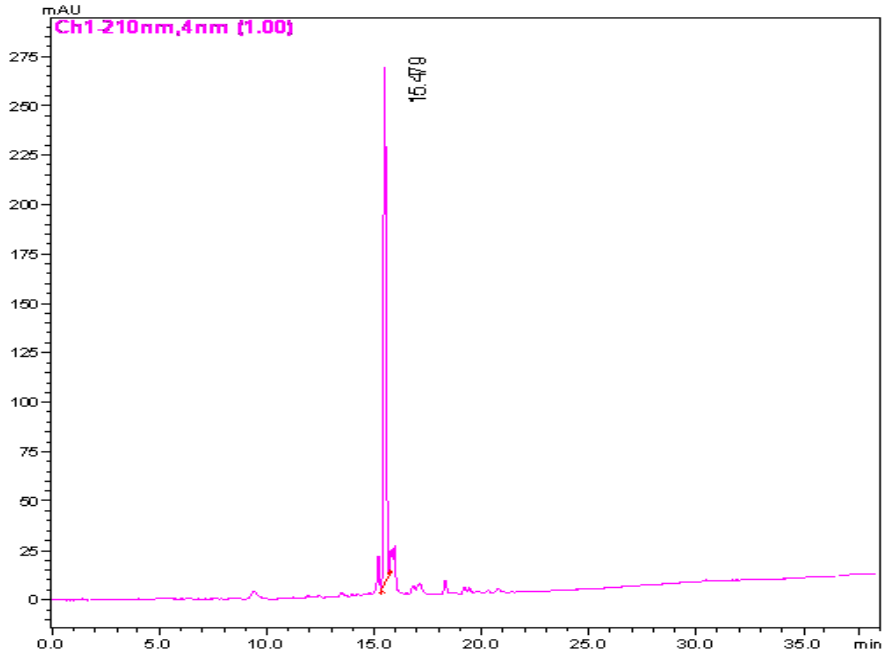

***Figure 3.6**: HPLC chromatogram of the Mimochrome IV Lys[3] peptide.*

3.3.2 Peptide-deuteroporphyrin coupling

The fully protected nonapeptide, except for the Lys^8 side chain, was coupled in solution to the deuteroporphyrin moiety. A small molar excess of the peptide (20%) was used. The porphyrin carboxyl groups were activated with HATU, which is one of the most efficient coupling reagent in peptide synthesis. In order to favour the formation of the bis-substituted deuteroporphyrin IX, the mixture of the activated porphyrin was slowly added to the nonapeptide solution. This procedure allows the activated porphyrin to be in the presence of excess of peptide. The completeness of the reaction was verified by RP-HPLC, following the disappearance of the peak with adsorption at 400 nm, corresponding to the free porphyrin.

The side chain protecting groups were removed by acid cleavage at 0 °C for 2.5 h. This treatment was performed twice. The reaction mixture was concentrated to approximately 1-2 mL. Extraction of the scavengers and precipitation of the crude product was achieved by addition of cold diethylether. The crude material was then dried in vacuo and purified by preparative RP-HPLC; the pooled fractions containing the desired product were

lyophilized.

The HPLC chromatogram of the pure product is reported in Figure 3.7a, showing the presence of a main peak at t_r 19,20 min.

The identity of the product was ascertained by mass spectrometry (Figure 3.7b (mass expected: 2753 u.m.a.; mass observed: 2751,91 ± 0.31 u.m.a.).

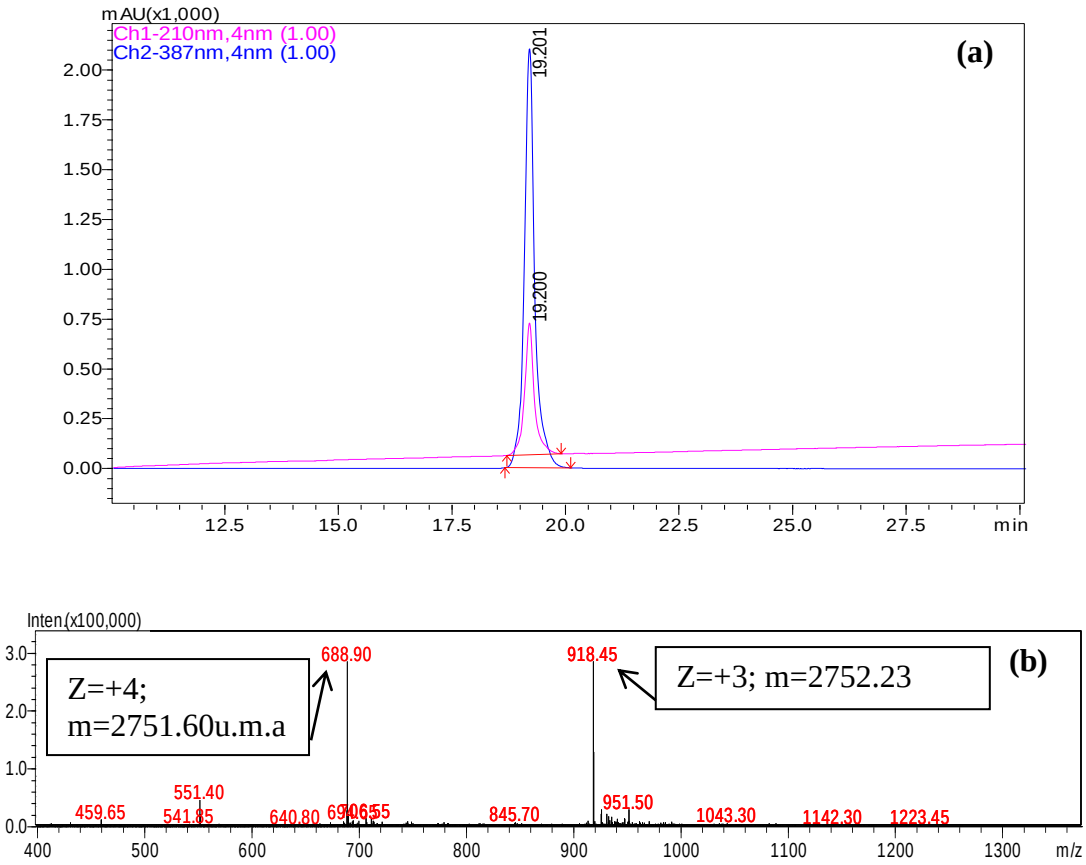

Figure 3.7 *(a) HPLC chromatogram and (b) mass spectrum of pure Mimochrome IV Lys[3] free base.*

3.3.3 Iron insertion

Basically, the reaction between the metal ion and a porphyrinic compound consists of *a)* the formation of the equatorial MN_4 plane; and *b)* the completion of the axial coordination sphere. However, certain considerations have to be made concerning the metalation procedure:

1. The solvent for the reaction should be able to dissolve the porphyrin as well as the metal compound, but without coordinating the metal ion with high affinity in order to avoid competition with the porphyrin.

2. The porphyrin has to be deprotonated in order to produce the negative P^{2-} ion that is present in the metal-porphyrin complex. The presence of strong acids in the reaction media will impede or even reverse metalation by shifting the protonation/ deprotonation equilibrium to the left.

$$H_4(P)^{2+} \rightleftharpoons H_3(P)^{+} \rightleftharpoons H_2(P) \rightleftharpoons H(P)^{-} \rightleftharpoons (P)^{2-}$$

3. To be able to react with the porphyrin macrocycle, the metal compound which carries the metal ion should dissociate, yielding an active (coordinatively unsaturated) species. Therefore, the metal complex should not be too stable otherwise it will not react with the porphyrin present in the reaction mixture. Other considerations are the availability, ease of handling, and solubility of the metal complexes in organic solvents.

4. After the incorporation of a metal ion with a positive charge greater than +2, it will bind one or more anions from the reaction medium to form a neutral species. Some metal ions prefer certain defined geometries, which require the addition of a neutral ligand (solvent, H_2O, O_2) to complete their coordination sphere.

The methods commonly used for the insertion of metal ions in the porphyrin macrocycle are listed below. The systems are characterized either by the solvent or the metal carrier used, depending on the more essential component. Since metalloporphyrins have characteristic UV-VIS properties, the reaction is usually monitored by spectrophotometry.

The acetate method

$$\mathbf{Zn(OAc)_2.xH_2O + H_2P} \xrightarrow[50\ ^oC]{\text{HOAc}} \mathbf{Zn(P) + 2\ HOAc + 2\ H_2O}$$

The acetate method includes all metalation reactions in which the protons of the porphyrin are transferred to acetate or propionate ions of the metal acetates/propionates. The solvents can be glacial acetic acid, or mixtures of $CHCl_3$/MeOH. This method can be applied to all divalent metals, except those which are unstable in acetic acid, and to some tri- and tetravalent metal ions. Often sodium acetate is added to further buffer the solution and to enhance deprotonation of the porphyrins. This method is considered the method of choice for the synthesis of manganese-porphyrin complexes.

The pyridine method

$$Mg(ClO_4)_2 + H_2P + 4\ Py \xrightarrow{Py} Mg(P)Py_2 + 2\ [PyH][ClO_4]$$

In those cases where the metalloporphyrin is very labile towards acids, the basic solvent pyridine is used for divalent metal ions. Pyridine is capable of dissolving the porphyrins as well as the metal salts, and the good complexing properties of pyridine allow the direct isolation of metalloporphyrin pyridinates. The same properties, however, impede the incorporation of metal ions with higher charges by forming pyridine complexes with the metal carrier, thus retarding the dissociation of the metal ion.

The dimethylformamide method

$$4\ CrCl_4 + 4\ H_2P + O_2 \xrightarrow[153\ ^oC]{DMF} 4\ Cr(P)Cl + 2\ H_2O + 4\ HCl$$

Weakly coordinating, high boiling oxygen-donor solvents such as dimethylformamide, tetramethylurea and sulfolan are excellent solvents for the metal carriers and porphyrins. The best results have been obtained with anhydrous metal chlorides (although they can be difficult to obtain and to handle), as the high boiling temperature forces the formed HCl to escape.

The metal carbonyl method

$$Re_2(CO)_{10} + H_2P \xrightarrow[195\ ^oC]{decalin} [Re(CO)_3]_2(P) + H_2 + 4\ CO$$

In metal carbonyls some of the CO groups may be eliminated, resulting in a coordinatively unsaturated species. This species acts as a Lewis acid, attacking the lone pairs of the porphyrin nitrogen atoms. This method is especially useful for the preparation of porphyrins containing the metals of groups VI to VIII.

Iron ion was inserted into Mimochrome IV Lys^3 according to the acetate method (Buchler, 1978).

Iron (II) acetate (10 molar excess) was added to a solution of pure Mimochrome IV Lys^3 free base in TFE/Acetic acid (6/4 v/v), and the reaction mixture was kept at 50°C for 2 h, refluxing under nitrogen. After 20 minutes, the reaction mixture started to turn slowly brown, and the HPLC chromatogram (Figure 3.8 a) showed the presence of a new peak at 18.32 min with the characteristic UV-visible spectrum of the iron (III) deuterophorphyrins at acidic pH, λ_{max} = 387 nm (Figure 3.8 b). The mass spectrum confirmed (Figure 3.8 c) the identity of the desired product (mass expected: 2807 u.m.a.; mass observed 2805.62 ± 0.18 u.m.a.).

The product was then purified by RP-HPLC and pooled fractions containing the pure product were lyophilized.

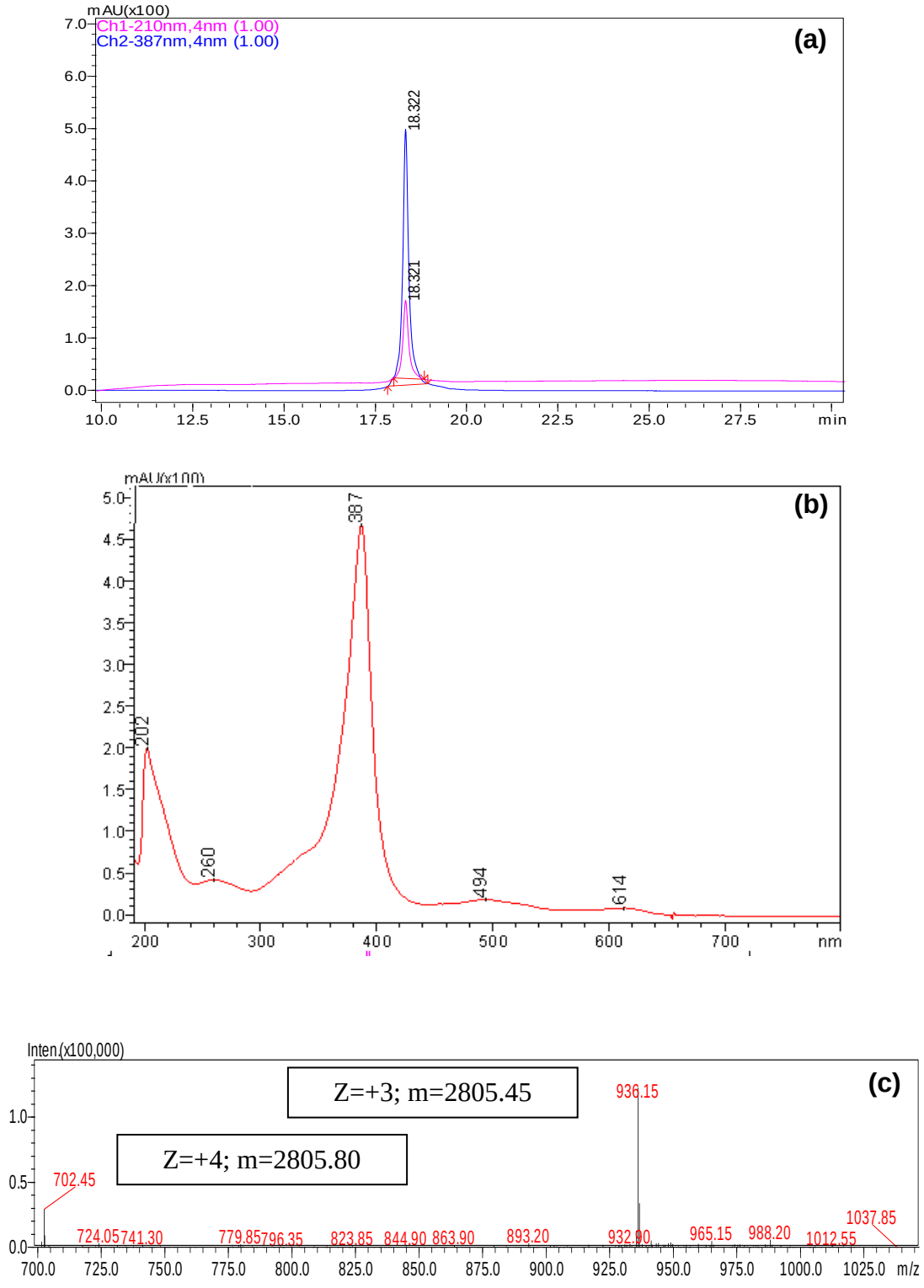

***Figure 3.8**: (a) HPLC chromatogram, (b) UV-vis and (c) mass spectra of pure Fe(III)-Mimochrome IV Lys[3].*

3.4 Synthesis of the recognition element: Ha_epitope

HA_epitope was synthesized by the solid-phase method using the Fmoc strategy. A cisteine residue was added at the N-terminus of the peptide sequence to simplify the functionalization protocol of Fe(III)-Mimochrome IV Lys3 with the epitope.

The peptide (Ac-Cys^{1}(Trt)-Tyr^{2}(tBu)-Pro^{3}-Tyr^{4}(tBu)-Asp^{5}(OtBu)-Val^{6}-Pro^{7}-Asp^{8}(OtBu)-Tyr^{9}(tBu)-Ala^{10}-NH_2) was synthesized following the protocol described in Chapter 3 (section 3.2.1) for Mimochrome IV Lys^{3} peptide.

In this case, the peptide was cleaved from the resin fully deprotected and purified via preparative RP-HPLC. The purity of the product was ascertained by analytical HPLC and MALDI-TOF spectrometry. Figure 3.9 reports the RP-HPLC chromatogram and the mass spectrum of the pure HA_epitope. The experimental molecular weight, 1268 uma, corresponds to the NA+ adduct (1245 + 23), and fully

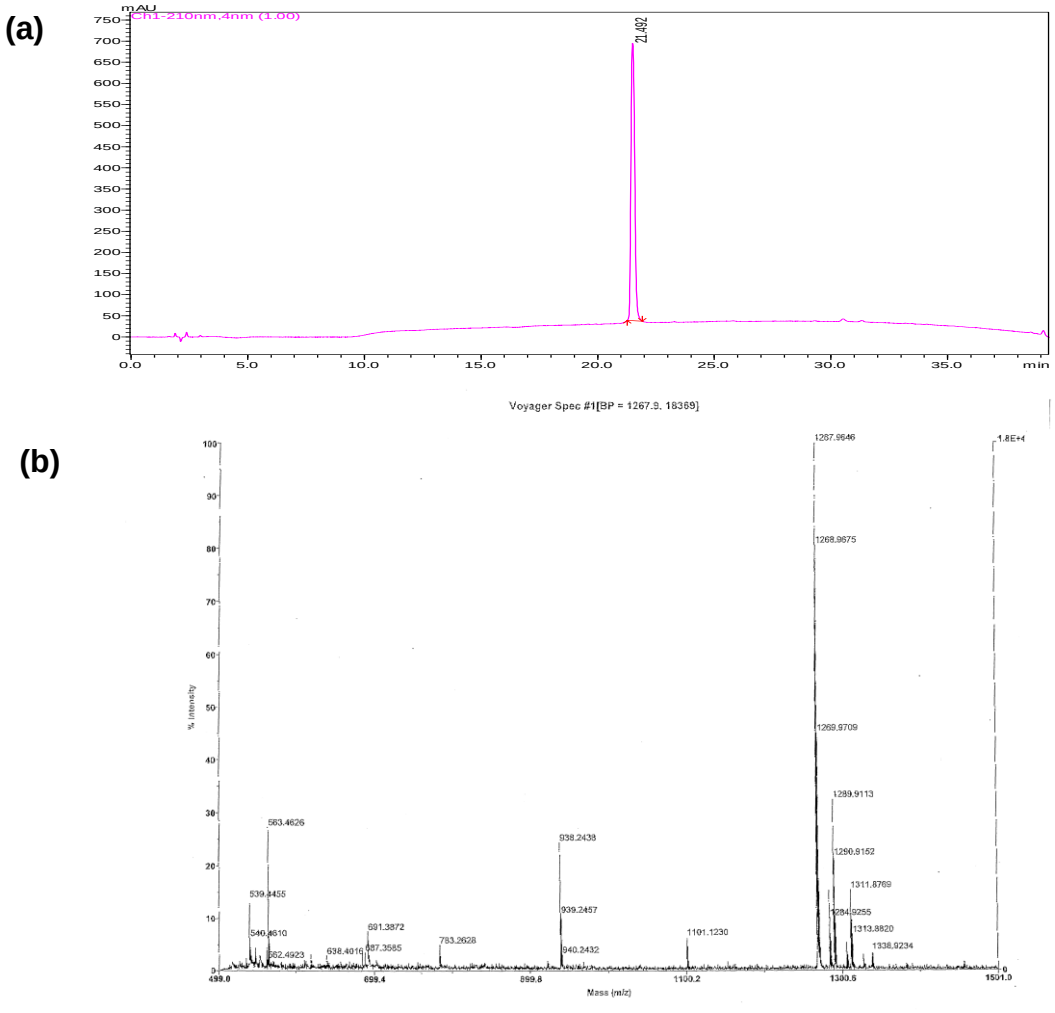

***Figure 3.9**: (a) HPLC chromatogram and (b) mass spectrum of pure HA_epitope.*

agree with the calculated mass (1245 uma), thus confirming the identity of the product.

3.5 Synthesis of the complex Fe(III)-Mimochrome IV Lys^3-Ha_ep

Fe-Mimochrome IV Lys^3 was modified with the HA_epitope utilizing the Sulfo-Succinimidyl-4-(N-maleimidomethyl)cyclohexane-1-carboxylate reagent (sulfo-SMCC, Figure 3.10), (Mattson et al., 1993).

Sulfo-SMCC is a water-soluble heterobifunctional crosslinker containing an N-hydroxysuccinimide (NHS) ester and a maleimide group. It allows covalent conjugation of amine- and sulfhydryl-containing molecules. It is often used to prepare antibody-enzyme and hapten-carrier protein conjugates in a two-step reaction scheme. NHS esters react with primary amines at pH 7-9 to form amide bonds, whereas maleimides react with sulfhydryl groups at pH 6.5-7.5 to form stable thioether bonds (Mattson et al., 1993). In aqueous solutions, NHS ester hydrolytic degradation is a competing reaction, whose rate increases with pH. The maleimide group is more stable than the NHS-ester group (Mattson et al., 1993). For these reasons, conjugations between Fe-Mimochrome IV Lys^3 and HA epitope was performed in two steps: first, the NHS-ester was coupled with the ε-amino group of one Lys of the heme-protein; in the second step, maleimide reaction with the N-terminal Cys of HA epitope was carried out.

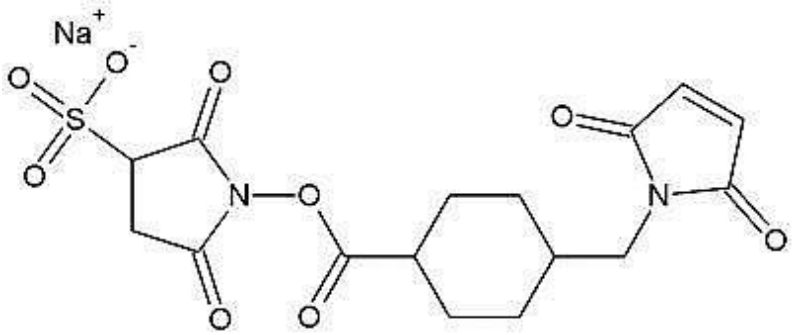

Figure 3.10 *Structure of sulfo-SMCC.*

3.5.1 Fe-Mimochrome IV Lys^3 functionalization with sulfo-SMCC

In order to obtain the mono-functionalized derivative, with only one Lys residue bound to the crosslinker, the reaction was carried out using a 1:1 molar ratio between Fe-Mimochrome IV Lys^3 and sulfo-SMCC, in 100 mM phosphate buffer, pH 7.2.

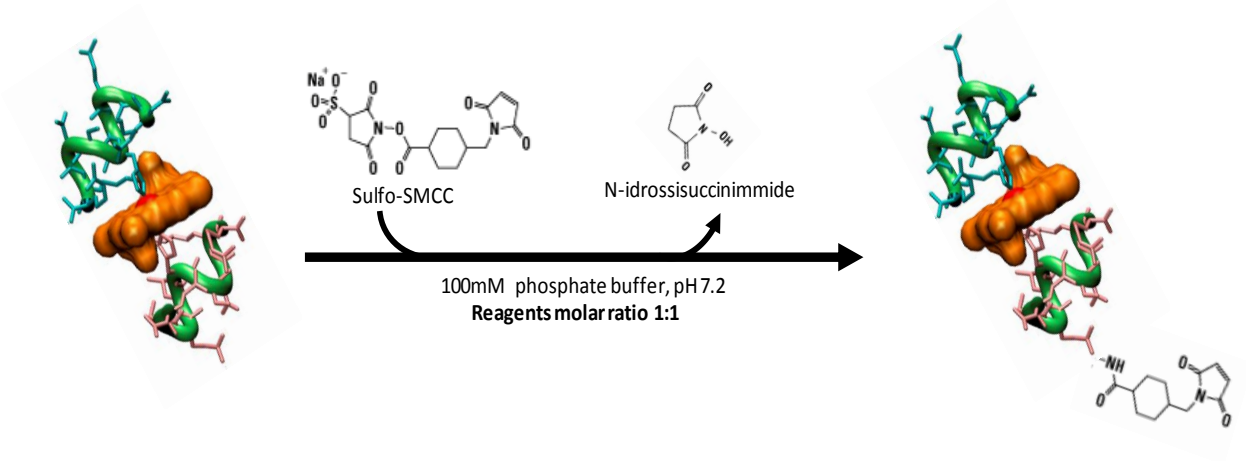

Figure 3.11 *First step of crosslinking reaction: activation of Fe(III)-Mimochrome IV Lys^3 with maleimido-group.*

After 1 hour, the proceeding of the reaction was controlled via LC-MS (Figure 3.12 a). The chromatogram shows the presence of two new peaks, at higher retention times respect to the starting molecule Fe(III)-Mimochrome IV Lys^3.

The analysis of the mass spectrum allowed the identification of the two peaks. The peak at t_r = 44.9 min corresponds to the unmodified Fe(III)-Mimochrome IV Lys^3, while the peaks at t_r = 48.6 min and t_r = 51.5 min correspond to the mono- and the bis-functionalized products, respectively.

Due to the high reactivity of the NHS moiety of the sulfo-SMCC towards primary amines, it is difficult to obtain only the desired, mono-substituted product. For this reason, the reaction was stopped, even though it was not completed. This is because further additions of sulfo-SMCC bring to the modification not only of the free Mimochrome, but also of the mono-functionalized species present in the reaction mixture. Figure 3.12c reports the mass spectrum of the mono-substituted product (mass expected: 3026 u.m.a., mass observed: 3024.12 ± 0.32 u.m.a.).

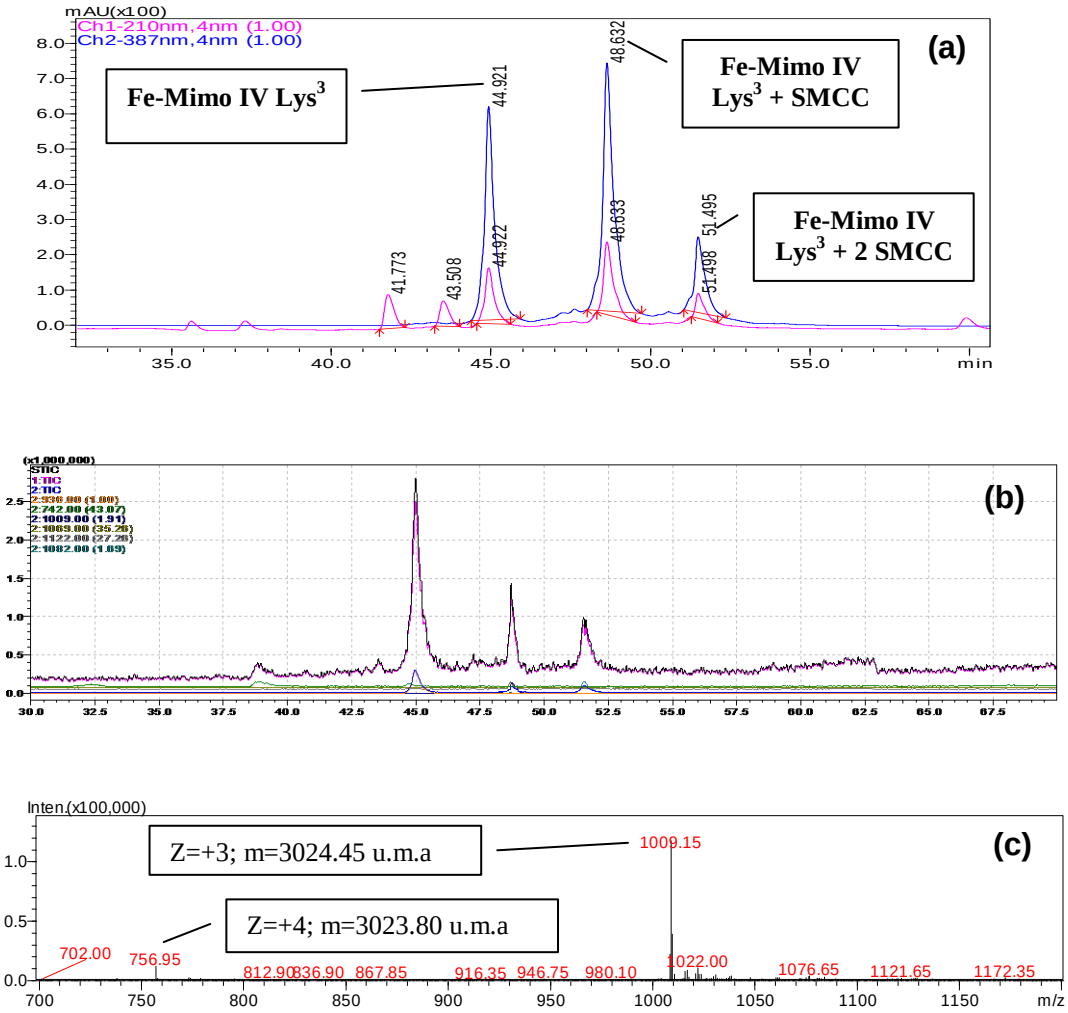

Figure 3.12 *(a) HPLC chromatogram, (b) mass chromatogram of the reaction mixture, and (c) mass spectrum of peak at* t_r *= 48.6 min.*

3.5.2 Fe-Mimochrome IV Lys^3 functionalization with HA_ep

The Fe(III)-Mimochrome IV Lys3 mono-sulfo-SMCC was used without further purification. HA_ep was added to the reaction mixture in a molar ratio 3.5 to the total Fe(III)-Mimochrome IV Lys^3.

The mixture was allowed to react for 2 hours at room temperature, under continuous stirring. The proceeding of the reaction was followed by LC-MS (Figure 3.14). After two hours, the analysis of the chromatogram and the mass spectra showed the complete functionalization of the Fe(III)-Mimochrome IV Lys^3-SMCC with HA_epitope.

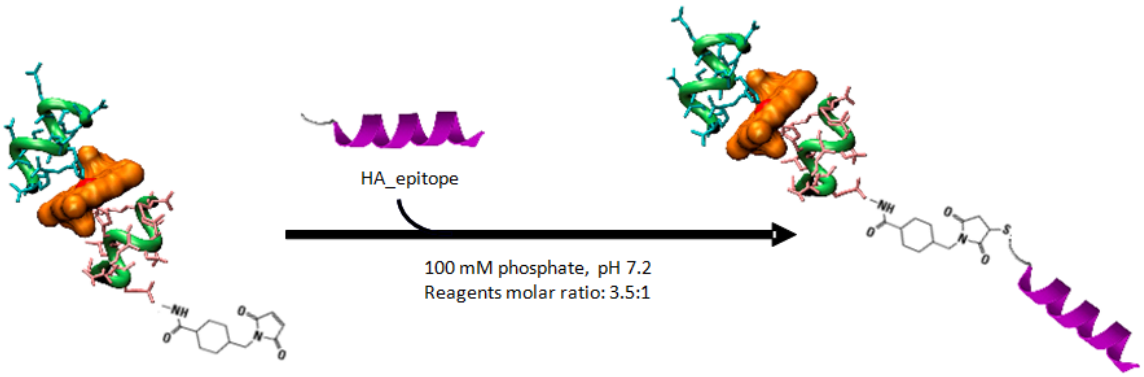

Figure 3.13: *Second step of crosslinking reaction: modification of Fe(III)-Mimochrome IV Lys^3-SMCC with HA_epitope.*

In the electrospray process a population of variably charged ions are generated (Figure 3.14 b), depending on the number of protonation sites in the peptide sequence.

The mass spectrum of the peak at t_r = 44.789 min (Figure 3.13 c) corresponds to the unmodified Fe (III)-Mimochrome IV Lys^3 (mass expected: 2808 u.m.a., mass observed: 2806.62 ± 0.42 u.m.a.).

The mass spectrum of the peak at t_r = 43.762 min (Figure 3.14 d) corresponds to HA_epitope functionalized with a molecule of sulfo-SMCC (mass expected: 1482 u.m.a., mass observed: 1482.80 u.m.a.).

The mass spectrum of the peak at t_r = 48.815 min (Figure 3.14 e) corresponds to the final desired product (mass expected: 4272 u.m.a., mass observed: 4271 u.m.a.).

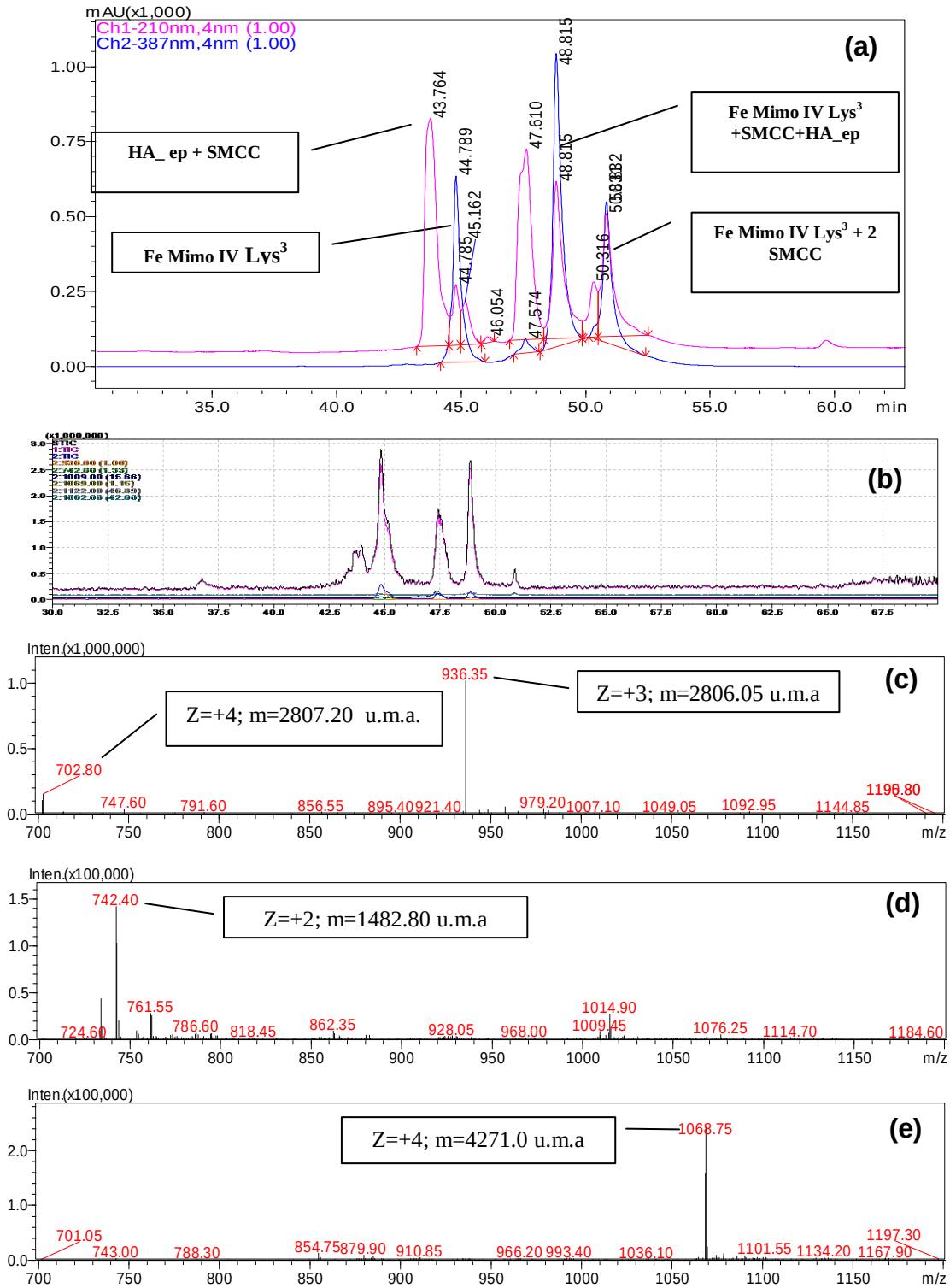

Figure 3.14: *(a) HPLC chromatogram, (b) mass chromatogram of the reaction mixture, and mass spectra of: (c) peak at t_r = 44.789 min, (d) peak at t_r = 43.762 min, (e) peak at t_r = 48.815 min.*

The reaction mixture was then purified by preparative HPLC, and the fractions corresponding to the desired product were collected and lyophilized. Figure 3.15 shows the chromatogram and the mass spectrum of the pure product (mass expected: 4272 u.m.a., mass observed: 4270.50 ± 0.12 u.m.a.).

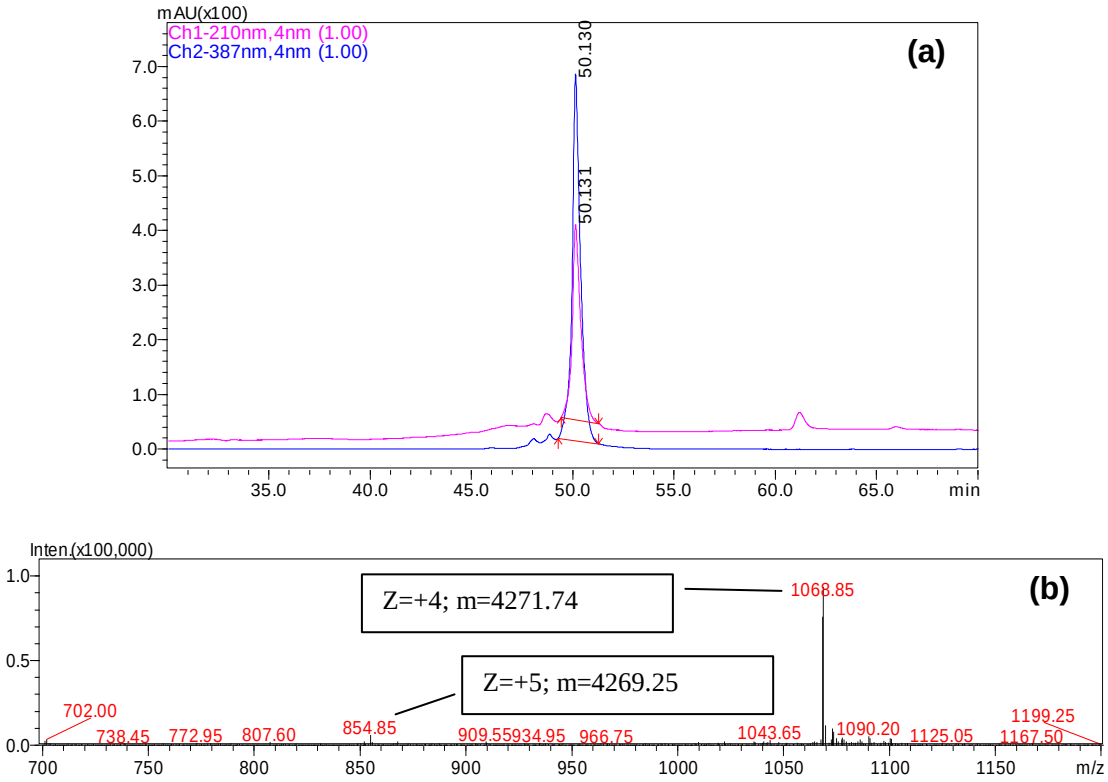

***Figure 3.15**: (a) HPLC chromatogram, and (b) mass relative to the pure Fe(III)-Mimochrome IV Lys^3-HA_ep conjugate.*

3.6 Voltammetric analysis of Fe(III)-Mimochrome IV Lys[3]

3.6.1 Voltammetric methods

The common characteristic of all the voltammetric techniques is that they involve the application of a potential (E) to an electrode and the monitoring of the resulting current (i) flowing through the electrochemical cell (Kounaves, 1997). In many cases the applied potential is varied or the current is monitored over a period of time (t). Thus, all voltammetric techniques can be described as some function of E, i, and t. They are considered active techniques (as opposed to passive techniques such as potentiometry) because the applied potential forces a change in the concentration of an electroactive species at the electrode surface by electrochemically reducing or oxidizing it.

The analytical advantages of the various voltammetric methods include:

1. excellent sensitivity with a very large useful concentration ranges (10^{-12} to 10^{-1} M), for both inorganic and organic species;
2. large number of useful solvents and electrolytes;
3. wide range of useful temperatures;
4. rapid analysis times (seconds);
5. simultaneous determination of several analytes.

In addition, these techniques are supported by a well-developed theory, leading to the possibility to determine kinetic and mechanistic parameters, the ability to reasonably estimate the values of unknown parameters, and the ease with which different potential waveforms can be generated and small currents measured.

A sensitive, electroanalytical method for detection of analytes in solution or on the surface of an electrode is Cyclic Voltammetry (CV) (Kounaves, 1997). It is perhaps the most effective and versatile electroanalytical technique available for the study of redox systems. It enables the electrode potential to be rapidly scanned in search of redox couples. Once located, a couple can then be characterized from the potentials of peaks on the cyclic voltammogram and from changes caused by varying the scan rate. CV is often the first experiment performed in an electrochemical study. It is rarely used for quantitative determinations, but it is widely used for the study of redox processes, to determine

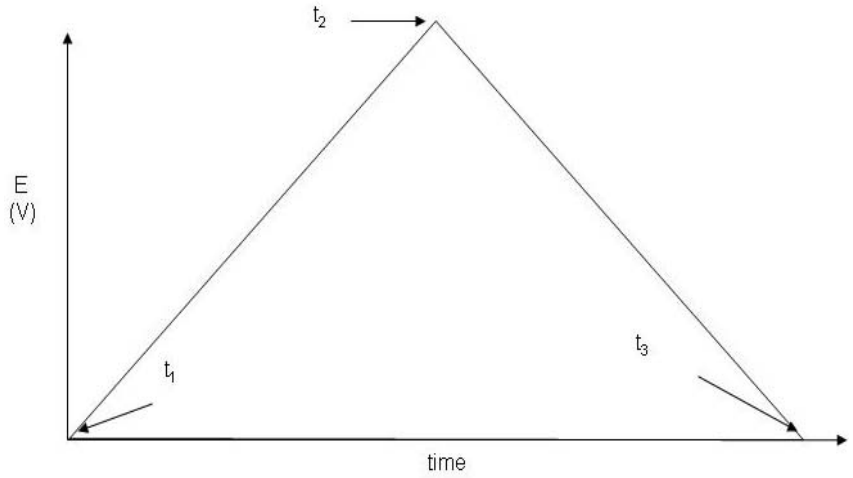

Figure 3.16: *Triangular waveform used in cyclic voltammetry.*

redox potentials, reaction mechanisms, chemical concentrations and kinetic rate constants. Cyclic voltammetry uses a triangular waveform to linearly ramp the potential through time and measuring the current as a function of the applied potential. Figure 3.16 is an example of the triangular waveform used for cyclic voltammetry. The potential is varied linearly with time, and the rate at which the potential is varied is called the sweep rate. A cyclic voltammetry experiment starts by scanning from t_1 to t_2 in a linear fashion. The scan then reverses direction back to the original potential at t_3. The detection limit of this technique is about $1*10^{-5}$ M.

Square-Wave Voltammetry (SWV) (Wang, 1994) is a large-amplitude differential technique in which a waveform composed of a symmetrical square wave, superimposed on a base staircase potential, is applied to the working electrode (Figure 3.17).

The net current, i_{net}, is obtained by taking the difference between the forward and reverse currents ($i_{for} – i_{rev}$) and is centered on the redox potential. The peak height is directly proportional to the concentration of the electroactive species and detection limits as low as $10^{–8}$ M are possible.

Square-wave voltammetry has several advantages: excellent sensitivity and the rejection of background currents, and speed. This speed, coupled with computer control and signal averaging, allows for experiments to be performed repetitively and increases the signal-to-noise ratio. Applications of square-wave voltammetry include the study of electrode kinetics, catalytic homogeneous

chemical reactions, determination of some species at trace levels, and its use with electrochemical detection in HPLC.

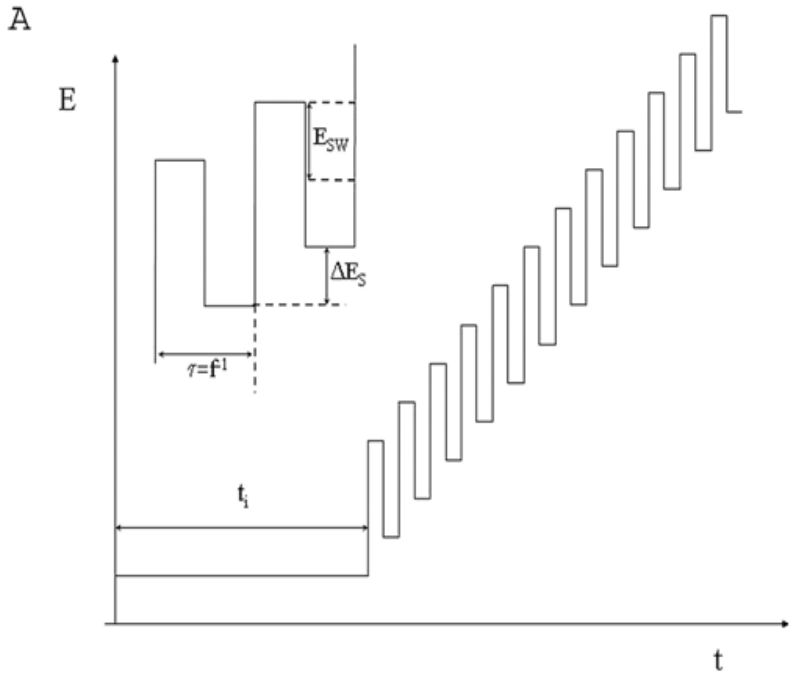

Figure 3.17: *Potential time waveform for square-wave voltammetry and definition of the different parameters: E_{sw} is the square-wave amplitude, ΔE_s the staircase step height, $t_p = \tau/2$ the pulse width.*

3.6.2 The electrochemical cell

The basic components of a modern electroanalytical system for voltammetry are a potentiostat, a computer, and the electrochemical cell. A typical electrochemical cell consists of the sample dissolved in a solvent, an ionic electrolyte, and three (or sometimes two) electrodes: a working (indicator) electrode, a reference electrode, and usually a counter (auxiliary) electrode. While the working electrode is the electrode at which the reaction of interest occurs, the reference electrode provides a stable potential (indipendent of the sample composition), against which the potential of the working electrode is compared. An inert conducting material, such as a platinum wire, is used as the current carrying auxiliary electrode.

Figure 3.18 : *The three electrodes electrochemical cell used for the measurements.*

The sample holders come in a variety of sizes, shapes, and materials. The type used depends on the amount and type of sample, the technique, and the analytical data to be obtained. The material of the cell (glass, Teflon, polyethylene) is selected to minimize reaction with the sample. An accurate temperature control is generally achieved by immersing or jacketing the cell in a constant temperature bath.

In Figure 3.18 is shown the electrochemical cell used for all the electrochemical measurements. The electrodes employed are listed below:

Working electrode: Glassy carbon (GC, 3mm dia.) or Gold (Au, 1.6 mm dia.)
Reference electrode: Ag | AgCl | NaCl 3 M
Auxiliary electrode: Platinum wire (Pt)

Prior to each measurement, the electrolytic solution was bubbled with argon for about 15-20 minutes to get rid off of any dissolved oxygen. During the measurement, the electrochemical cell was blanketed with argon. All the

measured potentials are measured against the Ag/AgCl 3 M NaCl reference electrode, the E°' are also reported against SHE.

3.6.3 Square wave and cyclic voltammetry of freely diffusing Fe(III)-Mimochrome IV Lys^3

The Fe^{III}/Fe^{II} reduction potential (E˚') of the diffusing Fe(III)-Mimochrome IV Lys^3 was determined by square-wave and cyclic voltammetry. All the measurements were performed using a glassy carbon electrode, at 25 C˚. A 0,1 M Fe(III)-Mimochrome IV Lys^3 solution in a 10 mM phosphate buffer at pH 7, 100 mM $NaClO_4$ was used. The sample volume in the electrochemical cell was 1 ml.

Figures 3.19, 3.20 and 3.21 report the square-wave voltammograms, for both the cathodic and the anodic scans, recorded at different scan rates.

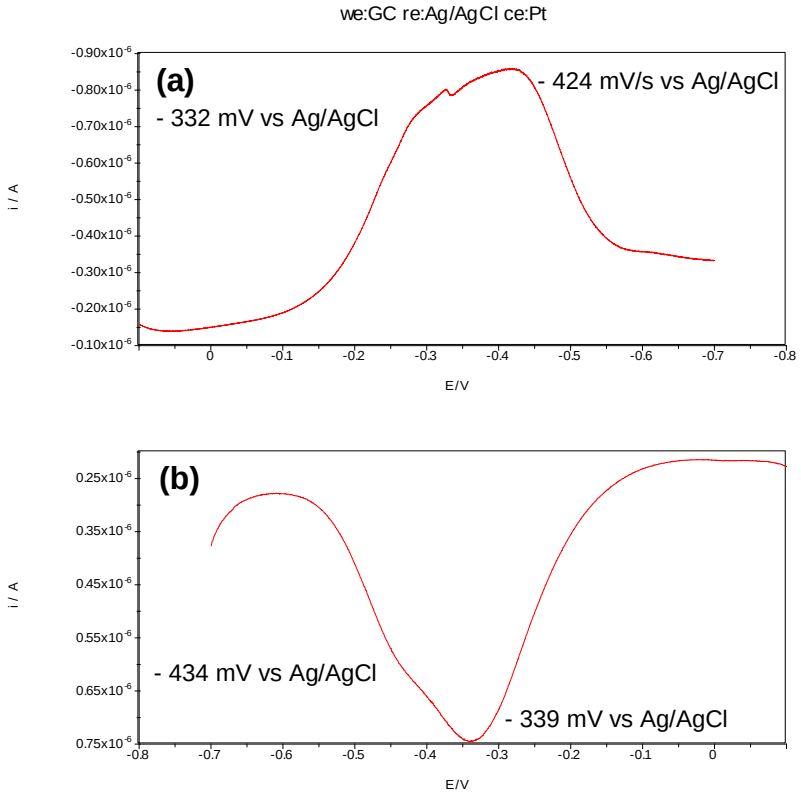

Figure 3.19: *Square-wave voltammograms of Fe(III)-Mimochrome IV Lys^3 at 3.7 mV/s on a glassy carbon electrode. (a) cathodic scan, (b). anodic scan.*

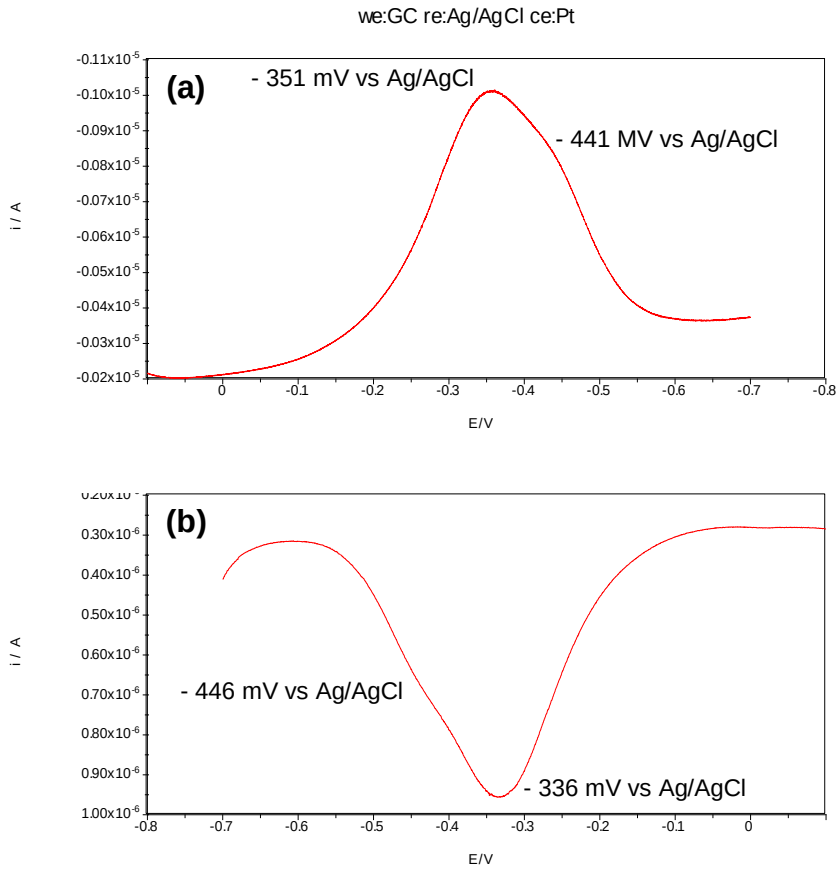

Figure 3.20 : *Square-wave voltammograms of Fe(III)-Mimochrome IV Lys*[3] *at 4.8 mV/s on a GC electrode. (a) cathodic scan, (b) anodic scan.*

Voltammograms recorded at low scan rate (3.7 mV/s) showed broad peaks in both scans, suggesting the presence of two signals at different potential. Increasing the scan rate (4.8 mV/s) the peaks in both the anodic and cathodic scans became sharper (Figure 3.20). At high scan rate (37.5 mV/s) both scans showed a single peak, with a well-defined voltammetric wave (Figure 3.21).

This finding is indicative of the electron transfer of a single species. The cathodic and anodic peaks are located at -350 and -333 mV, respectively. Interestingly, the peak current intensity ratio (Ip,c/Ip,a) is ≈1, indicating that Fe(III)-Mimochrome IV Lys[3] molecule undergoes a reversible electrochemical reaction (Jiang et al., 1997). The formal potential is obtained as below:

$E°' = (Ep^{cat} + Ep^{an})/2 = -340$ mV vs Ag/AgCl

E°' of the Ag/AgCl 3 M NaCl reference electrode = +209 mV vs SHE

E°'= -340 mV + 209 mV = -131 mV vs SHE

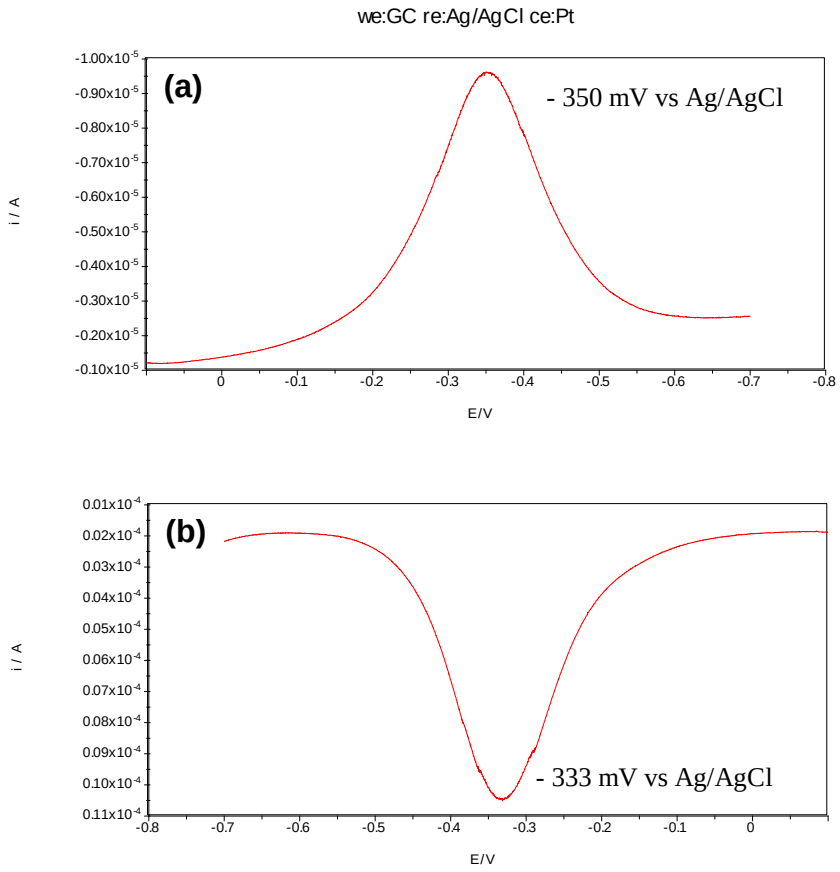

Figure 3.21 : *Square-wave voltammograms of Fe(III)-Mimochrome IV Lys*[3] *at 37.5 mV/s on a GC electrode. (a) cathodic scan, (b) anodic scan.*

This value is in good agreement with previous reported for other Mimochrome molecules (Lombardi et al., 2003; Ranieri et al., 2010).

In the voltammograms obtained at lower scan rates, the broad peak observed in both cathodic and anodic scans can be related to the presence of a second species, absorbed on the electrode surface, that contributes to the total signal registered. In the voltammograms recorded at 3.7 mV/s is clearly visible a second peak, both in cathodic and in the anodic scans, with the maximum intensity values located at -424 mV (Fig. 3.19 a) and -434 mV (Fig. 3.19 b), respectively. This peak can be assigned to the molecule adsorbed on the electrode surface, a common

phenomenon observed in the direct electrochemical measurements of heme-proteins and models (Chattopadhyay and Mazumda, 2000; Hu, 2001). In this specific case, it is likely that the adsorption of Fe(III)-Mimochrome IV Lys^3 on the surface of the glassy carbon electrode causes a major exposition of the heme group to the solvent. As a consequence, the redox potential of the adsorbed species is more negative than the E°' value for the freely diffusing protein in solution.

$E°' = (Ep^{cat} + Ep^{an})/2 = -444$ mV vs Ag/AgCl

E°'= -444 mV + 209 mV = -234 mV vs SHE

This hypothesis is supported by the finding that the E°' value measured for the adsorbed species is in a good agreement with the values obtained for some iron-porphyrins (e.g. Fe-porphyrin IX- bis imidazole -235 mV vs SHE, Fe-mesoporphyrin bis imidazole -285 mV vs SHE)(Kassner, 1972).

Results of cyclic voltammetry measurements are consistent with the SWV observations. Figure 3.22 reports the cyclic voltammograms obtained at three different scan rates: 0.025 V/s (Figure 3.22 a), 0.5 V/s (Figure 3.22 b) and 5 V/s (Figure 3.22 c).

The cyclic voltammogram registered at the highest scan rate (Figure 3.22 c) consists of a single, well-defined signal arising from the quasi-reversible one-electron reduction-oxidation process of the heme-iron of the freely diffusing molecule.

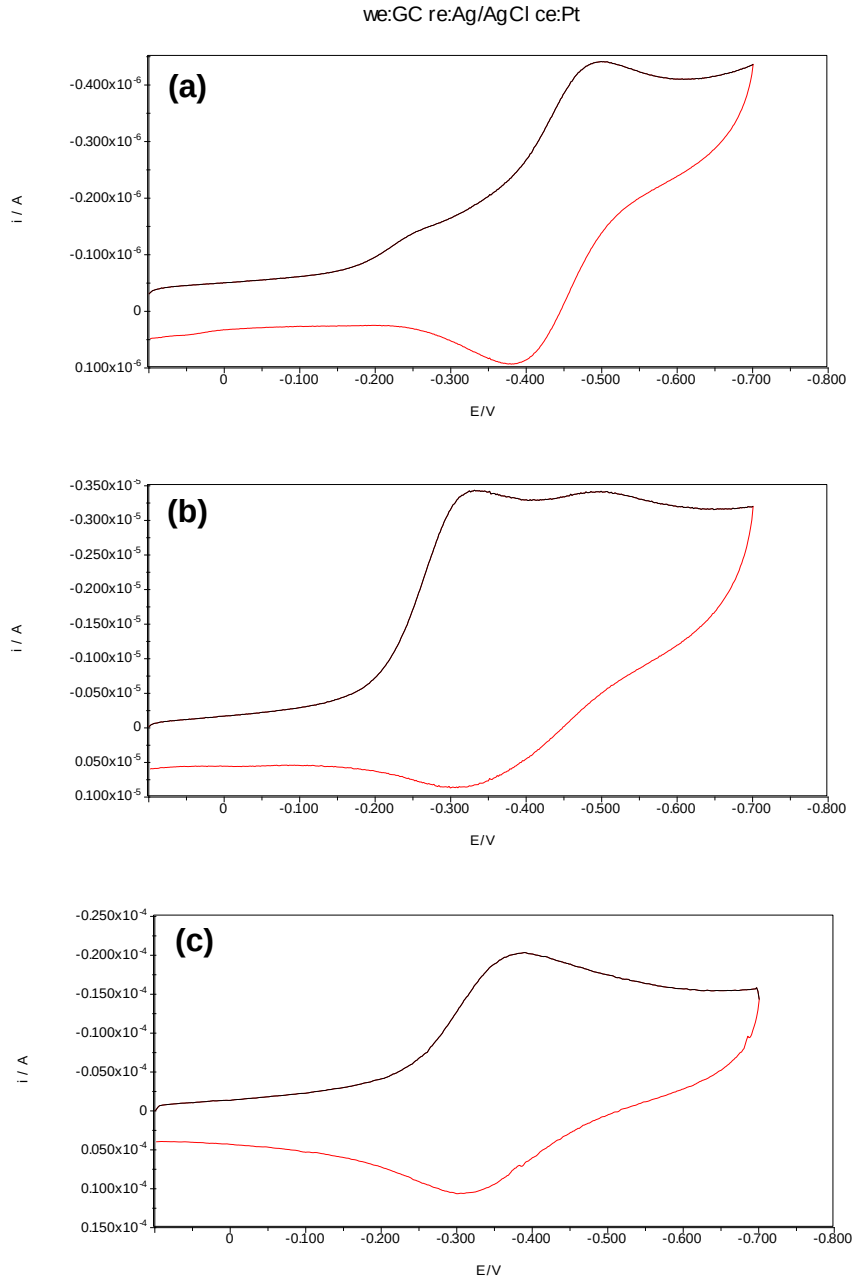

Figure 3.22 : *Cyclic voltammograms of diffusive Fe(III)-Mimochrome IV Lys*[3] *at different scan rates on a glassy carbon electrode. (a) 0.025 V/s, (b) 0.5 V/s, (c) 5 V/s.*

The cathodic and anodic peaks are located at -372 and -306 mV, respectively. The peak potential separation is ≈ -66 mV, in good agreement with the expected theoretical value of -59 mV, for a reversible mono-electronic process. This indicate that the Fe(III)-Mimochrome IV Lys[3] molecules possess reversible electrochemical behavior. The formal potential is -339 mV vs Ag/AgCl and -130 mV vs SHE. This

value is in good agreement with the one obtained by SWV experiments, and it represents the redox potential of the freely diffusing molecule.

Similarly to the finding observed in SWV measurements, at lower scan rate it is possible to observe the adsorption phenomenon. In fact, in the voltammogram registered at 0.025 V/s (Figure 3.22 a), a species with a more negative redox potential is particularly evident. The E°' value of - 234 mV is the same measured for the adsorbed molecule in SWV experiments. In the scan performed at 0.50 mV/s it is possible to note the presence of both the diffusing and the adsorbed species.

Analysis of freely diffusing Fe(III)-Mimochrome IV Lys^3 confirmed that this heme-protein model is able to exchange electrons with the electrode surface in a reversible process. Therefore the immobilization of the molecule on a gold electrode via covalent binding was carried out, in order to study its electrochemical behavior once anchored on a surface.

3.7 Immobilization of Fe(III)-Mimochrome IV Lys^3 on the electrode surface

3.7.1 Immobilization method

One of the crucial steps in the development of third generation electrochemical biosensors is the proper immobilisation of the electron transfer element on the electrode surface, since its electron transfer activity must be preserved (Collings and Caruso, 1997). In fact, for heme-proteins, which exhibit direct electron transfer to the electrode surface, the orientation, distribution, organization and proximity of the heme-group respect to the electrode surface are parameters of outmost relevance.

Several strategies have been employed to immobilize molecules on electrodes, such as physical adsorption (Yaropolov et al., 1996), covalent or electrostatic attachment to electrochemically modified surfaces (Quan and Shin, 2004) and to self-assembled monolayers (SAMs) (Gooding et al., 2001; Chaki and Vijayamohanan, 2002).

The self-assembly method for the anchoring of enzymes or other bio-molecules displays a number of advantages relatively to other approaches, such

as high reproducibility, molecular level control (e.g. distribution on the surface), vicinity to the surface, which allows direct electron transfer (Gooding et al., 2001).

The most studied systems make use of the strong affinity between thiols or disulphides and gold substrates (Ulman, 1996; Schreiber, 2004; Love et al., 2005). Some biomolecules, containing thiol or disulphide groups in their structure, may spontaneously bind to gold surfaces without any functionalization. However, the main reported routes (Hyung et al., 1997) relate to the chemical modification of bio-molecules through the introduction of terminal thiol groups (Hegner et al., 1993), or the formation of SAMs containing specific groups with subsequent non-covalent (Hyung et al., 1997) or covalent (Gooding et al., 2001) attachment of biomolecules.

When the alkanethiol has proper functionalities, such as carboxylic acid or amine, chemical anchoring of the biomolecule to the SAM can be realized through the formation of peptide bonds. Nevertheless, the success of the chemical reaction involves the activation of either the amine or carboxylic acid moieties in the SAMs, through the use of appropriate coupling reagents (Quan and Shin, 2004; Disley et al., 1998; Mirsky et al., 1997), such as 1-ethyl-3-(dimethylaminopropyl)carbodiimide hydrochloride / N-hydroxysuccinimide (EDC/NHS).

In the present work, the immobilisation strategy employed involves the modification of a gold electrode surfaces with a SAM of 11-mercaptoundecanoic acid (11-MUA). The carboxylic group at the end of the alkanethiol is activated as hydroxysuccinimide ester, which reacts with primary amines, such as the ε-amino group of the free Lys residue on one of the peptide chains of Fe(III)-Mimochrome IV Lys^3.

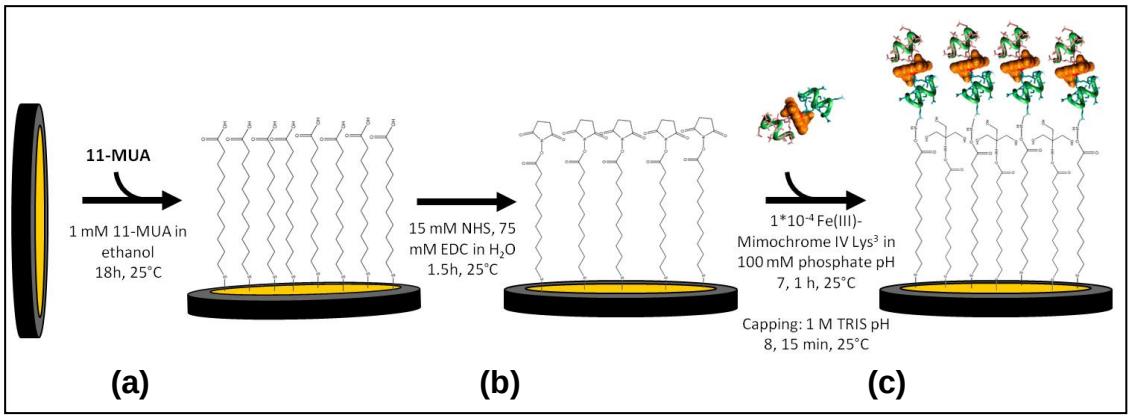

Figure 3.23: *Representation of the steps of the electrode surface modification: (a) gold coating with 11-MUA, (b) activation of the carboxylic groups with EDC/NHS and (c) Fe-Mimochrome IV Lys3 coupling, with final capping with Tris solution.*

3.7.2 Electrode surface modification with a SAM of 11-MUA

The monolayer of 11-mercaptoundecanoic acid was formed by exposing clean gold electrodes to a solution of freshly prepared 1.0 mM 11-MUA in ethanol (Figure 3.23, step a). The electrodes have an exposed working surface of 1.6 mm. The gold electrodes were allowed to sit for 18 hours at room temperature in the thiol solution, to obtain maximum monolayer packing. Then, they were removed from the SAM solution and thoroughly rinsed with ethanol.

SAM formation was ascertained by studying the electron-transfer reaction of a redox probe, the $K_3Fe(CN)_6$, on the SAM-modified surfaces, by taking advantage

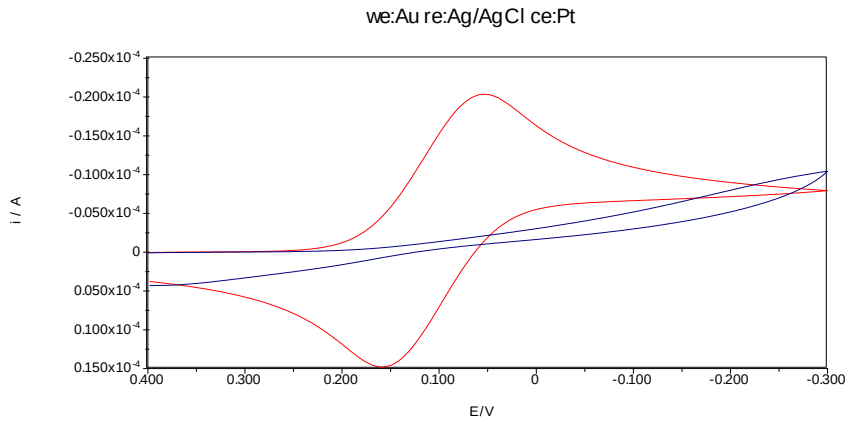

Figure 3.24: *Cyclic voltammograms of freely diffusive $K_3Fe(CN)_6$ on bare (red line) and SAM coated (blue line) gold electrode.*

of the ability of alkanethiol SAMs to block the electron transfer between the metal surface and a redox species in solution (Garcìa-Raya et al., 2008).

Figure 3.24 shows cyclic voltammograms for the bare gold and a SAM-modified electrode in 10 mM $K_3Fe(CN)_6$ in ethanol/10 mM $NaClO_4$ (50/50 v/v), at a potential scan rate of 0.05 V/s. The cyclic voltammogram of the bare gold electrode shows a CV with a shape typical of a diffusion-controlled reversible redox couple (Figure 3.24, red line). On the opposite, in the presence of the SAMs the electron transfer for the Fe^{3+}/Fe^{2+} couple is totally absent (Figure 3.24, blue line), thus suggesting the formation of a monolayer which blocks the redox reaction. The 11-MUA SAM is completely formed after 18 h of modification time, according to literature data (Garcìa-Raya et al., 2008).

3.7.3 SAM activation and Fe(III)-Mimochrome IV Lys^3 anchoring

In order to couple proteins via their amino groups, typically the 1-ethyl-3-(3-dimethylamino-propyl)carbodiimide and N-hydroxysuccinimide procedure is used to activate a carboxylic group on the surface (Cass and Ligler, 1998).

The SAM coated electrode was immersed in a solution of EDC 75 mM / NHS 15 mM for 1.5 hours at room temperature (Figure 3.23, step b), then removed from the activating solution and thoroughly rinsed with deionized water (Patel et al., 1997). The activated electrode surface was immediately immersed in a 0.1 M Fe(III)-Mimochrome IV Lys^3 solution in 0.1 M phosphate buffer, pH 7, for 1 hour at room temperature.

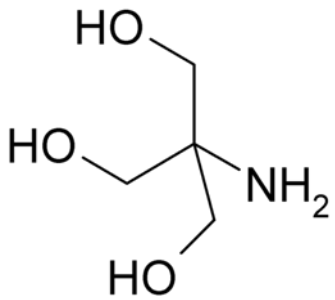

Figure 3.25: *Structure of tris(hydroxymethyl)amino methane.*

After covalent coupling, the surface was rinsed with deionized water to remove unreacted protein molecules. A 1 M solution of Tris (2-Amino-2-hydroxymethyl-propane-1,3-diol) buffer, pH 8, was used to quench the activated carboxyl groups of 11-MUA, in order to eliminate further chemical reaction with free amines (Balasubramanian et al., 2006). Electrodes were immersed in Tris solution for 15 minutes, then rinsed with deionized water and stored into phosphate buffer solution till the electrochemical measurements have been performed.

3.7.4 Square wave and cyclic voltammetry of Fe(III)-Mimochrome IV Lys^3 immobilized on the gold electrode

The Fe^{III}/Fe^{II} reduction potential (E°') of the immobilized Fe(III)-Mimochrome IV Lys^3 was determined by square-wave and cyclic voltammetry. All measurements were performed by deeping the Fe(III)-Mimochrome IV Lys^3 coated electrode in 1 ml of 10 mM phosphate buffer at pH 7, at 25 °C.

Figure 3.26 shows the square wave voltammograms, for the cathodic and anodic curves, of the immobilized molecule. The scans were performed at a scan rate of 37.5 mV/s.

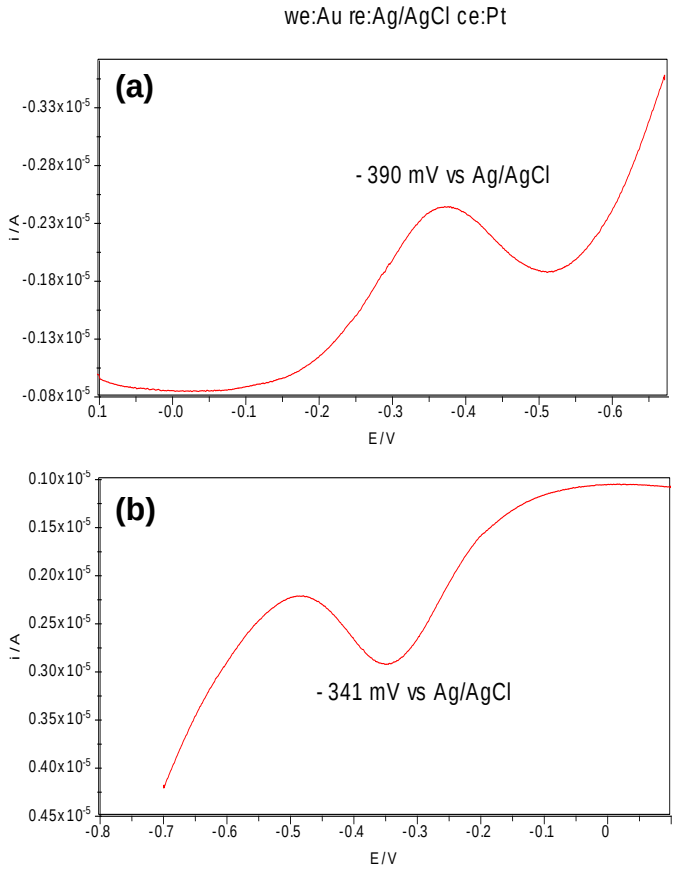

Figure 3.26 : *Square-wave voltammograms of Fe(III)-Mimochrome IV Lys^3 immobilized on a SAM coated gold electrode, at 37.5 mV/s, (a) cathodic scan, (b) anodic scan.*

The covalently immobilized Fe(III)-Mimochrome IV Lys[3] exhibits a pair of well-defined redox peaks located at - 390 and - 341 mV/s, respectively, with a E°' = - 365 mV vs Ag/AgCl and - 156 mV vs SHE. The average ratio of cathodic and anodic peak current intensities is 0.85, this value remains constant even when scans at different scan are registered. This finding clearly demonstrates a reversible electrode reaction and also excludes involvement of dioxygen in the reduction process.

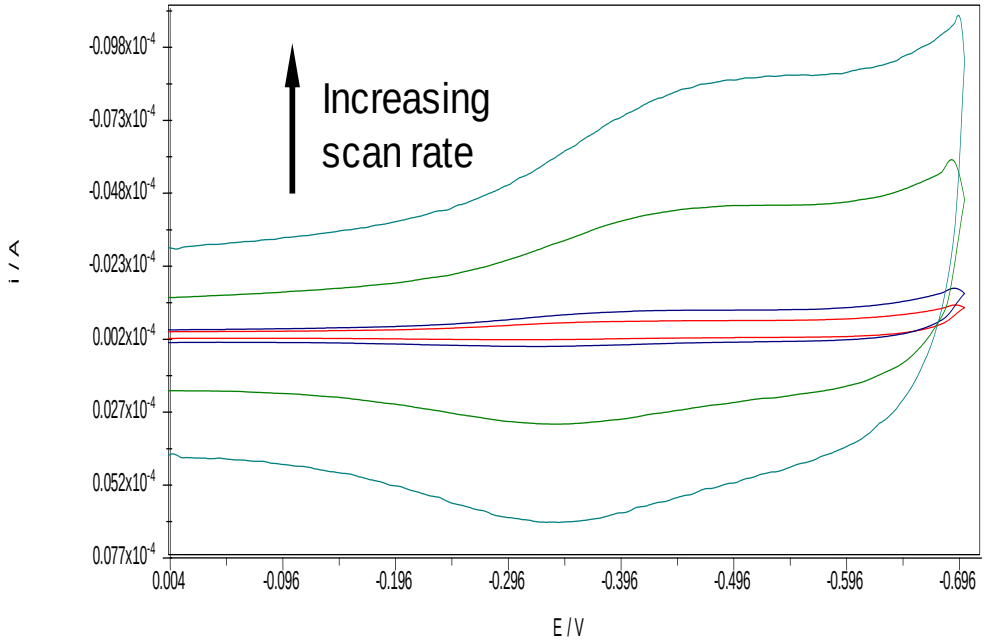

Figure 3.27: *Cyclic voltammograms of Fe(III)-Mimochrome IV Lys[3] immobilized on a SAM coated gold electrode, at different potential scan rates: 0,5 V/s line red; 1 V/s line blue; 5 V/s line green; 10 V/s line cyano.*

Cyclic voltammetry scans were also performed at different scan rates, in the potential range 40-500 mV (Figure 3.27). The peak current intensity varies linearly as a function of the scan rate (Figure 3.28), indicating that the peptide is bound to the electrode surface (Ranieri et al., 2009). The measured peak potential

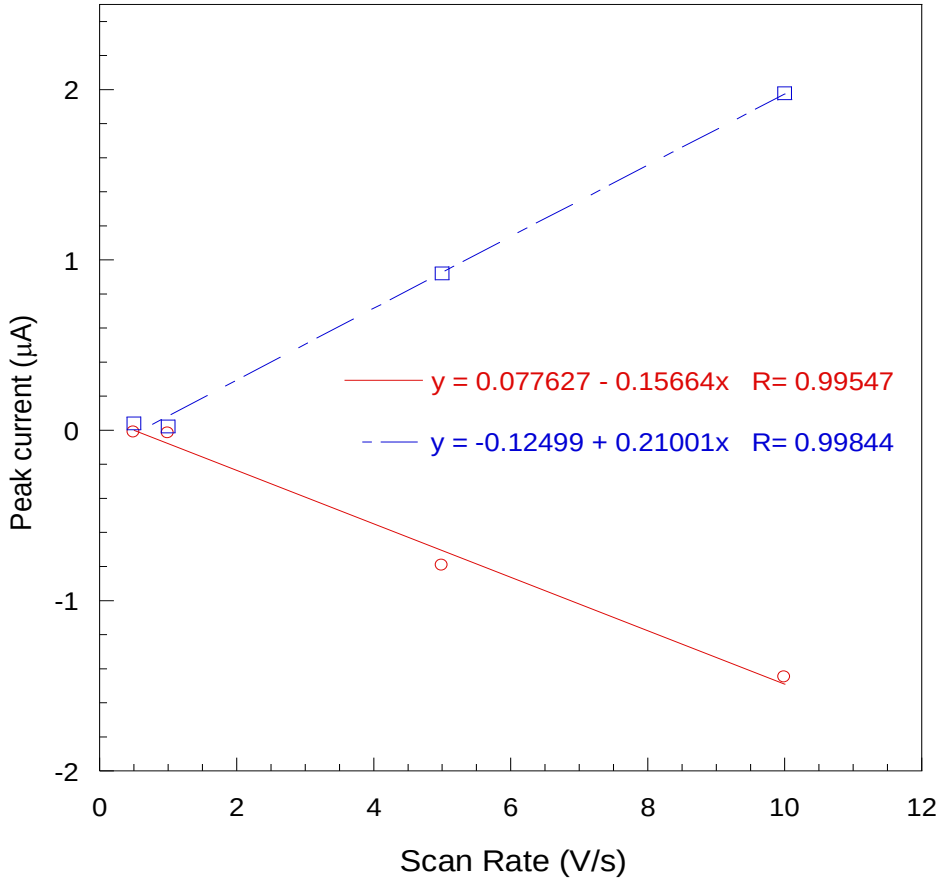

Figure 3.28: *Linear dependence of the peak current intensity from the scan rate; line red cathodic peaks; line blue anodic peaks.*

separation measured slightly increases with scan rate, ranging from -77 to -110 mV, indicating that once bound to the 11-MUA coated electrode, Fe(III)-Mimochrome IV Lys^3 undergoes a surface controlled quasi-reversible process. Similar results were reported for the direct electron transfer of Microperoxidase-11 (MP-11) bound to a chitosan-graphene electrode with a 11-mercaptoundecanoic SAM (Zhou et al., 2010).

The measured redox potential (E°') of the immobilized Fe(III)-Mimochrome IV Lys^3 shows a 25 mV anodic shift, when compared to the potential observed for the freely diffusing protein in the same medium. This observation is consistent with

literature data reported for Microperoxidase-11 (Jiang et al., 1997; Zhou et al., 2010). The shift is probably due to the changes in the environment of the protein-iron assembly, which occur when the peptide is covalently bound to the SAM.

3.8 Square wave and cyclic voltammetry of Fe(III)-Mimochrome IV Lys^3-HA_epitope immobilized on the gold electrode

The conjugate Fe(III)-Mimochrome IV Lys^3-HA_epitope was immobilized on the gold electrode coated with a SAM of 11-mercaptoundecanoic acid following the procedure previously described for Fe(III)-Mimochrome IV Lys^3.

The Fe^{III}/Fe^{II} reduction potential (E°') of the immobilized Fe(III)-Mimochrome IV Lys^3-HA_epitope complex was determined by square-wave and cyclic voltammetry. All measurements were performed immersing the Fe(III)-Mimochrome IV Lys^3 coated electrode in 1 ml of 10 mM phosphate buffer, pH 7, 100 mM $NaClO_4$, at 25 °C.

Figure 3.29 reports the square wave voltammograms of the immobilized conjugate, both for the cathodic and the anodic scans, performed at a scan rate of 37.5 mV/s.

Each scan shows a single peak, with a well-defined voltammetric wave, indicative of the electron transfer of a single species. The cathodic and anodic peaks are located at -407 and -369 mV, respectively, and the peak current intensity ratio (Ip,c/Ip,a) is ≈ 1.1; the peak potential separation measured is ≈ 0.52 mV. This finding indicates that the Fe(III)-Mimochrome IV Lys^3 molecules undergo a reversible electrochemical reaction, even when functionalized with the epitope. The formal potential measured is E°' = -384 mV vs Ag/AgCl and -175 mV vs SHE.

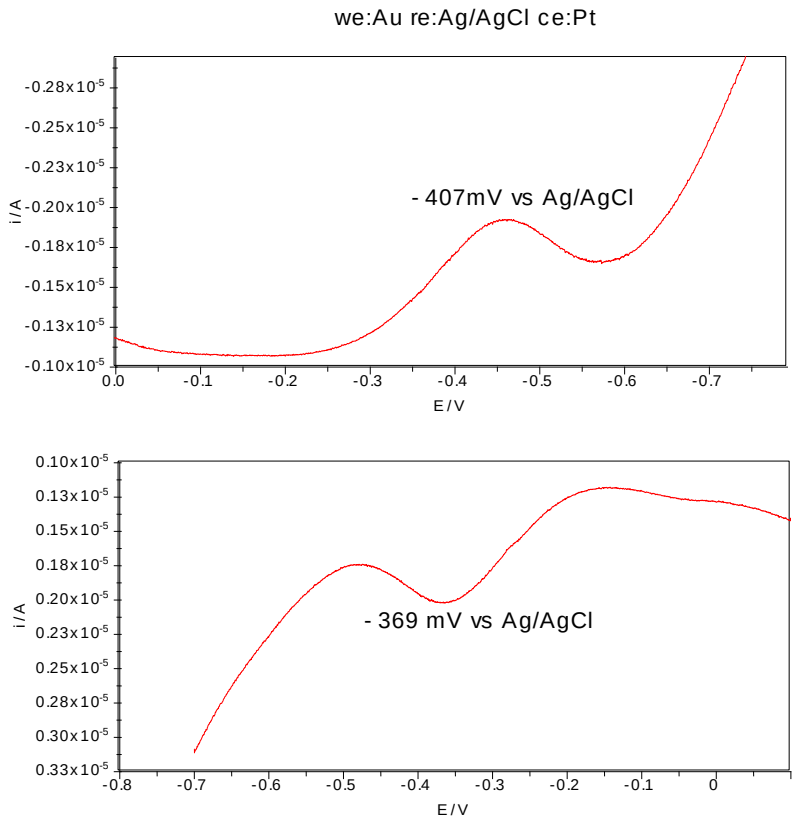

Figure 3.29: *Square-wave voltammograms of Fe(III)-Mimochrome IV Lys*^{3}*-HA_epitope complex immobilized on a SAM coated gold electrode, at 37.5 mV/s, (a) cathodic scan, (b) anodic scan.*

The dependence of peak current intensity from the scan rate was determined from cyclic voltammetry scans, performed at different scan rates in the potential range 1 - 10 V (Figure 3.30). Figure 3.31 reports the linear increase of the peaks current intensity with increasing scan rate. This indicates that the Fe(III)-Mimochrome IV Lys^{3}-HA_epitope conjugate is immobilized onto the electrode surface.

The measured peak potential separation slightly increases with scan rate up to 2 V/s, as observed for other molecules of the Mimochrome series (Ranieri et al., 2010).

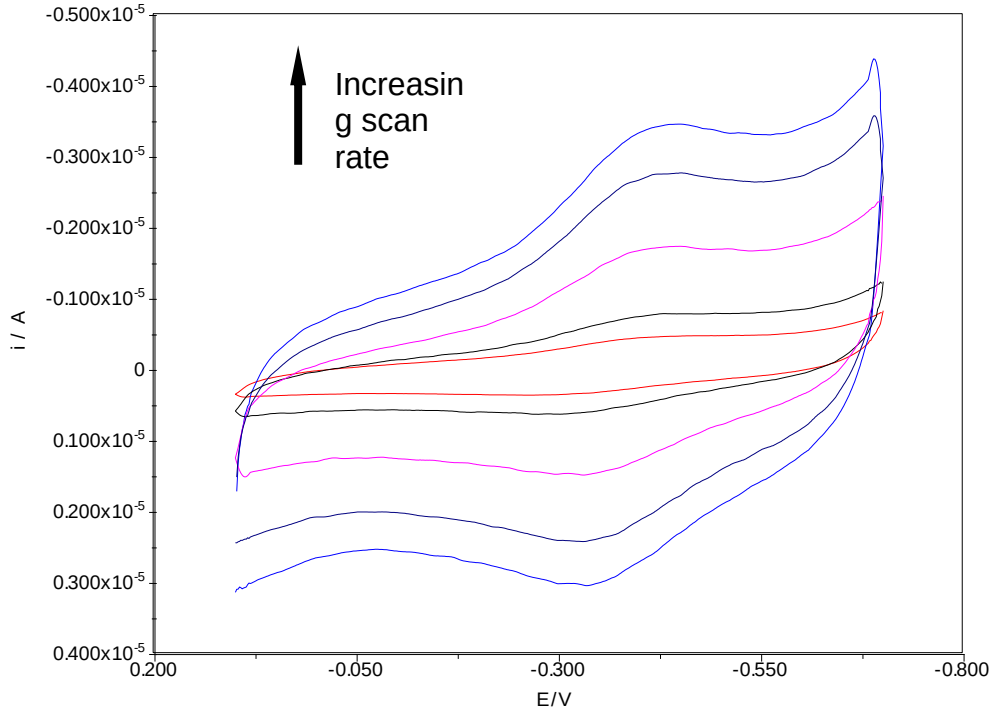

Figure 3.30: *Cyclic voltammograms of Fe(III)-Mimochrome IV Lys^3-Ha_ep immobilized on a SAM coated gold electrode, at different potential scan rates: (1 - 10 V/s).*

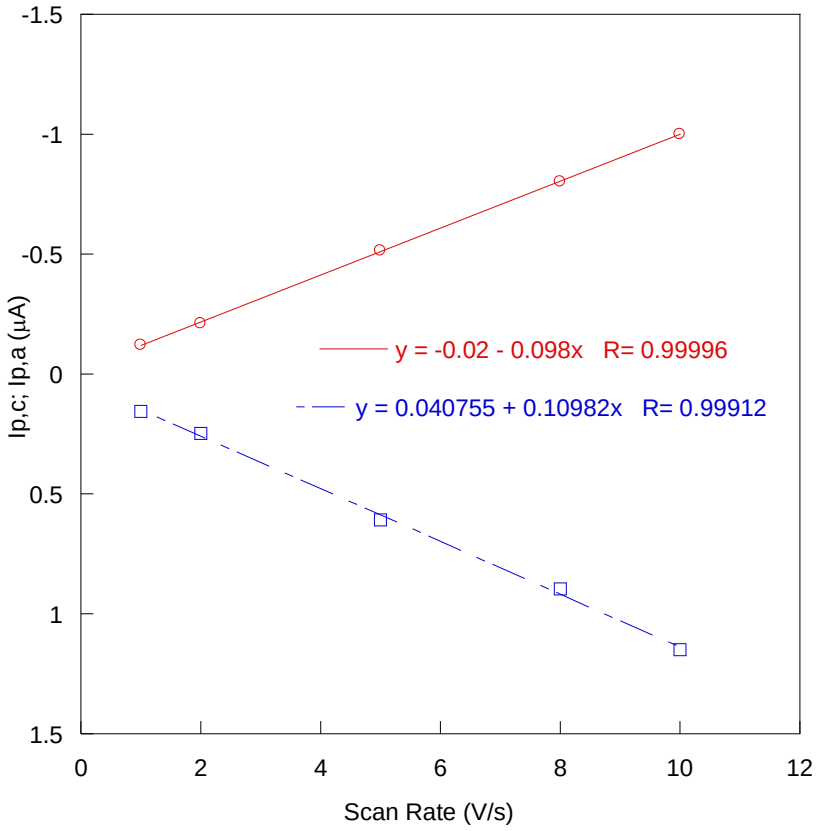

Figure 3.31: *Linear dependence of the peak current intensity from the scan rate for the immobilized Fe(III)-Mimochrome IV Lys^3-HA_ep; line red cathodic peaks; line blue anodic peaks.*

Table 3.1 reports the E° values of Fe(III)-Mimochrome IV Lys^3 in different environment. As discussed before, the covalent binding of the molecule on the gold substrate causes the formal potential to shift towards more negative values (25 mV) relatively to the freely diffusing molecule.

The observed potential shift toward negative values may be caused by the interaction of the molecule with the anionic SAM. Probably, the SAM carboxyl groups were not completely quenched by the reaction with TRIS. Therefore, the presence of free negatively charged groups on the SAM surface could shift the E° to more negative values. A further shift of E° toward negative values (-19 mV) was observed upon functionalization of Fe(III)-Mimochrome IV Lys^3 with the epitope HA. This finding is in agreement with the negatively charged residues present in the epitope sequence.

All the results so far obtained show that Fe(III)-Mimochrome IV Lys^3 electrochemical properties are very sensitive to small changes in the environment.

Table 3.1: *Comparison of the* E°' values measured for Fe(III)-Mimochrome IV Lys^3 in different environments.

Mimochrome IV Lys^3	**E°' measured (mV vs SHE)**
Freely diffusing	- 131
Immobilized on gold	-156
Functionalized with HA_ep and immobilized on gold	- 175

3.9 Antibody detection

The immunosensor was tested for the detection of specific Anti-HA_epitope monoclonal antibodies.

The assay procedure consisted of placing the sensor in an electrochemical cell containing 1.0 ml of measurement buffer (10 mM phosphate, pH 7). After registering the control voltammograms (t = 0), 2 µg of mAb anti-HA_epitope ([mAb] = $2*10^{-3}$ M) were added directly in the electrochemical cell. The modified electrode surface was allowed to incubate for 10 minutes, under stirring, prior to performing the electrochemical detection of the binding event. Then, SW voltammograms were recorded every 10 minutes to monitor the time-response of the sensor.

As shown in Figure 3.32, in the presence of the target antibody, there is a significant decrease of the Faradic current. After 30 minutes the signal is completely suppressed.

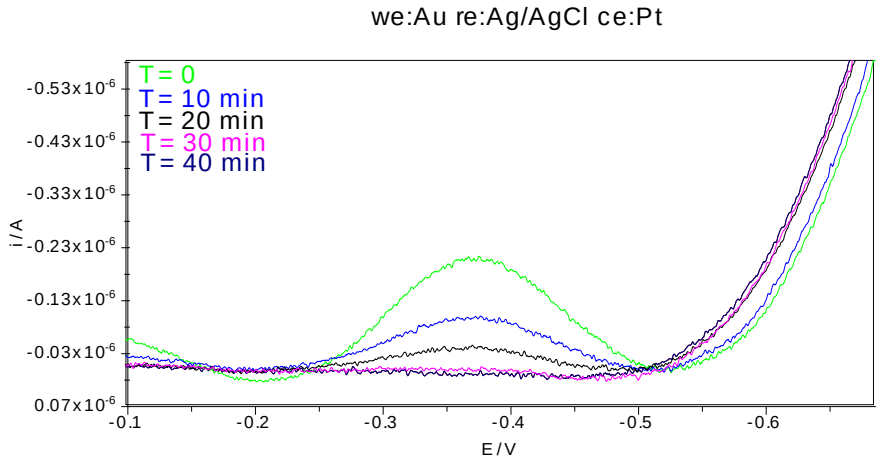

Figure 3.32: *The response of the electrode coated with Fe(III)-Mimochrome IV Lys[3]-HA_epitope complex before (green line) and after exposure to 2 mM target antibody.*

The decrease in current intensity upon binding of anti-HA_epitope IgG may reflect the changes in the interfacial microenvironment arising from the formation of the immunocomplex on the electrode surface. Probably, after Ab binding, the transducer is immersed in a protein environment that hinders electron transfer, causing the lowering of the electrochemical signal. This interpretation is consistent with literature data (Liu et al., 2008; Liu and Gooding, 2009; Yan et al., 2001). Gooding and co-workers reported similar observations on two immunoaffinity biosensors for the detection of anti-biotin IgG, in which the transducer is represented by small redox probes, such as ferrocene (Liu et al., 2008; Liu and

Gooding, 2009). The same behavior was already observed for viologen modified electrodes, in the detection of anti-biotin IgG (Yan et al., 2001).

To proof that this response was related to the specific interaction of anti-HA_epitope antibody with HA_epitope, a control measurement was performed employing an electrode coated with Fe(III)-Mimochrome IV Lys^3, devoid of the recognition element. In this case, only slight lowering in current, upon exposure to the target antibody, was observed (Figure 3.33).

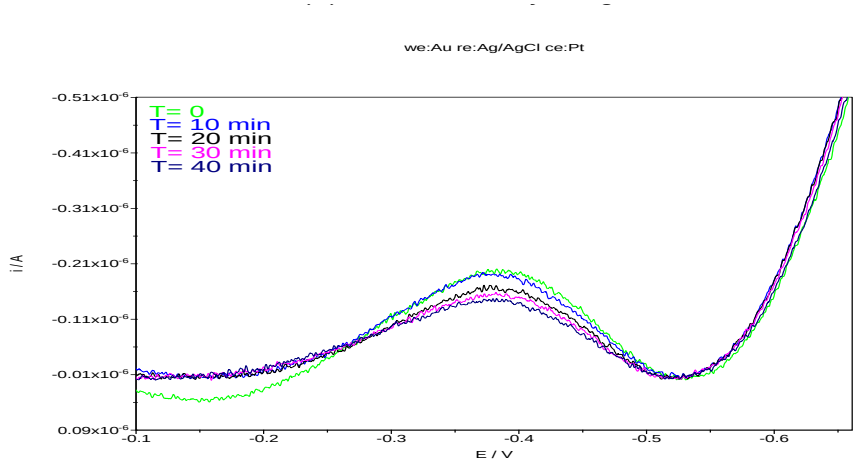

Figure 3.33: *The response of the electrode coated with Fe(III)-Mimochrome IV Lys^3 complex before (green line) and after exposure to 2 mM target antibody.*

These results indicate that anti-HA_epitope IgG selectively associate with the HA_epitope sites on the electrode surface, and only this selective interaction leads to a change in the electrochemistry of Fe(III)-Mimochrome IV Lys^3.

3.10 Conclusions

The application of a newly synthesized heme-protein model, Fe(III)-Mimochrome IV Lys^3, as signal transducer in a label-free immunoaffinity electrochemical biosensor was investigated, as reported in this chapter.

The artificial heme-protein was characterized by the electrochemical point of view, to understand its ability to exchange electrons with an electrode surface. Fe(III)-Mimochrome IV Lys^3 showed a well- defined electrochemical behavior, both freely diffusing than covalently bound to a gold electrode surface. For this reason, the next step in the development of the biosensor provided the functionalization of the heme-protein with the recognition element: the specific epitope recognized by the antibody to be detected. In fact, the model immunosensor developed is based on revealing the antigen-antibody recognition event.

The complex Fe(III)-Mimochrome IV Lys^3-HA_epitope was covalently immobilized on the gold electrode surface through the activated terminal carboxyl groups contained in the 11-MUA monolayer. The direct electron transfer of Fe(III)-Mimochrome IV Lys^3, once conjugated to the epitope, was evaluated by SW and cyclic voltammetry. The molecule showed a reversible behavior, with well-defined signals, demonstrating that the coupling with epitope has not remarkable influence on the redox properties of Fe(III)-Mimochrome IV Lys^3.

Preliminary experiments on the target antibody detection were performed in the presence of an excess of anti-HA_epitope IgG. The developed biosensor demonstrated to respond to the presence of the specific antibody. The detection of the antibody in solution occurs via the attenuation of Fe(III)-Mimochrome IV Lys^3 current intensity, as the antibodies bind to the HA_epitope. In the absence of the epitope the signal remains quite unchanged, thus demonstrating that signal changes are due to specific antigen-antibody interactions.

In summary, we have developed a new model of a label free immunoaffinity electrochemical sensor, based on the modulation of amperometric signals of surface-bound redox species. Further experiments to determine the limits of detection of the antibodies are required. Nevertheless, but the results so far obtained demonstrate the ability of the developed system to function as an immunobiosensor.

An important advantage of the biosensor model here described resides in the simplicity of construction, which allows the functionalization with different

recognition element in reasonable time at low costs. Therefore, it could be applied in the near future to a wide range of antigen-antibody pairs, as well as to receptor-ligand recognition. This finding may open numerous interesting perspectives in diagnostic field.

Chapter 4: Bio-catalytic electrochemical biosensors

4.1 Introduction

As previously described, engineered protein-based biosensors represent a further advancement in the detection of chemical substrates, compared to those made up of natural enzymes (Lambrianou et al., 2008). In fact, the use of native proteins, especially in the case of enzymes, cannot adequately embrace the limit of detection and the level of stability required for an usable sensor, since natural proteins are often subjected to degradation or denaturation by heat, organic solvents, extreme values of pH, and ionic strength. Therefore, a simpler enzyme model would have greater stability towards these destructive conditions, and it would be more useful for the afore-mentioned biotechnological applications (Moore et al., 1996). Another limitation in the use of natural enzymes is that, once immobilized on the electrode, they generally require an electron transfer mediator, which allows the electrochemical communication between the electrode and the enzyme active site. On the opposite, the direct and efficient communication between the electrode and the active site should be possible using a suitable immobilized small catalyst (Figure 4.1). In addition, a smaller catalyst would allow a higher density of active sites on the electrode surface, and hence, an enhanced amperometric sensitivity.

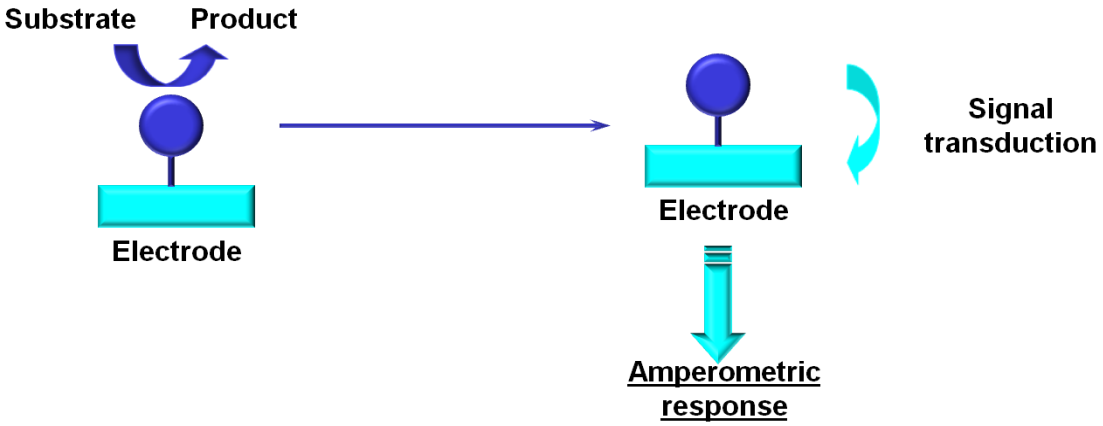

Figure 4.1: *Schematic representation of a bio-catalytic electrochemical biosensor.*

For these reasons, an electrode on which the immobilized enzyme is replaced by a simple and low-molecular-weight engineered enzyme could be desirable for

studying advanced models of electrochemical catalytic biosensors (Moore et al., 1996).

In this chapter, the application of the artificial enzyme Fe(III)-Mimochrome VI (figure 4.2) in the development of a totally sinthetic electrode surfaces is discussed. In the following paragraphs are reported: a brief description of the synthetic protocol, the analysis of Fe(III)-Mimochrome VI direct electron transfer in solution and adsorbed on a modified electrode surface, and its ability of electrochemically reduce dioxygen.

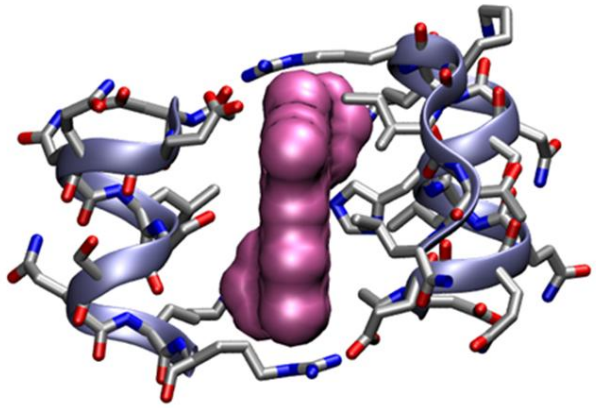

R= Ac-Asp-Glu-Gln-Gln-Leu-His-Ser-Gln-Lys-Arg-Lys-Ile-Thr-Leu-NH_2

R'= Ac-Asp-Glu-Gln-Gln-Leu-Ser-Ser-Gln-Lys-Arg-NH_2

Figure 4.2: *Figure 4.2 shows a model structure of Mimochrome VI, generated using the Visual Molecular Dynamics software (VMD: http://www.ks.uiuc.edu/Research/vmd/) (Humphrey et al., 1996). The aminoacid sequence of the two chains are shown, in which the heme iron-binding histidine is in blue and the two lysine residues bound to the two heme propionate groups are in red.*

4.2 Synthesis of Fe(III)-Mimochrome VI

4.2.1 Peptides synthesis

Peptides were synthesized by the solid-phase method using the Fmoc strategy, and they were coupled to deuteroporphyrin in solution to afford Mimochrome VI. The decapeptide (Ac-Asp^{1}(OtBu)-Glu^{2}(OtBu)-Gln^{3}(Trt)-Gln^{4}(Trt)-Leu^{5}-Ser^{6}(tBu)-Ser^{7}(tBu)-Gln^{8}(Trt)-Lys^{9}(Mmt)-Arg^{10}(Pbf)-NH_2) and the tetradecapeptide (Ac-Asp^{1}(OtBu)-Glu^{2}(OtBu)-Gln^{3}(Trt)-Gln^{4}(Trt)-Leu^{5}-His^{6}(Boc)-Ser^{7}(tBu)-Gln^{8}(Trt)-Lys^{9}(Mmt)-Arg^{10}(Pbf)-Lys^{11}(Boc)-Ile^{12}-Thr^{13}(tBu)-Leu^{14}-NH_2) were synthesized following the protocol described in Chapter 3 (sections 3.2.1 and 3.2.2) for Mimochrome IV Lys^{3}.

Fully protected peptides amide, except for the Lys^{9}, were generated from the resin separately, following the same protocol. They were cleaved from the resin by applying a solution of TFA/TIS/DCM (1/1/98 v/v/v) (triisopropylsilane: TIS; dichloromethane: DCM). Fractions eluted from the resin were checked by TLC and pooled if they contained the desired product. Analytical RP-HPLC (Vydac C18 column, using a gradient of acetonitrile in 0.1% aqueous TFA, 50% to 90% over 20 min, flow rate 1 mL min^{-1}) showed a main peak for both the protected peptides. Purification was accomplished by precipitation in ice-cold water, as previously described for Mimochrome IV Lys^{3} peptide. Both peptides were homogeneous as determined by analytical HPLC and by MALDI mass spectrometry (MALDI/MS).

Since Mimochrome VI is an asymmetrical complex, after the synthesis of the two peptides, their coupling with porphyrin was performed in two steps: first, we obtained the mono substituted intermediate decapeptide-deuteroporphyrin IX, then this intermediate was coupled with the tetradecapeptide.

4.2.2 Decapeptide-deuteroporphyrin coupling

The fully protected decapeptide, except for the Lys^9, was coupled in solution to the deuteroporphyrin ring. In order to favour the formation of the mono substituted deuteroporphyrin IX, the peptide solution was slowly added to the activated porphyrin.

The crude product was purified on a silica gel column to eliminate unreacted deuteroporphyrin IX, and its purity was estimated by analytical RP-HPLC.

From the chromatogram shown in Figure 4.3 a is possible to note the presence of two peaks: the first, with a t_r of 25.429 min corresponds to the mono-substituted decapeptide-DPIX, while the second, with t_r = 32.63 min corresponds to the bis-substituted species, decapeptide-DPIX-decapeptide.

The first peak was collected from the analytical RP-HPLC and its identity was confirmed by MALDI/MS spectrometry (Figure 4.3 b) (2980 u.m.a.).

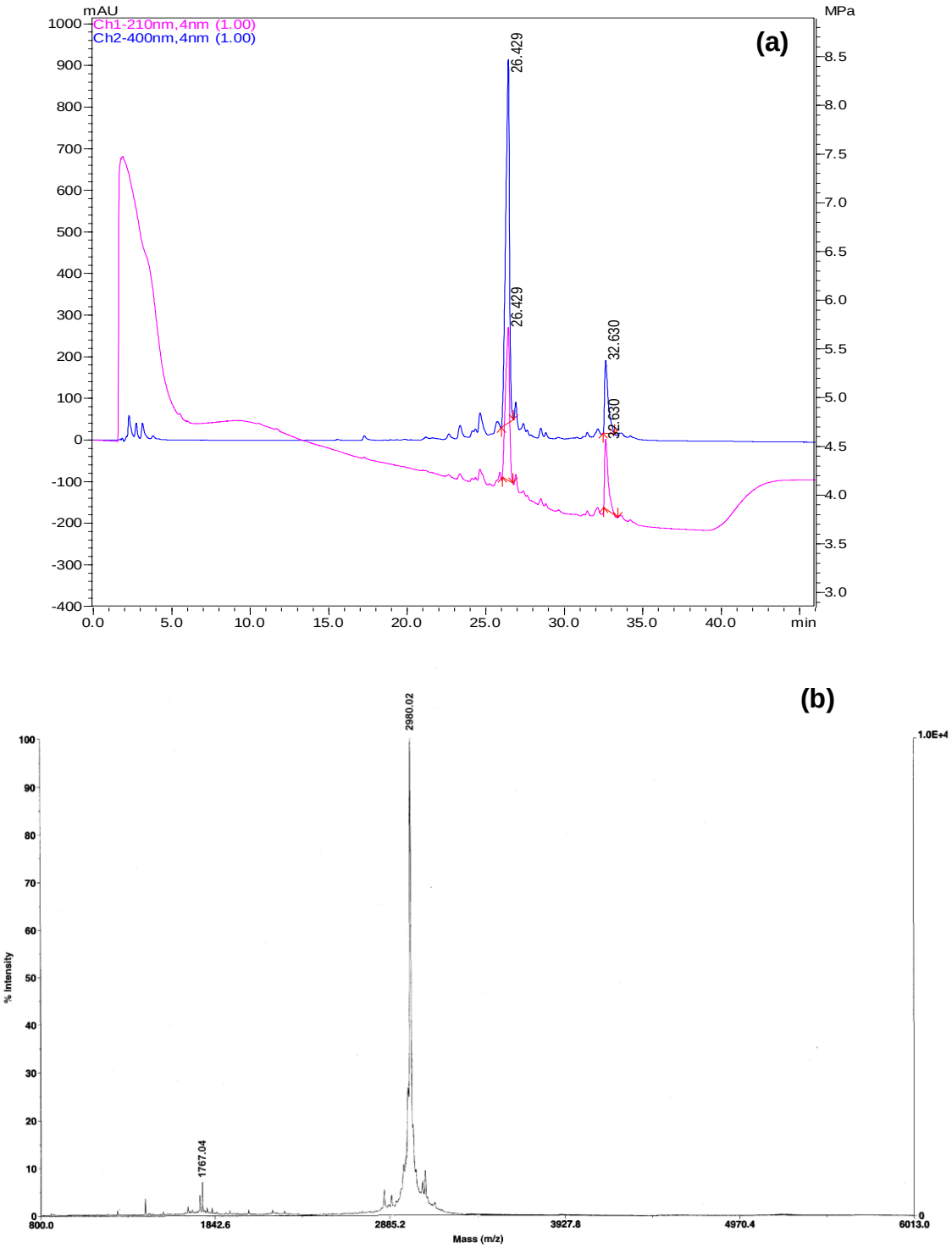

Figure 4.3: *(a) HPLC chromatogram and (b) mass spectrum of the decapeptide-porphyrin complex.*

4.2.3 Coupling of the tetradecapeptide to the mono substituted intermediate

Mimochrome VI free base, was synthesized by coupling the tetradecapeptide to the mono-substituted intermediate. The reaction was carried out adding 20% TFE (v/v) to the reaction mixture to avoid aggregation of peptide and porphyrin in solution.

The reaction was allowed to proceed at room temperature for 2 hours. The reaction progress was followed by analytical HPLC and by tlc. When reaction was complete, the mixture was evaporated under reduced pressure up to 20% of the volume, and precipitated with cold diethylether, and finally centrifuged. The crude product was dried in vacuo. Side chain deprotection was achieved by addition of the cleavage mixture (0.75 g phenol in thioanisole/H2O/EDT/TFA 0.25/0.5/0.5/8.75, v/v/v/v) (1,2-ethanedithiol: EDT) at 0 °C for 2.5 h. This treatment was performed twice. The reaction mixture was concentrated on a rotary evaporator to a volume of approximately 1-2 mL. Extraction of the scavengers and precipitation of the crude product was achieved by addition of cold diethylether. The crude material was then dried in vacuo and purified by preparative RP-HPLC; the pooled fractions containing the desired product were lyophilized. Analytical RP-HPLC (Figure 4.4 a) indicated that the purified product was > 99% pure, and ESI/MS (Figure 4.4 b) confirmed the expected molecular weight (expected mass: 3498 u.m.a; observed mass: 3498.62 ± 0.43 u.m.a).

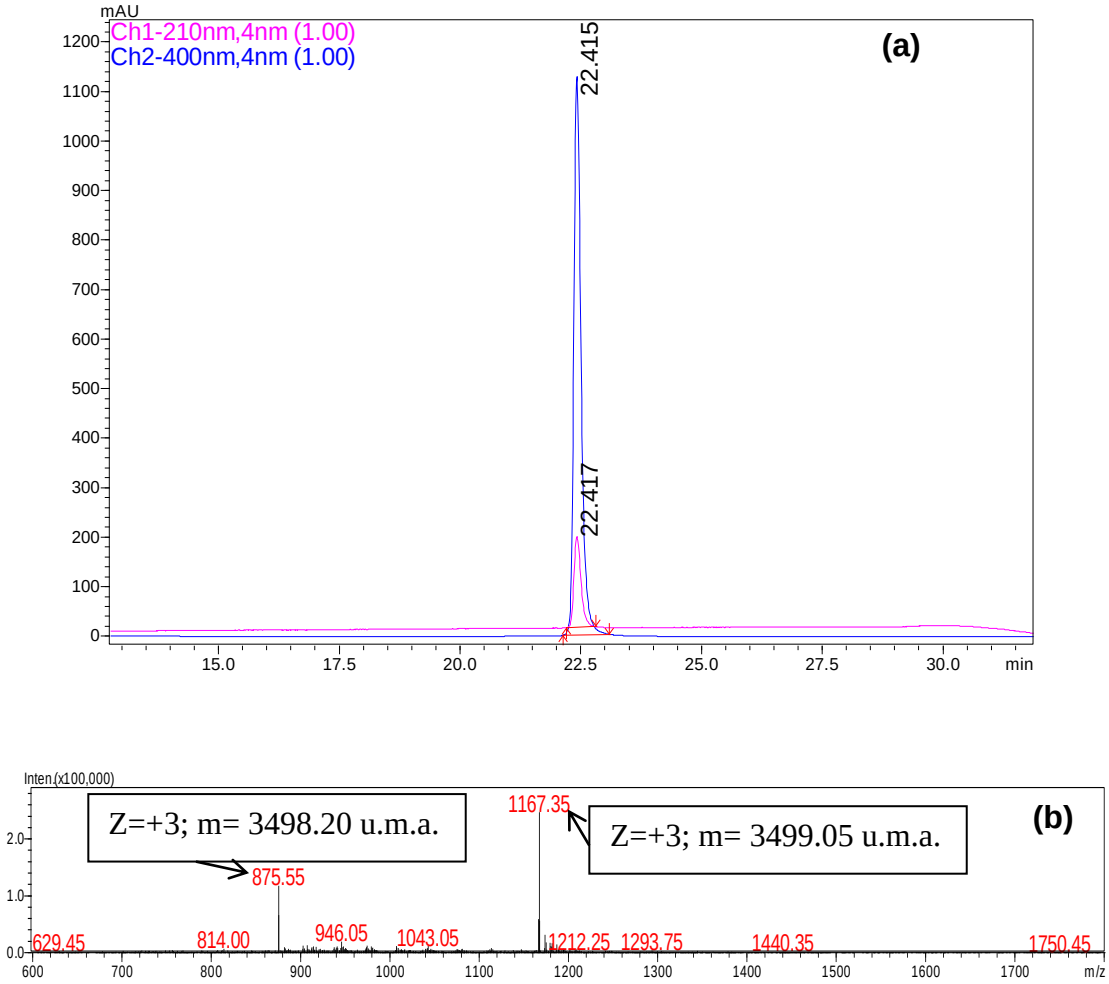

***Figure 4.4**: (a) HPLC chromatogram and (b) mass spectrum of the pure Mimochrome VI free base.*

4.2.4 Iron insertion

Iron ion was inserted into Mimochrome VI according to the acetate method (Buchler, 1978), as previously described for Fe(III)-Mimochrome IV Lys[3].

Iron (II) acetate (10 molar excess) was added to a solution of pure Mimochrome VI free base in TFE/Acetic acid, and the reaction mixture was kept at 50 °C for 2 h, refluxing under nitrogen. After 20 minutes the reaction mixture started to turn slowly brown, and the HPLC chromatogram showed the presence of a new peak at 23.77 min with the characteristic UV-visible spectrum of an iron (III) porphyrin at acidic pH.(Figure 4.5 b). When the reaction was complete, the product was purified by RP-HPLC and the pooled fractions containing the pure product were analized by analytical HPLC (Figure 4.5 a) and ESI-MS.

The mass spectrum confirmed (Figure 4.5 c) the identity of the desired product Fe(III)-Mimochrome VI (expected mass: 3552 u.m.a; observed mass: 3551.67 ± 0.12 u.m.a.).

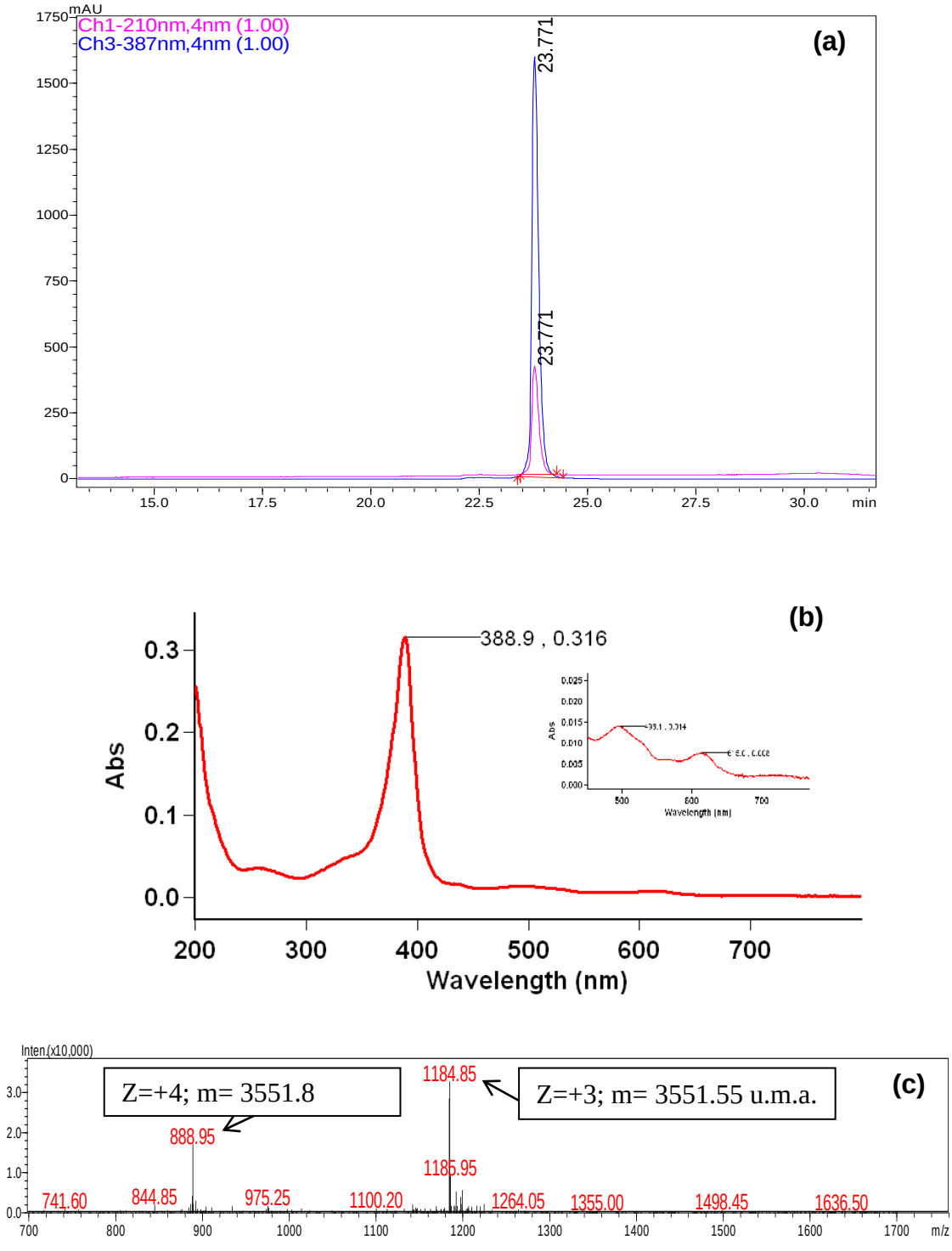

Figure 4.5: *(a) HPLC chromatogram, (b) UV-vis and (c) mass spectra of pure Fe(III)-Mimochrome VI.*

4.3 Voltammetric analysis of Fe(III)-Mimochrome VI

Cyclic voltammetry experiments reported in this chapter were performed in collaboration with the Bioinorganic chemistry group directed by professor Marco Sola at the University of Modena and Reggio Emilia.

4.3.1 Cyclic voltammetry of freely diffusing Fe(III)-Mimochrome IV Lys[3]

The Fe^{III}/Fe^{II} reduction potential (E°') of the diffusing Fe(III)-Mimochrome VI was determined by cyclic voltammetry. All measurements were performed using a gold electrode (1 mm dia.), at 20 C°. The electrode was coated with a SAM of 4-mercapto-pyridine. A saturated calomel electrode (SCE) was used as reference electrode. Fe(III)-Mimochrome VI concentration was 1 µM in a 5 mM phosphate buffer pH 7, 20 mM $NaClO_4$. The sample volume in the electrochemical cell was 0,5 ml, and before starting the measurements the sample was bubbled with argon, in order to avoid the presence of any dissolved oxygen. All the measured potentials are referred to SHE.

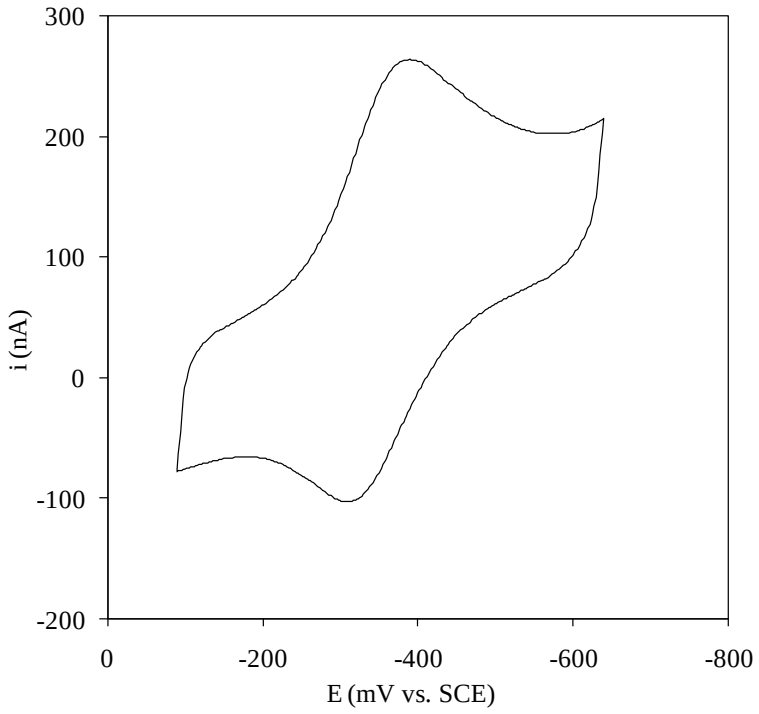

Figure 4.6: *Cyclic voltammogram for diffusing Mimochrome VI at a polycrystalline gold electrode coated with a SAM of 4-mercapto-pyridine.*

The cyclic voltammogram registered at 2 V/s (Figure 4.6) is clearly due to a specific electrochemical species, a pair of well-defined redox peaks clearly appears in the potential region between 0.0 and -0.7 V, corresponding to the electron transfer process between the heme-protein in solution and the electrode surface.

The cathodic and anodic peaks are located at - 370 and - 310 mV vs SCE, respectively, and the peak potential separation measured is about - 60 mV, indicating that the Fe(III)-Mimochrome VI molecules possess a reversible electrochemical behavior. The formal potential E°' is - 99 mV vs SHE.

4.3.2 *SAM deposition and Fe(III)-Mimochrome VI adsorption*

The immobilization strategy employed involves the modification of a gold electrode surfaces with a SAM of decane-1-thiol (DT). Electrode coating with the decane-1-thiol (DT) SAM was done by dipping the cleaned electrode into a 1 mM ethanolic DT solution for 12 h at 4 °C and then rinsing the electrode with deionized water.

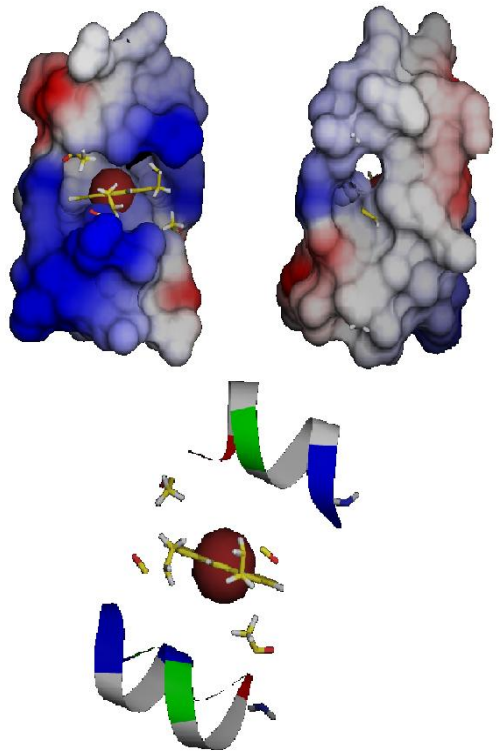

Figure 4.7: *Electrostatic potential of two sides of Mimochrome VI computed using the NOC software.*

Adsorption of the artificial heme-protein was achieved by dipping the functionalized electrode into a freshly prepared 1 µM Fe(III)-Mimochrome VI solution made up in 5 mM phosphate buffer at pH 7, for 4 h at 4 °C. Fe(III)-Mimochrome VI was adsorbed on this modified electrode taking advantage of the hydrophobic interaction between the SAM and the non-polar patch of the heme-peptide, including residues of both R and R' chains. In Figure 4.7 is shown the electrostatic potential of two sides of Fe(III)-Mimochrome VI computed using the NOC software (Chen et al., 2007). Positive and negative charge are shown in blue and red color, respectively. The structure on the right showing the hydrophobic

patch is that which likely faces the decane-1-thiol-coated Au electrode. The helix-heme-helix sandwich motif of Mimochrome VI is also shown.

4.3.3 *Cyclic voltammetry on the electrode surface*

The Fe^{III}/Fe^{II} reduction potential (E°') of the immobilized Fe(III)-Mimochrome VI was determined by cyclic voltammetry. All measurements were performed immersing the Fe(III)-Mimochrome VI coated electrode in 0,5 ml of 5 mM phosphate buffer at pH 7 at 20 °C. All the measured potentials are reported against SHE.

Figure 4.8 reports the cyclic voltammogram obtained at a scan rate of 2 V/s. It consists of a single well-defined signal arising from the quasi-reversible one-electron reduction/oxidation process of the heme iron.

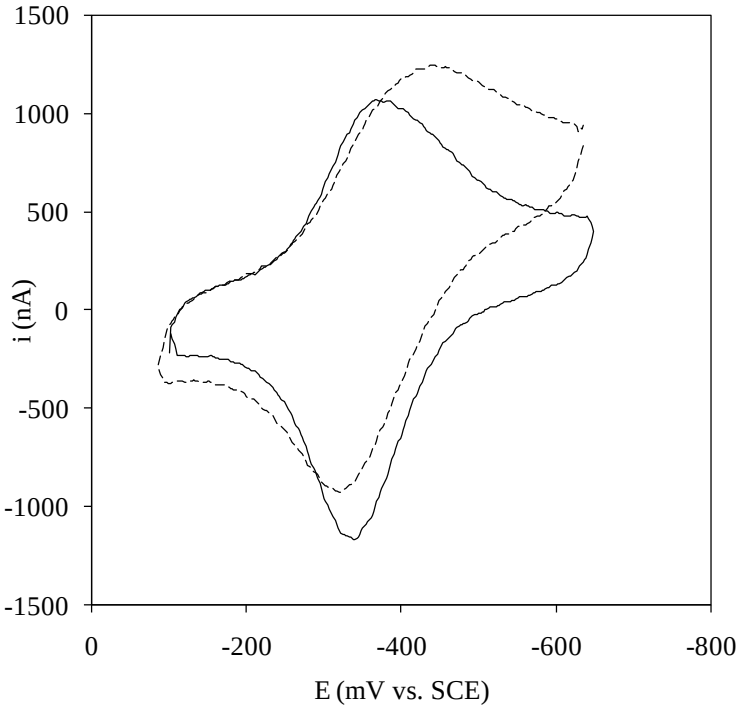

Figure 4.8: *Cyclic voltammograms for Mimochrome VI immobilized on a polycrystalline gold electrode coated with a SAM of decane-1-thiol. Solid line: cathodic scan starting from a poise at positive (oxidizing) potential; dotted line: anodic scan starting from a poise at negative (reducing) potential.*

The current intensity is linearly dependent on the scan rate, as expected for a diffusionless electroactive species (Figure 4.9). Repeated cycling does not affect the voltammograms from 5 to 35 °C, indicating that the peptide monolayer is stable. Above 35 °C, currents decrease due to peptide desorption and/or

unfolding. Peptide coverage of the functionalized electrode surface resulted to be 23.5±0.9 pmol cm^{-2}, which is similar to the value of 19 pmol cm^{-2} obtained for microperoxidase-11 in analogous conditions (Liu et al., 2010; Ruzgas et al., 1999) and for cytochrome *c* on carboxyalkanethiol SAMs (Tarlov et al., 1991; Battistuzzi et al., 2007). Fe-Mimochrome VI yielded no electrochemical response on anionic (1:1 mixed 11-mercapto-1-undecanoic acid – 11-mercapto-1-undecanol) and cathionic (cysteamine) SAMs, consistent with the low net charge of both redox states (see below).

It is worthy of note that the apparent E°' value (determined as the average of the cathodic and anodic peak potentials) is dependent on the potential scan rate, v, and on whether the potential scan is started from a reducing (negative potentials, dotted line) or oxidizing (positive potentials, solid line) poise (Figure 4.8).

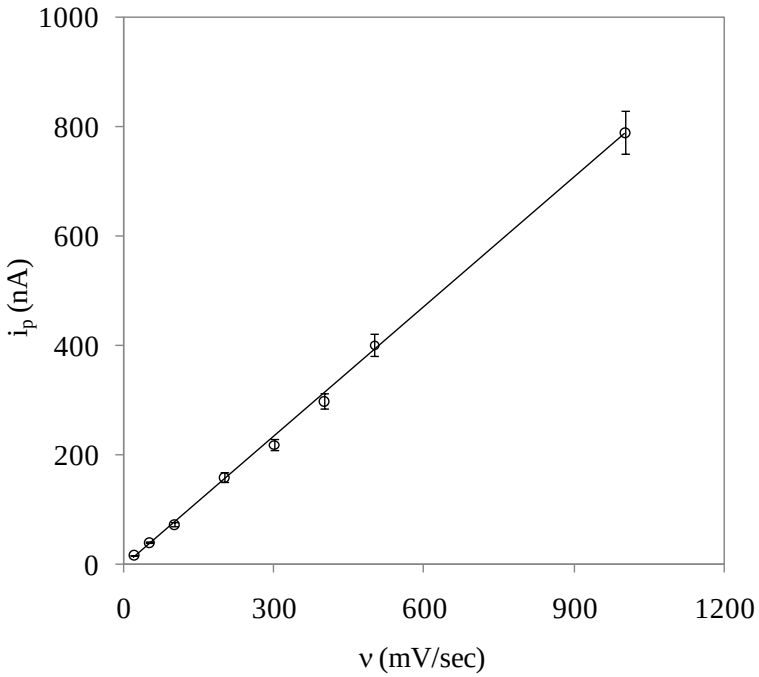

Figure 4.9: *Current intensity as a function of the scan rate for Mimochrome VI immobilized on a polycrystalline gold electrode coated with a SAM of decane-1-thiol.*

For v higher than 2 V/s (Figure 4.10) the scan rate dependence of E° is lost and two distinct and constant E°' values are obtained (Figure 4.8). This behaviour indicates that two redox state-dependent electrochemically active conformers of Fe-Mimochrome VI exist, which interconvert depending on the applied potential. At

low scan rates, the experimental E°’ would be the result of an average of the individual potentials weighted over the conformer populations, whereas at high scan rates the individual voltammetric features can be recognized, and thereby the individual E°’ values determined (Table 4.1).

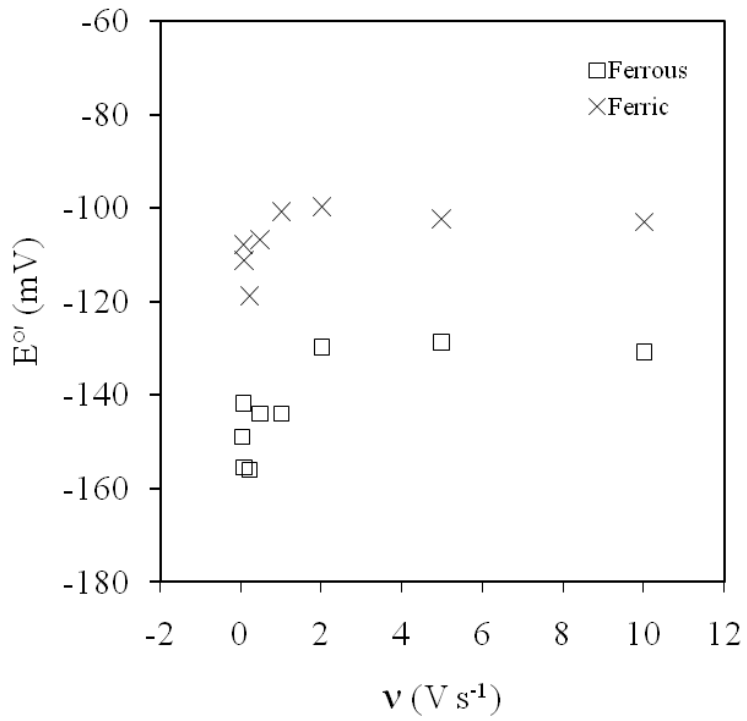

Figure 4.10: *E°’ values for Mimochrome VI immobilized on a gold electrode coated with a SAM of decane-1-thiol measured at varying scan rates (0.02-10 V/s).*

These conformers have been termed “high-potential” (HP) and “low-potential” (LP), corresponding to the voltammetric response obtained starting from an oxidizing and reducing poise, respectively. The measured E°’ values for the two conformers are: -106 mV (for the HP) and -131 mV (for the LP) vs SHE. The HP and LP conformers likely differ in the heme surrounding environment. This hypothesis is supported by analysis of the CD spectra in the Soret region (Figure 4.11) for the oxidized and reduced Fe-Mimochrome VI in solution.

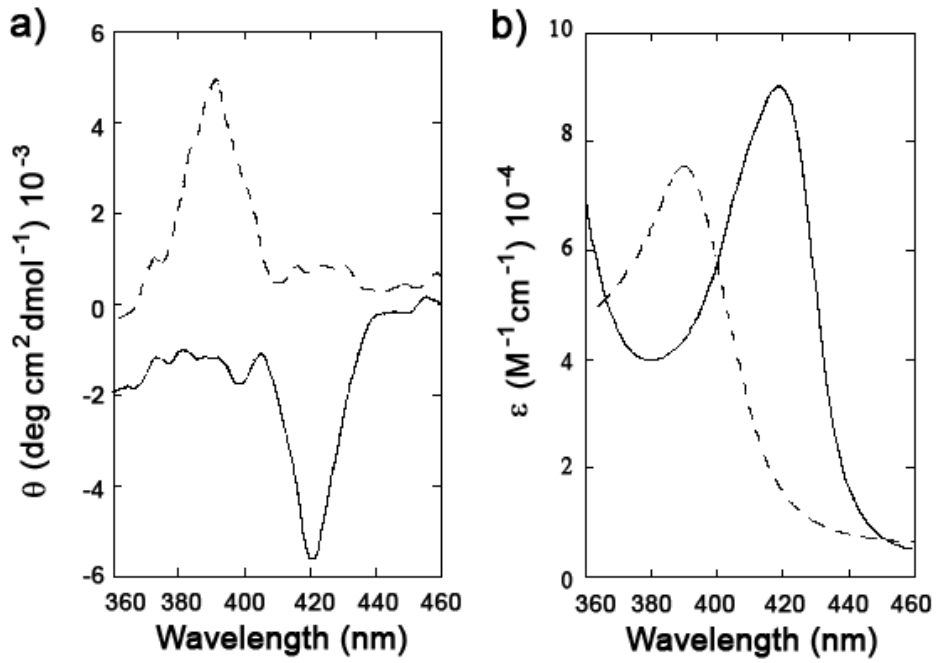

Figure 4.11. *CD spectra of Fe-MimochromeVI in the Soret region, in 5.0 mM phosphate buffer at pH 7. Dotted line: CD spectrum of ferric MimochromeVI, solid line CD spectrum of ferrous Fe-Mimochrome VI (a). Corresponding absorption spectra (b).*

In particular, the CD spectrum of oxidized Fe-Mimochrome VI, in aqueous phosphate buffer (5.0 mM, pH 7), displays a positive Cotton effect with a maximum at 390 nm. Reduced Fe-Mimochrome VI, obtained by sodium dithionite addition to the ferric form, display a negative Cotton effect with a minimum at 420 nm. The induced Cotton effect in the Soret region of heme-proteins has proven to be a useful probe for investigating protein conformational change. It is well known that the shape and the intensity of the induced Cotton effect in the Soret region is strictly related to the composition and structural organization of the polypeptide surrounding the heme (Mayer, 1978; Myer and Pande, 1978). CD analysis on previously developed Mimochromes demonstrated that the induced Soret Cotton effect in this class of molecules is related to the coupling between porphyrin (π-π*) and peptide backbone (n-π* and π-π*) transitions, and that the sign of the Cotton effect depends on the relative orientation of the peptide chains respect to the porphyrin plane (Lombardi et al., 2001; Nastri et al., 1997; D'Auria et al., 1997;

Nastri et al., 1998; Lombardi et al., 1998; Lombardi et al., 2003; Di Costanzo et al., 2004). In particular, a detailed analysis on the structurally characterized derivatives revealed that the flexibility of the linker between the peptide and the deuteroporphyrin ring allows each peptide chain to be positioned either above or below the porphyrin plane (D'Auria et al., 1997; Lombardi et al., 2003; Di Costanzo et al., 2004). These arrangements produce enantiomeric configurations around the metal ion, i.e. Δ or Λ: the Λ configuration gives rise to a positive Cotton effect, whereas the Δ configuration gives rise to a negative effect. Therefore, it is possible to hypothesize that the two redox forms of Fe-Mimochrome VI in solution correspond to two conformers differing in the configurations around the metal ion. This conclusion can be extended to electrode-immobilized LP and HP forms of Fe-Mimochrome VI. It is likely that protein-electrode interactions decrease the rate of conformer interconversion, so that at reasonably high potential scan rates the nuclear coordinates of each conformer can be "frozen", irrespective of the initial redox state of the metal.

4.3.4 Thermodynamic and kinetic aspects of the electron transfer reaction of Mimochrome VI adsorbed on the electrode surface

The E°' values for both immobilized conformers are more negative compared to the single freely diffusing species observed in the same conditions (Figure 4.13) (Table 4.1).

This can be explained considering that the oxidized and reduced states of Fe-Mimochrome VI features a net charge of 0 and -1, respectively. Therefore the adsorption process (involving hydrophobic interactions) stabilizes selectively the oxidized form of the heme-peptide which, bearing a zero charge, binds more strongly to the SAM. Such a cathodic shift is different for the two conformers, probably because of peculiar conformational features which affect the strength of the adsorption process, possibly also including a different rearrangement of solvent molecules at the SAM-peptide interphase. We note that similar E°' values were determined for microperoxidase-11 in solution (-0.134 V, vs. SHE) and adsorbed on alkanethiolate SAMs (-0.118 V) (Liu et al., 2010). The lower E°' values of both peptide systems in solution with respect to class I cytochromes c (E°' values from approximately +0.200 to +0.350 V vs. SHE) (Casalini et al., 2008) is the result of the enhanced accessibility of the heme group to solvent, which

favors the ferric state, and of the presence of a water or hydroxide ion axially bound to the heme iron in place of the Met ligand (Battistuzzi et al., 2005; Battistuzzi et al., 2004).

Mimochrome VI	***E°',[b] (V)***	***ΔG°'$_{rc}$[c] (kJ mol^{-1})***	***ΔS°'$_{rc}$ (JK^{-1} mol^{-1})***	***ΔH°'$_{rc}$ (kJ mol^{-1})***	***k_s (s^{-1})***	***λ (eV)***	***ΔH$^{\#}$ (kJ mol^{-1})***	***r (Å)***
Adsorbed HP conformer[d]	***-0.106***	***+10.2***	***-66***	***-9.1***	***92***	***0.51***	***-12.3***	***5.0***
Adsorbed LP conformer[e]	***-0.131***	***+12.6***	***-50***	***-2.1***	***33***	***0.48***	***-11.7***	***6.2***
freely diffusing	***-0.099***	***+9.5***	***+35***	***+20***	***-***	***-***	***-***	***-***

Table 4.1: *Thermodynamic and kinetic parameters for the electron transfer process of Mimochrome VI*[a]
[a] *Average errors on E°', ΔG°'$_{rc}$, ΔS°'$_{rc}$, ΔH°'$_{rc}$, k_s, λ, ΔH$^{\#}$, $r_{MC\text{-}VI}$ are ±0.002 V, ±0.2 kJ mol^{-1} , ±2 J K^{-1} mol^{-1}, ±0.3 kJ mol^{-1}, ±2 s^{-1}, ±0.03 eV, ±0.6 kJ mol^{-1}, ±0.4 Å respectively.*
[b] *at 20 °C.*
[c] *Corresponding to peptide-based ΔH°'$_{rc}$ (see text).*
[d] *Stable Fe-Mimochrome VI conformation with the Fe(III) heme, corresponding to the voltammetric response obtained starting from an oxidizing poise (see text).*
[e] *Stable Fe-Mimochrome VI conformation with the Fe(II) heme, corresponding to the voltammetric response obtained starting from a reducing poise (see text).*

The enthalpy ($\Delta H°'_{rc}$) and entropy ($\Delta S°'_{rc}$) changes for the Fe(III) to Fe(II) reduction (where the subscript rc stands for the iron 'redox couple') for both conformers of immobilized Fe-Mimochrome VI, determined from the E° measurements at variable temperature (Figure 4.12), are negative (Table 4.1). Therefore, the reduction potentials turn out to be the result of opposite and thereby partially compensatory thermodynamic contributions, a behavior common to heme proteins (Battistuzzi et al., 2005; Battistuzzi et al., 2004).

The same scheme holds for freely diffusing Fe-Mimochrome VI as well, which however features positive enthalpy and entropy changes (Table 4.1).

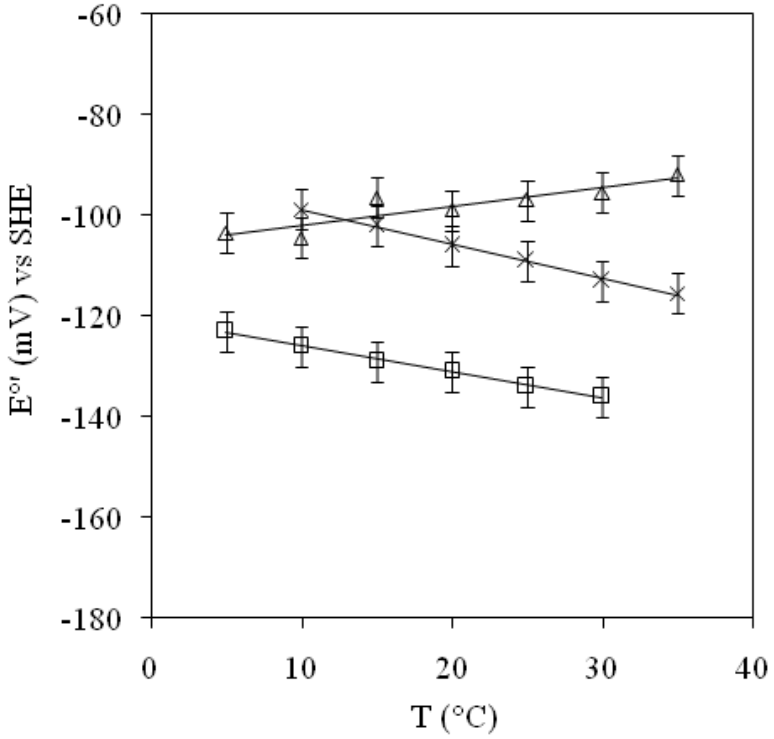

Figure 4.12: *E°' vs. T plots for immobilized and for diffusing Mimochrome VI Ferric conformer (×); Ferrous conformer (□); diffusion (Δ). Solid lines are least-squares fits to the data points.*

It is now well documented that this thermodynamic scenario is the signature of the dominant role played by solvent reorganization effects as effectors of the reduction thermodynamics (Battistuzzi et al., 2005; Battistuzzi et al., 2004). In particular, the reduction-induced changes in the hydrogen bonding network between the water molecules and surface residues within the hydration sphere of the molecule can be considered to a first approximation as the only determinants of the measured reduction entropy. However, these solvent reorganization effects are known not to contribute to the overall free energy change of the reaction due to exactly compensatory enthalpy and entropy changes. Therefore, the determinants of free energy change of the reaction (i.e the E°'' value) would be peptide-based and, considering that the corresponding entropy changes are conceivably small compared to solvation effects, the $\Delta G°'_{rc}$ values can be assumed to first approximation to correspond to the peptide-based $\Delta H°'_{rc}$ term (Battistuzzi et al., 2005; Battistuzzi et al., 2004). As a result, adsorption of the

heme peptide on the SAM through van der Waals interactions induces a large change in the reduction thermodynamics of Fe-Mimochrome VI. Several factors may account for this: alteration of reduction-induced changes in the network of hydrogen bonds at the peptide-solvent interface, the interaction with ions in solution and, to much lesser extent, the peptide conformational degrees of freedom. Yet, the much lower change in reduction free energy is determined by the enthalpy-based stabilization of the oxidized peptide on the non-polar SAM due to its zero charge.

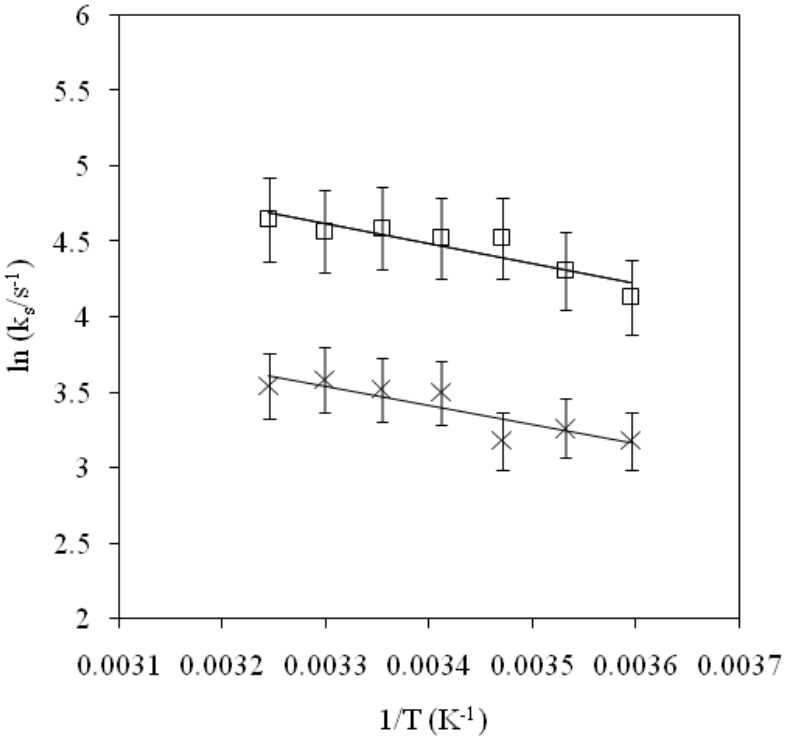

Figure 4.13: *Arrhenius plot for the ferric (×) and ferrous (□) conformer of Mimochrome VI immobilized on a polycrystalline gold electrode coated with a SAM of decane-1-thiol in 5 mM phosphate buffer at pH 7. Solid lines are least-squares fits to the data points.*

The rate constant of peptide-electrode heterogeneous ET (k_s) has been determined from the scan rate dependence of the anodic and cathodic peak potentials, according to Laviron (Laviron, 1979). The activation enthalpy ($\Delta H^{\#}$) and the reorganization energy (λ) values have been determined from the temperature dependence of k_s (Figure 4.13) and from the Marcus theory. The Marcus equation for the heterogeneous electron transfer process is (Marcus and Sutin, 1985):

$$k_s = \nu_0 e^{[-\beta(r-r_0)]} e^{\left(-\frac{\Delta G^{\#}}{RT}\right)} = \nu_0 e^{[-\beta(r-r_0)]} e^{\left(-\frac{\lambda}{4RT}\right)} \qquad 1)$$

where $\Delta G^{\#} = \lambda/4$, ν_0 is the frequency factor, β and r are the electronic tunneling factor for the peptide matrix and the distance between the metal center of adsorbed peptide and the electrode surface (tunneling distance), respectively.

As in these systems the entropic term of the free activation energy is negligible(Yee and Weaver, 1977; Nahir et al., 1994), $\Delta H^{\#}$ would correspond to $\Delta G^{\#}$ and can obtained by the Arrhenius equation. In this way, λ can be easily calculated. The calculated values for the adsorbed ferric and ferrous conformer are 0.51 and 0.48 eV, respectively (Table 4.1). The above equation can be arranged in the form:

$$\ln k_s = \ln \nu_0 - \beta(r - r_0) - \frac{\Delta G^{\#}}{RT} \qquad 2)$$

Using a ν_0 value of $6 \cdot 10^{12}$ s^{-1} and a mean β values of 1 $Å^{-1}$ and r_0 = 3 Å (Nahir et al., 1994; Tarlov and Bowden, 1991; Hildebrandt and Murgida, 2002; Ulmann, and Kostic, 1995) *r* values of 23.0 and 24.2 Å have been determined for the "ferric" and "ferrous" conformers, respectively (Table 4.1) (Figure 4.14). Assigning the DT SAM an upper value of tunnelling distance of 18 Å, corresponding to the length of a fully extended DT chain (Reipa et al., 1999), the distance of closest approach between the solvent exposed heme edge and the SAM surface would be of 5.0±0.4 Å and 6.2±0.4 Å. The difference in ET distance for the two conformers may be ascribed to the abovementioned redox state-dependent conformational features which may result in differences in the molecular volume and/or orientation toward the electrode. Manual docking of the

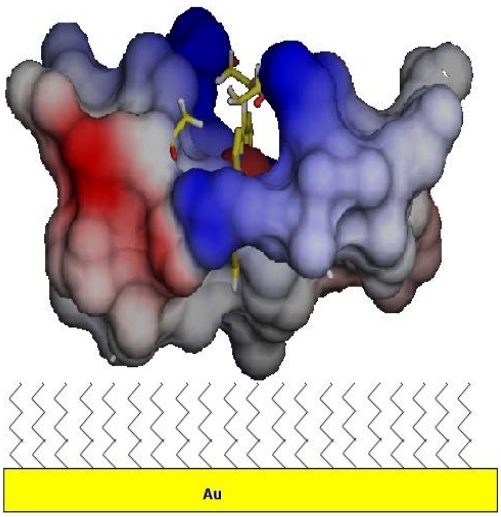

Figure 4.14: *Cartoon showing the orientation of Mimochrome VI onto an ideally flat DT-coated gold electrode surface obtained from manual docking of the heme-peptide.*

Fe-Mimochrome VI molecule on an ideally flat DT-coated electrode surface carried out in such a way as to maximize the contact of the heme-peptide with the hydrophobic patch, yields an orientation of the construct with the heme plane nearly perpendicular to the SAM surface. The calculated SAM-heme iron distance of 5.7 Å is in good agreement with those determined above from the kinetic data (Figure 4.14).

4.3.5 Electrocatalytic reduction of dioxygen

Figure 4.15 shows the electrochemical response of adsorbed Fe-Mimochrome VI in the presence of increasing oxygen concentration (obtained by increasing the time of exposure of the electrochemical cell, initially under argon) to air. The corresponding increase in intensity of the cathodic peak, with a concomitant decrease of the anodic current indicates that immobilized Fe-Mimochrome VI in these conditions is able to electrocatalytically reduce dioxygen at the heme iron, as observed previously for five-coordinate heme iron-containing cytochrome *c* variants (Battistuzzi et al., 2004; Casalini et al., 2010). The mechanism for O_2 reduction likely implies an oxidative addition of O_2 to Fe(II), yielding a Fe(III)-O_2^- derivative, which then dissociates. After a few catalytic cycles, the CV response taken after dioxygen removal contains the initial Fe-Mimochrome VI signal, indicating that the overall process is reversible. Re-use of the Fe-Mimochrome VI-functionalyzed electrode is limited by the natural loss of immobilized peptide from the adsorbed layer. The ability of immobilized Fe-Mimochrome VI to carry out reductive dioxygen turnover at the electrode is an essential finding for further applications. In fact, it constitutes a prerequisite for exploring the mono-oxygenase/hydroxylase activity toward a substrate, in conditions where electrons are pumped into the molecular systems by the electrode.

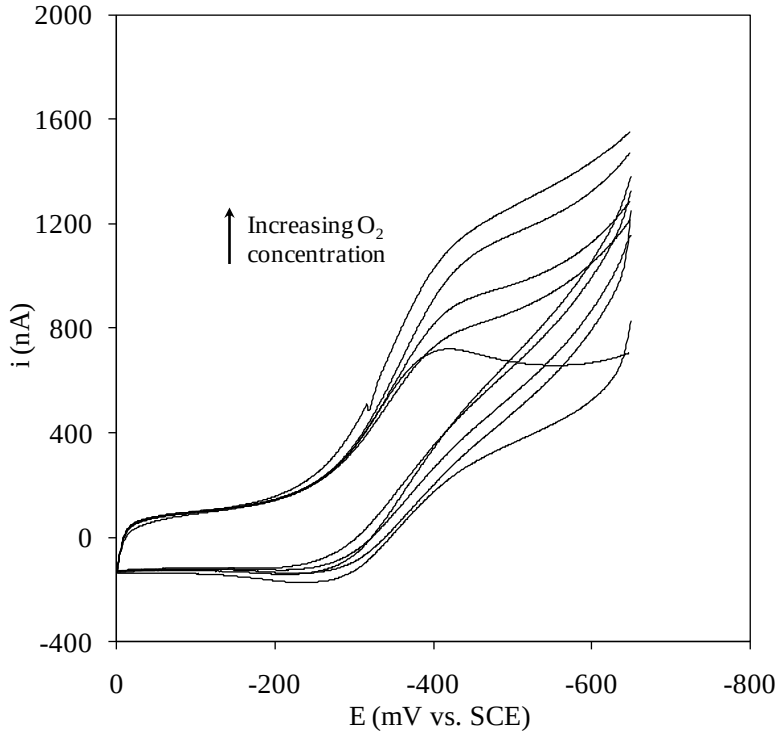

Figure 4.15: *Cyclic voltammograms for Mimochrome VI immobilized on a polycrystalline gold electrode coated with a SAM of decane-1-thiol in 5 mM phosphate buffer at pH 7, recorded at different exposure times of the electrochemical cell (initially under argon) to air at normal atmospheric pressure. Sweep rate, 0.1 Vs^{-1}. T = 20°C.*

It is interesting to notice that Fe-Mimochrome VI, such a small heme-protein model, behaves like a natural protein. In particular, it showed an electrochemical behavior comparable to five-coordinate heme iron-containing cytochrome *c* variants (Bortolotti et al., 2006; Casalini et al., 2008; Casalini et al., 2010). In fact, it reproduces the properties of the Met80Ala cytochrome c mutant to electrocatalitically reduce dioxygen (Casalini et al., 2008), with the same mechanism proposed for Mimochrome VI.

4.4 Conclusions

Mimochrome VI was developed to engineer into the Mimochrome scaffold a catalytic site, by creating a cavity able to accommodate small molecules and/or substrates. Therefore, it is an attractive system to be used as novel catalyst or as a constituent of hybrid synthetic interfaces in electrochemical biosensors.

To understand the possibility of the application of Mimochrome VI in the field of biosensing, the iron complex of this molecule was characterized by the electrochemical point of view. In particular, first the electrochemical properties of the freely diffusing species were determined.

Subsequently, the thermodynamics and kinetics of the electron transfer process for the Fe^{III}/Fe^{II} couple of Fe-Mimochrome VI immobilized on a SAM-coated electrode were determined.

This is a very important result, since this work constitute the first exemple of a complete analysis of the thermodynamic parameters that contribute to the reduction potential of a totally synthetic five-coordinated heme-protein (Ranieri et al., 2010)

Finally, the ability of the molecule to catalytically turn over molecular oxygen has been established.

All the results here reported show that Fe-Mimochrome VI, suitably immobilized on an electrode surface, maintains its redox properties and the chemistry of the five-coordinate heme iron. The most intriguing feature is that it is able to catalytically reduce dioxygen, similarly to five-coordinated cytochrome c variants. This study opens the way to the development of electrocatalytic hybrid Mimochrome-modified electrode surfaces for biosensing in the clinical and pharmaceutical areas.

Chapter 5: Concluding remarks and future perspectives

The main goal of this thesis was to develop sensitive third-generation electrochemical biosensors, based on artificial heme-protein mimetics. These new devices would be able to detect analyte of clinical interest in complex matrices. In order to accomplish this goal, the first step of this work was to select a suitable transduction method, to obtain label-free generic biosensors, that could be applied to the detection of a wide range of analytes, simply by varying the recognition element.

The field of third generation biosensors grew a few years ago when it was found that direct electrochemistry with redox proteins is possible without using a co-substrate (Armstrong and Cox, 1987), but efficient direct electron transfer reactions have been reported for a restricted number of redox enzymes. In fact, direct ET can be difficult to achieve and the electron transfer rates between the majority of redox proteins and electrode surfaces are prohibitively slow. There are several possible reasons for this (Zhang and Li, 2004).

Direct electron transfer can be difficult to achieve, and the electron transfer rates between the majority of redox proteins and electrode surfaces are often prohibitively slow (Zhang and Li, 2004). There are several possible reasons, as reported in the following:

- Unfavourable orientation of protein molecules on electrode surface may hinder electron exchange between the electrode and the electroactive centre of the proteins, which is usually deeply buried inside the polypeptide chains, especially in larger proteins.
- The "bad" orientation may increase the distance between the redox centre and the electrode surface, thus limiting the direct electrochemistry of the molecules (Zhang and Li, 2004).
- The monolayer concentration/coverage of the redox protein on the electrode surface decreases as the protein size increased, thus resulting in low electrochemical signals.
- Natural proteins can also denaturate on the electrode surface, blocking the electron exchange (Heller, 1990; Armstrong, 1990).

Our strategy to overcome the above limitations was the exploitation of artificial proteins, designed on rational bases to possess the required activity, structural

robustness (to prevent denaturation on the electrode surface), and small size (to simplify the electron transfer path to the electrode and increase surface coverage).

For application in biosensor technology, we have employed a particular class of heme-protein models, named Mimochromes.

This work was divided into two parts:

(i) the construction of an affinity electrochemical biosensor based on the redox transducer Fe(III)-Mimochrome IV Lys^3; and

(ii) the development of a bio-catalytic electrochemical biosensors based the artificial enzyme Fe(III)-Mimochrome VI.

The first part of this thesis was focused on the translation of a biological interaction, the antigen-antibody binding, into an electrical signal using the esa-coordinated heme-protein model Fe(III)-Mimochrome IV Lys^3 as signal transducer. This model was developed starting from a class of analogs (Fe(III)-Mimochrome IV, Fe(III)-Mimochrome IV 8Lys and Fe(III)-Mimochrome IV 8Glu), synthesized and characterized in a previous PhD thesis. They showed a good ability in exchanging electrons with solid electrodes, making them suitable for application in biosensor technology.

Starting from this point, the new model was developed to simplify its binding to a solid electrode surface and its functionalization with a recognition element. The most popular methods to bind a protein on a solid surface or to another protein, is by introducing functional groups on the ε-amino group of the Lys residues side chain. For this reason, two Gln residues in the sequence of the parental Fe(III)-Mimochrome IV were substituted with Lys.

The newly synthesized molecule was electrochemically characterized, using square wave and cyclic voltammetry, to understand its ability to exchange electrons with an electrode surface. Fe(III)-Mimochrome IV Lys^3 showed a well-defined electrochemical behavior, when freely diffusing to a glassy carbon electrode surface.

A method to covalently immobilise the peptide to a gold electrode surface was developed. The immobilization of biomolecules onto surfaces of electrically-conducting materials is an active area of research, useful for a range of applications, involving the construction of electrochemical biosensors. A general methodology that is currently being used for this purpose, is the self-assembly of

various functional groups onto specific surfaces. In this work, the best immobilization of Fe(III)-Mimochrome IV Lys^3 was obtained employing a SAM of 11-mercaptoundecanoic acid, activated at the terminal carboxyl group with an hydroxysuccinimide ester, which reacts with primary amines, such as the ε-amino group of the free Lys residue on one of the peptide chains of the molecule.

Electrochemical studies allowed us to understand that, once covalently bound to the gold surface, Fe(III)-Mimochrome IV Lys^3 maintains its redox properties. Its electrochemical behaviours were consistent with literature data.

The next step in the development of the biosensor was focused on the functionalization of the heme-protein with the chosen recognition element, a specific epitope recognized by the antibody to be detected. In fact, the immunosensor developed uses an epitope as biorecognition element, in order to detect the specific antibody, which constitutes the analyte to be determined. The chosen biorecognition element was a synthetic epitope (HA_ep) of the hemagglutinin A of the human *influenza* virus, Haemophilus Influenzae. A rapid and simple functionalization protocol was developed to bind the epitope to the heme-protein mimetic, employing the heterobifunctional crosslinker sulfo-SMCC. This makes our model immunosensor really versatile. In fact, it can be easily used for the application to a wide range of analytes, by simply changing the recognition element.

The complex Fe(III)-Mimochrome IV Lys^3-HA_epitope was covalently immobilized on the gold electrode surface through the activated terminal carboxyl groups contained in the 11-MUA monolayer. The direct electron transfer of Fe(III)-Mimochrome IV Lys^3, once conjugated to the epitope, was evaluated by SW and cyclic voltammetry. The molecule showed a reversible behavior, with well-defined signals, demonstrating that the coupling with epitope has not remarkable influence on the redox properties of Fe(III)-Mimochrome IV Lys^3.

Preliminary experiments on the target antibody detection were performed in the presence of an excess of anti-HA_epitope IgG. The developed biosensor demonstrated to respond to the presence of the specific antibody. The detection of the antibody in solution occurs via the attenuation of the Fe(III)-Mimochrome IV Lys^3 current signal as antibodies bind to the HA_epitope. In the absence of the epitope, presence of the antibody does not cause any changes in the signal.

The development of this model biosensor system and the first experiments in analyte detection were done to proof the working hypothesis. We have developed a new model of a label free immunoaffinity electrochemical sensor based on the modulation of amperometric signals of surface-bound redox species. Further experiments are required, in order to determine the limits of detection of the antibodies. Therefore, the system will be optimized and eventually applied to the recognition of other analytes, of clinical and pharmaceutical interest.

The second part of this project was focused on the application of the artificial enzyme Fe(III)-Mimochrome VI in the development of a totally sinthetic catalytic electrode surfaces. Mimochrome VI was developed to engineer into the Mimochrome scaffold a catalytic site, by creating a cavity able to accommodate small molecules and/or substrates. It is an attractive system to be exploited as novel catalyst or as a constituent of hybrid synthetic interfaces in electrochemical sensing devices.

To understand the possibility of the application of Fe(III)-Mimochrome VI in the field of biosensing, the iron complex of this molecule was characterized by the electrochemical point of view. In particular, the ability of exchange electrons with an electrode surface was investigated performing cyclic voltammetry experiments on the freely diffusing molecule at a gold electrode coated with a SAM of 4-mercapto-pyridine. Fe(III)-Mimochrome VI showed a quasi reversible, well-defined electrochemical behavior.

The next step was related to the biosensor assembly. Fe(III)-Mimochrome VI was adsorbed on a gold electrode coated with a SAM of decane-1-thiol, taking advantage of the hydrophobic interaction between the SAM and the non-polar patch of the heme-peptide. Cyclic voltammetry analysis of the adsorbed molecule allowed to study the electrochemical behaviour of Mimochrome VI. Notably, once adsorbed on the SAM coated electrode, two redox state-dependent electrochemically active conformers of Fe-Mimochrome VI were detected, which interconvert depending on the applied potential. This hypothesis was supported by analysis of the CD spectra in the Soret region of the oxidized and reduced Fe-Mimochrome VI, in solution.

The thermodynamics and kinetics of the electron transfer process for the Fe(III)/Fe(II) couple of Fe-Mimochrome VI, adsorbed on the SAM-coated gold

electrode, were also determined, in order to verify that the immobilization produces a stable hybrid interface allowing for fast heterogeneous electron transfer (ET). In these conditions, Fe-Mimochrome VI was found to maintain its redox properties and the chemistry of a five-coordinate heme iron; and it was also able to exchange electrons with the electrode at a reasonable rate.

The developed biosensor was tested for the ability of catalytically reduce dioxygen. The reaction was followed by cyclic voltammetry: the adsorbed Fe-Mimochrome VI was able to electrocatalytically reduce dioxygen at the heme iron, as previously observed for five-coordinate heme iron-containing cytochrome *c* variants. This study opens the way to the development of electrocatalytic hybrid Mimochrome-modified electrode surfaces for biosensing in the clinical and pharmaceutical areas.

In summary, the developed biosensor models, based on the use of totally synthetic heme-protein mimetics and peptides interfaces, demonstrated the possibility of creating a new class of third generation electrochemical biosensors, potentially applicable to the detection of a wide range of analytes. Their possible applications range from environmental, food and clinical analysis.

Future work of this project will include a deep investigation of the response of the immunosensor, at different concentration of the specific antibody, in order to determine the detection limit.

It would be also interesting to proof the biosensor working with a different recognition element/analyte pair, such as biotin and streptavidin, or a larger antigen and the corresponding antibody.

Future studies would also include further investigation of the immobilization methods of Fe-Mimochrome VI with different SAMs, adsorbed or covalently linked, to improve the electron transfer rate and the stability of the system.

Experimental section

Chapter 6: Experimental section

6.1 Solid phase peptide synthesis

Since R. B. Merrifield's report (Merrifield, 1963) on the solid phase chemical synthesis of peptides and small proteins, solid-phase peptide synthesis (SPPS) has become a widely utilized technique for the production of peptides and small proteins.

The basic idea of the solid-phase approach involves the covalent attachment (anchoring) of the growing peptide chain to an insoluble polymeric support (resin); in this way unreacted soluble reagents can be removed simply by filtration and washing, without losses of the growing peptide chain. Subsequently, the insoluble peptide-resin is elongated by addition of α-amino- and side-chain-protected amino acid residues in a series of addition reactions, which must be performed with high yields. Excess soluble reagents are used to drive sequential coupling and deprotection reactions to completion. The repetitive nature of the coupling and deprotection steps has led the major portion of the SPPS method to automation.

The acid-labile Boc group or base-labile Fmoc-group are used for the *N*-α-protection of amino acids. The general scheme of SPPS using Fmoc chemistry is illustrated in Figure 3.2. Fmoc- protected amino acids are most popular in SPPS since a mild basic treatment, using piperidine, can be used for the Fmoc-group removal at every stage. The final cleavage and deprotection of the peptidyl resin is accomplished using TFA. An *N*-α-derivatized amino acid is attached to an insoluble (solid) support, *via* a flexible linker. The *N*-α-blocking group is then removed (deprotected) and the amino acid-linker-support is thoroughly washed with solvent. The next amino acid (which is also *N*-α-protected) is then coupled to the amino acid-linker-support directly in the presence of coupling reagents. The coupling may also be carried out using peptides instead of single amino acids: this method is referred to as fragment condensation (Simmerman et al., 1982). After the completeness of the coupling reactions, the *N*-α-dipeptide (or oligopeptide)-linker-support is washed with the solvent. The deprotection/coupling cycle is repeated until the desired sequence of amino acids is generated. The peptide-linker-support is cleaved to obtain the peptide as a free acid or amide, depending on the chemical nature of the linker. The cleavage reagent also removes the amino acid side chain protecting groups, which are stable to the deprotection

reagent. These steps may be carried out as either a batch process, where the support is filtered between each step, or as a continuous flow process, where the support is always solvated during reagent exchange and the release of the protecting groups is monitored spectrometrically.

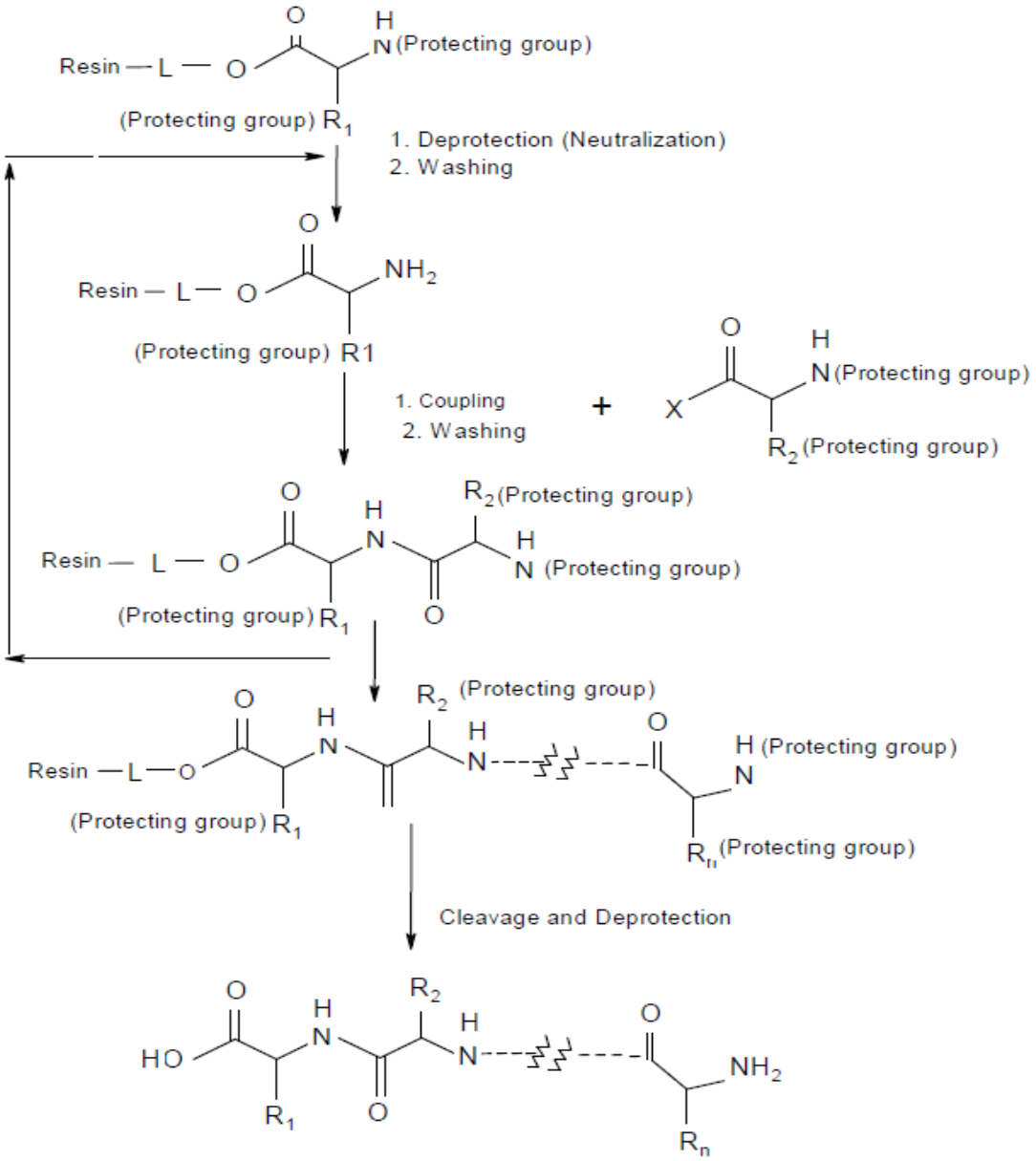

Figure 6.1: *General approach to solid phase peptide synthesis using Fmoc chemistry. Peptides are synthesized from the C-terminus to the N-terminus by stepwise addition of N-α-amino- and side chain-protected amino acid residues to an insoluble polymeric support (resins). Final cleavage of the peptidyl resin and side chain deprotection is achieved using TFA.*

Materials and Methods

6.1.1 Materials

All 9-fluorenylmethoxycarbonyl (Fmoc) protected amino acids, Sieber amide resin and coupling reagents: Nhydroxybenzotriazole (HOBt), 2-(1H-benzotriazole-1-yl)-1,1,3,3 tetramethyluronium hexafluorophosphate (HBTU), and benzotriazole-1-oxy-tris-pyrrolidino-phosphonium hexafluorophosphate (PyBOP) were purchased from NovaBiochem (EMD Biosciences, La Jolla, CA). PAL-PEG-PS resin was purchased from Applied Biosystems.

Silica gel 60 (230-400 mesh) was from Merck. Precoated silica G-60 plates, F254, were used for thin-layer chromatography (tlc).

All solvents used in the peptide synthesis and purification were anhydrous and HPLC grade respectively, and were supplied by Romil. Piperidine and scavengers (ethanedithiol, thioanisol, triisopropylsilane) were from Fluka. N,N-Diisopropylethylamine (DIPEA), trifluoroacetic acid (TFA) were supplied from Applied Biosystems. N,N-dimethylformamide (DMF), dichloromethane (DCM), pyridine, ethanol, methanol and ninhydrin reagent and 1-methyl-2-pyrrolidone (NMP) were supplied by Romil. Deuteroporphyrin IX was from Porphyrin Products. Iron(II) acetate, tetramethylsilane, sulfo-SMCC and EDTA were from Sigma Aldrich. Solvent mixtures are indicated in the respective sections.

6.1.2 Solid phase synthesis of peptides

Mimochrome IV Lys^3 peptide, HA_epitope, Mimochrome VI decapeptide, Mimochrome VI tetradecapeptide were synthesized using Fmoc solid phase peptide synthesis (SPPS) on an ABI 433 automatic peptide synthesizer on a 0.25 mmol scale for Mimochrome VI tetradecapeptide, and 0.2 mmol scale for HA_epitope, Mimochrome VI decapeptide and Mimochrome IV Lys^3 peptide. The resin used for the Mimochrome peptides was the super acid labile Sieber Amide (substitution level 0.52 mmol/g). For the HA_epitope, the resin used was the PAL-PEG-PS (substitution level 0.16 mmol/g). For the synthesis of the four peptides the following amino acids were used:

Mimochrome IV Lys^3: Fmoc-Glu(OtBu)-OH, Fmoc-Ser(tBu)-OH, Fmoc-Lys(Boc)-OH, Fmoc-Leu-OH, Fmoc-His(Trt)-OH, Fmoc-Asn(Trt)-OH , Fmoc-Lys(Mmt)- OH, Fmoc-Arg(Pbf)-OH.

Mimochrome VI decapeptide: Fmoc-Asp(OtBu)-OH; Fmoc-Glu(OtBu)-OH; Fmoc-Gln(Trt)-OH; Fmoc-Leu-OH; Fmoc-Ser(tBu)-OH; Fmoc-Lys(Mmt)-OH; Fmoc-Arg (Pbf)-OH.

Mimocrome VI tetradecapeptide: Fmoc-Asp(OtBu)-OH; Fmoc-Glu(OtBu)-OH; Fmoc-Gln(Trt)-OH; Fmoc-Leu-OH; Fmoc-His(Boc)-OH; Fmoc-Ser(tBu)-OH; Fmoc-Lys(Mmt)-OH; Fmoc-Arg(Pbf)-OH; Fmoc-Lys(Boc)-OH; Fmoc-Ile-OH; Thr(tBu)-OH.

HA_epitope: Fmoc-Cys(Trt)-OH; Fmoc-Tyr(tBu)-OH; Fmoc-Pro-OH; Fmoc-Asp(OtBu)-OH; Fmoc-Val-OH; Fmoc-Ala-OH.

For all the peptides the same synthetic procedures were used. The first step was the synthesis of the fully protected peptides. The synthetic procedure can be summarized as follow.

The α- Fmoc group, was removed at the beginning of every cycle with a 20% piperidine solution. After deprotection, the resin was washed with NMP to remove the piperidine. The peptide resin was then ready for coupling. All amino acids were coupled using a 0.45 M HBTU/HOBT solution in DMF. In the coupling step, the activated Fmoc aminoacid reacts with the amino-terminal group of the growing peptide chain to form a peptide bond. Deprotection and coupling steps were repeated with each subsequent amino acid, until the chain assembly was completed. When the coupling was complete, the resin was washed with NMP. Peptides N-terminal amino groups were acetylated with acid acetic (1mmol, 57 µl).

6.1.3 Cleavage of the peptides from the resin

6.1.3.1 Cleavage and deprotection of HA_epitope

The final peptide product was released from the resin in its fully deprotected form by treatment with TFA. Some scavengers (i.e., molecules that react preferentially with free radical and other reactive species released during the cleavage reaction) like thioanisole, ethanedithiol and anisole were added to avoid undesirable modification of the peptide during the cleavage process. At the end of the synthesis, the resin was washed three times each with DMF, DCM and methanol and allowed to dry. To cleave the peptide from the resin and deprotect the side chains, the resin was transferred to a flask and a freshly prepared cleavage mixture (2% anisole, 5% thioanisole, 3% ethanedithiol, 90% TFA; 10 ml) was added, and the reaction mixture was incubated for 2 hours (1 hour in an ice bath, 1 hour at room temperature) with stirring. The resin was filtered and the solution was collected by draining it into a 50-ml glass flask, then the resin were washed again with undiluted TFA. The crude peptide was precipitated immediately by adding 5 volumes of cold diethyl ether to the collected reaction mixture. The mixture was centrifuged, the supernatant was removed and the precipitate was washed twice with three volumes of cold diethyl ether. The peptide was dried to remove diethyl ether, redissolved in water and lyophilized.

6.1.3.2 Mmt deprotection and cleavage of Mimochromes peptides

The protocol of Mmt deprotection and cleavage from the resin was the same for all the Mimochromes peptides.

After the final assembly on the resin, the N-ε Mmt protecting group of the Lys residue was removed by repeated treatments with a solution containing 10% acetic acid and 20% trifluoroethanol (TFE) in CH_2Cl_2 (10 ml) for 15min. Each step was repeated until no yellow or red trityl cations were detected in the eluent .

The product thus obtained, was transferred into a reaction vessel. To release the peptide from the resin, 3-4 resin volumes of a freshly prepared cleavage mixture (1%TFA in DCM, 20 ml) were added. The acidic mixture was incubated for 2 minutes, under mixing. The solution was filtered with a vacuum pump, into an ice-cold flask containing 2 ml of 10% pyridine/methanol (v/v). Finally, the resin was washed with DCM and methanol. The reaction was followed by TLC

(chloroform/methanol/acetic acid 80:18:2); each step was repeated until no product was detected in the collected fractions. The fractions containing the product were combined.

6.1.4 Purification of the peptides

6.1.4.1 Purification of HA-epitope

Purification of the fully deprotected peptide was accomplished by preparative RP-HPLC (Shimadzu LC-8A, equipped with a SPD-M10 AV detector), on a 2.2 cm Vydac C18 column, at a flow rate of 22 mL min^{-1}, with a gradient of acetonitrile in 0.1% aqueous TFA, 5% to 95% over 35 min. The pooled fractions containing the desired products were lyophilized. The peptide was homogeneous as determined by analytical HPLC and by MALDI mass spectrometry (MALDI/MS). MALDI/MS measurements were made on a Voyager DE instrument Perkin-Elmer operating at the Centro di Metodologie Chimico-Fisiche, University of Naples Federico II.

240 mg of pure product (83% yield were obtained on the basis of the resin initial substitution level).

6.1.4.2 Purification of Mimochrome peptides

The pooled fractions obtained from the cleavage reaction were evaporated under reduced pressure up to 5% of the volume. Ice-cold water was added to the residue and the mixture was cooled on ice to aid precipitation of the protected peptide. The product was filtered, washed several times with fresh water, and dried under vacuum to give the crude C-terminal peptide amide.

Analytical RP-HPLC (Vydac C18 column, using a gradient of acetonitrile in 0.1% aqueous TFA, 50% to 90% over 20 min, flow rate 1 mL min^{-1}) showed a main peak for all the protected peptides: therefore the coupling reaction was performed without further purification of the peptides.

The side chain protecting groups were found to be stable in both deprotection and cleavage reactions.

The yield of reaction are the followings:

- Mimochrome IV Lys^3 peptide: 240 mg of product (62% yield)
- Mimochrome VI tetradecapeptide: 570 mg of product (70% yield)
- Mimochrome VI decapeptide: 320 mg of product (80% yield)

6.1.5 Coupling of Mimochrome peptides to deuteroporphyrin

6.1.5.1 Synthesis of Mimochrome IV Lys^3 free base

The coupling reaction between the carboxyl groups of the porphyrin scaffolds and the free ε amino groups of Lys^8 was achieved by using HATU as activant.

The coupling reaction was performed in DMF at room temperature.

The first step was the deuteroporphyrin activation. The deuteroporphyrin IX dihydrochloride (24 mg, 0.042 mmol, M.W. 583.5 g/mol) was dissolved in a small volume of DMF and DIEA (0.2 mmol, M.W., 129,24 g/mol; density, 0.742 g/mL). Then, 2 equivalents of HATU (M.W., 380.23 g/mol), other 2 equivalents of DIEA were added to this solution, and the reaction mixture was allowed to react for 15 min. In the following step, the activated deuteroporphyrin was added to a solution containing the peptide (214 mg, 0.1 mmol, M.W. 2146 g/mol) in DMF and DIEA (3 equivalents). Additional DIEA was added to bring pH at ~ 7/8. In order to favour the formation of the *bis*-substituted deuteroporphyrin IX, the mixture of the activated porphyrin was slowly added to the solution of the nonapeptide. This approach gave good average yields.

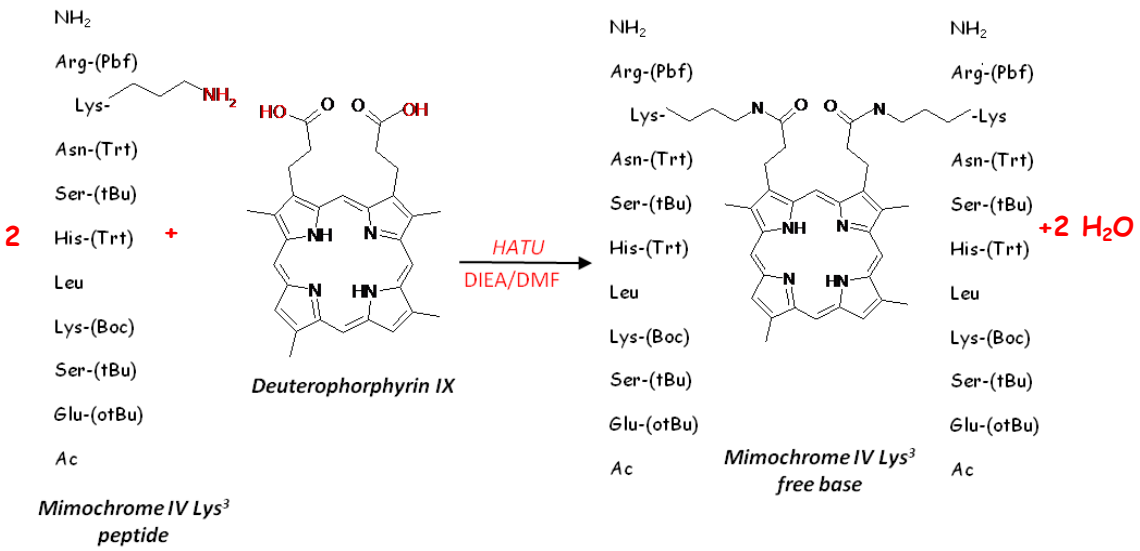

Figure 6.2: *Schematic representation of Mimochrome IV Lys^3 coupling.*

The proceeding of the reaction was followed by analytical RP-HPLC on a Vydac C_8 colum. After completion of the reaction (usually in 24 hours) the mixture was evaporated to dryness and extracted with chloroform and acid water (10%

citric acid p/v) to eliminate the reagents (DIEA, HATU and the peptide). The organic phase was anydrificated and evaporated under vacuum.

The next step was the deprotection of the aminoacid side chains. It was achieved at room temperature by addition of the cleavage mixture (TIS/H_2O/EDT/TFA 0.1/2.5/2.5/9.5, v/v/v/v). The thiol-based scavengers were added to avoid any side reaction that might occur when the protecting groups were removed from the peptide side chains. The deprotection was complete in 2 h; then, the solvent that contained the crude product was evaporated under reduced pressure to 5% of the volume. Ice-cold diethyl ether was added to the residue and the mixture was cooled on ice to aid product precipitation. The mixture was centrifuged, the supernatant was removed and the precipitate was washed twice with three volumes of diethyl ether. The peptide was dried, redissolved in water and then it was further purified by HPLC on a Vydac C_{18} column (2.2 x 25 cm; 10 µm), eluted with a linear gradient of acetonitrile 0.1 % TFA (v/v) from 5 % to 90% over 66 min, at a flow rate of 22 ml/min. The fractions containing the desired products were pooled, verified by LC-ESI-MS (Figure 3.6 a,b) and lyophilized. 52 mg of pure product (53% yield) were obtained.

6.1.5.2 Synthesis of Mimochrome VI free base

Synthesis of the decapeptide-deuteroporphyrin mono-substituted derivative: the Mimochrome VI decapeptide (100 mg, 0.040 mmol), deuteroporphyrin IX·2HCl (28 mg, 0.048 mmol, and DIEA (0.032 mL, 0.184 mmol) were dissolved in 30 mL of DMF. A solution of PyBop (25 mg, 0.048 mmol), HOBt (7.5 mg, 0.048 mmol), and DIEA (0.017 mL, 0.096 mmol) in DMF (10 mL) was then added dropwise. The reaction mixture was stirred for 3 h at room temperature, and the pH was verified every 20 min, and adjusted with DIEA, if necessary. The reaction was monitored by analytical HPLC (Vydac C8 column, using a gradient of acetonitrile in 0.1% aqueous TFA, 50% to 90% over 20 min), and by tlc (solvent system chloroform/methanol 90:10, R_f = 0.52). The reaction mixture was evaporated under reduced pressure up to 20% of the volume, and precipitated with cold diethylether. The crude product was purified on a silica gel column (5 × 60 cm), with stepwise elution using a chloroform/methanol gradient from 0 to 10% methanol. The product was eluted at 10% methanol, and obtained in a 48% yield.

Analytical RP-HPLC (Figure 4.3 a) and MALDI/MS spectrometry (Figure 4.3 b) confirmed the purity and the identity of the product (2980 amu).

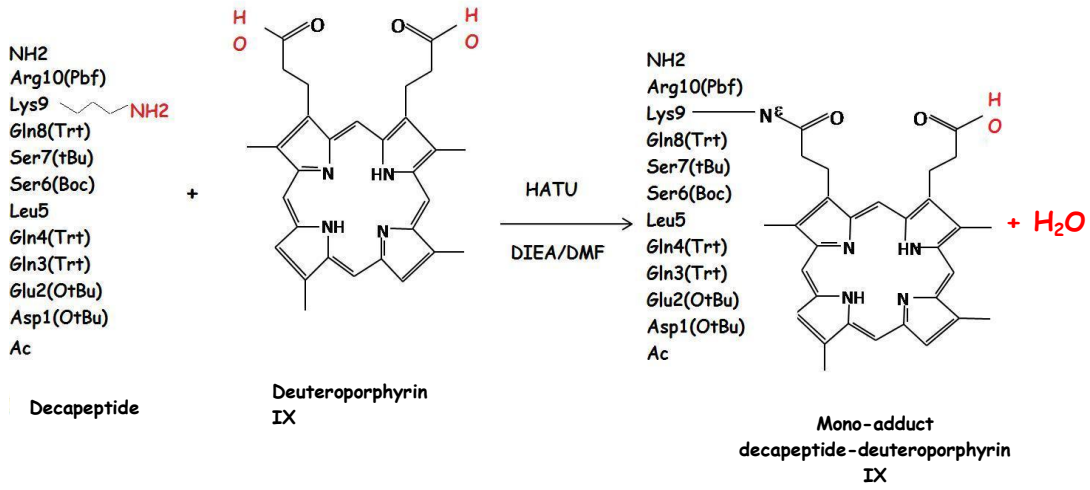

Figure 6.3: *Schematic representation of the decapeptide-deuteroporphyrin coupling.*

<u>*Synthesis of Mimochrome VI free base:*</u> monopeptide adduct (50 mg, 0.017 mmol), tetradecapeptide (52 mg, 0.017 mmol), and DIEA (0.009 mL, 0.051 mmol) were dissolved in 16 mL of 20% TFE in DMF. A solution of HATU (6.5 mg, 0.017 mmol) in 1 mL of DMF was then added dropwise, and the reaction was allowed to proceed at room temperature for a total of 2 h. The pH was checked during the reaction time. The reaction progress was followed by analytical HPLC (Vydac C8 column, using a gradient of acetonitrile in 0.1% aqueous TFA, 50% to 90% over 20 min, flow rate 1 mL min^{-1}), and by tlc (solvent system chloroform/methanol 90:10, R_f = 0.80). The reaction mixture was evaporated under reduced pressure up to 20% of the volume, and precipitated with cold diethylether, and finally centrifuged.

The crude product was dried in vacuo. Side chain deprotection was achieved by addition of the cleavage mixture (thioanisole/H_2O/EDT/TFA 0.25/0.5/0.5/8.75, v/v/v/v) (1,2-ethanedithiol: EDT) at 0 °C for 2.5 h. This treatment was performed twice. The reaction mixture was concentrated on a rotary evaporator to a volume of approximately 1-2 mL. Extraction of the scavengers and precipitation of the crude product was achieved by addition of cold diethylether. The crude material was then dried in vacuo and purified by preparative RP-HPLC (Vydac C18 column, using a gradient of acetonitrile in 0.1% aqueous TFA, 10% to 80% over 35 min);

the pooled fractions containing the desired product were lyophilized, affording 25 mg (7.2×10^{-3} mmol, yield 42%) of Mimochrome VI. Analytical RP-HPLC (Figure 4.4 a) indicated that the purified product was > 99% pure, and ESI-MS (Figure 4.4 b) confirmed the expected molecular weight (3502 amu).

6.1.6 Iron insertion

Iron ion was inserted into Mimochrome IV Lys^3 and Mimochrome VI according

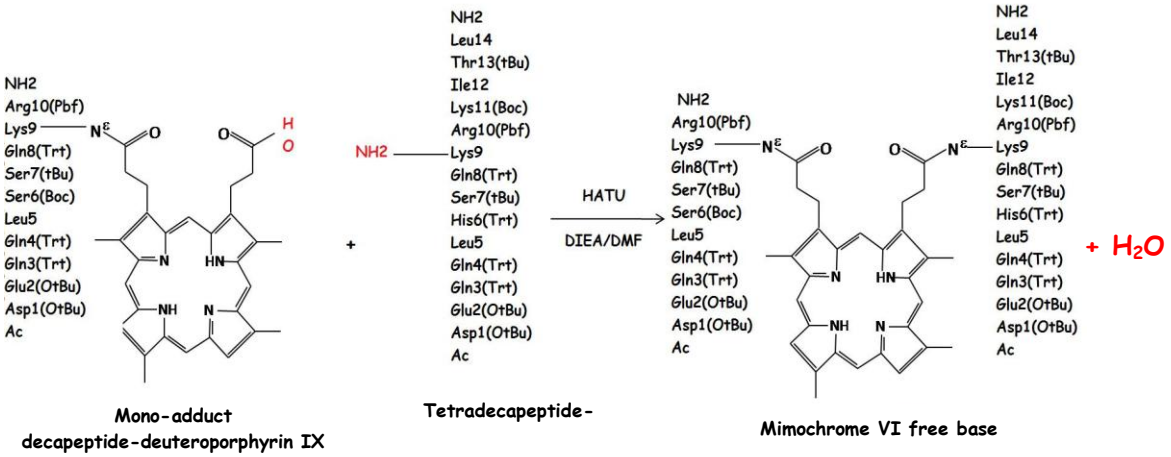

Figure 6.4: *Synthesis of Mimochrome VI free base.*

to literature procedures (Buchler, 1978). Iron (II) acetate (10 molar excess) was added to a solution of pure Mimochromes free bases in TFE (≈ 2×10^{-6} mol, final concentration, 1.0×10^{-4} M), and the reaction mixture was kept at 50 °C for 2 h, refluxing under nitrogen. The reaction was monitored by analytical HPLC. The solvent was then removed under vacuum, and the product was purified to homogeneity by preparative RP-HPLC (Vydac 2.2 cm C18 column at 22 mL min^{-1}, using a gradient of acetonitrile in 0.1% aqueous TFA, 10% to 80% over 58.4 min for Fe(III)-Mimochrome VI, 5 % to 90% over 66 min for Fe(III)-Mimochrome IV Lys^3). Pure products were obtained as the TFA salt (yeld was 44% for Fe(III)-Mimochrome IV Lys^3 and 54% for Fe(III)-Mimochrome VI). ESI-MS confirmed the expected molecular weight (Figure 3.7 c, 4.5 c) (Fe(III)-Mimochrome IV Lys^3 2806 amu, Fe(III)-Mimochrome VI: 3552 amu).

6.2 Synthesis of the conjugated Fe(III)-Mimochrome IV Lys^3-Ha_ep

6.2.1 Fe-Mimochrome IV Lys^3 activation with sulfo-SMCC

Because of the high hydrophilicity of the sample, Fe (III)-Mimochrome IV Lys^3 solution was assayed for its concentration by UV-vis spectroscopy. A sample of the molecule (≈ 1 mg) was dissolved in 500 µl of H_2O 0.1% TFA. This stock solution was diluted 1:1000. The diluted sample was transferred in a quartz cuvette with a path length of 1 cm, and its UV-Visible spectrum recorded (Figure 6.5) (on a Cary Varian 5000 UV Spectrophotometer, see below). The concentration of the solution was determined as follow:

Abs = 0.348; ε = 103.000 $M^{-1}cm^{-1}$; l = 1 cm

[Mimo IV Lys^3] = 3.4 mM; n_{mimo} = 1.7*10^{-6} mol → 5.5 mg

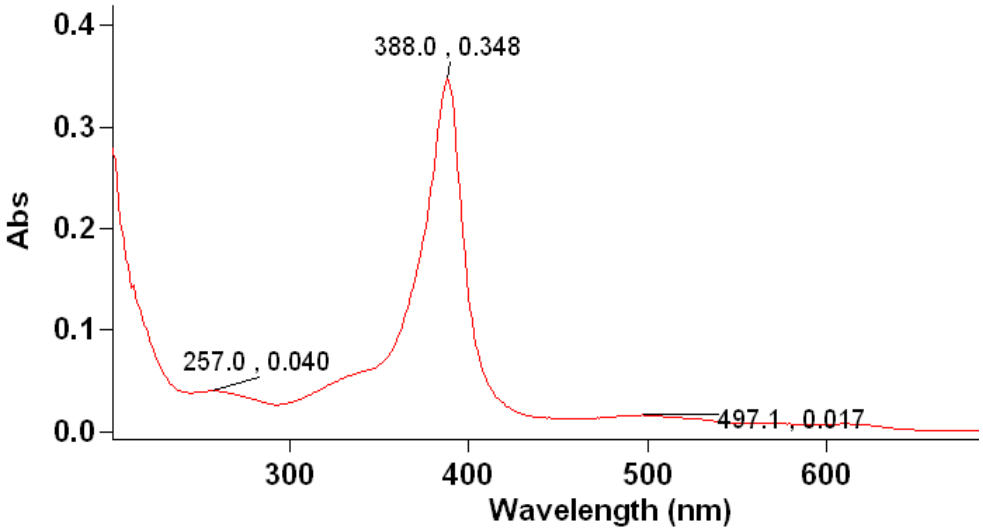

Figure 6.5: *UV-vis spectrum of Fe(III)-Mimochrome IV Lys3 in H2O 0.1 % TFA (pH 2).*

250 µl of the stock solution were added to 1 ml of 100 mM phosphate buffer, pH 7.2 (reaction buffer), to reach a final concentration 0.68 mM of the molecule. A solution of sulfo-SMCC (1 eq, 0.42 mg, dissolved in the reaction buffer) was added to the Fe(III)-Mimochrome IV Lys^3 solution. The reaction was carried out for 1 hour at room temperature, under stirring. After 1 hour, the proceeding of the reaction was controlled via LC-MS (Figure 3.11). The chromatogram (Figure 3.11 a) showed the presence of two new peaks corresponding to the mono- and the bis-functionalized products (see section 3.5.1).

6.2.2 Fe-Mimochrome IV Lys^3 functionalization with HA_ep

The Fe(III)-Mimochrome IV Lys3 mono-sulfo-SMCC was used without further purification. HA_ep was added to the reaction mixture in a molar ratio 3.5 to the activated Fe(III)-Mimochrome IV Lys^3 (3*10^{-6} mmol, 3.7 mg HA_ep).

The mixture was allowed to react for 2 hours at room temperature, under continuous stirring. The proceeding of the reaction was followed by LC-MS (Figure 3.13). After two hours, the analysis of the chromatogram and the mass spectra showed the complete functionalization of the Fe(III)-Mimochrome IV Lys^3-SMCC with HA_epitope. The product was purified to homogeneity by preparative RP-HPLC (Vydac 1 cm C18 column, using a gradient of acetonitrile in 0.1% aqueous TFA, 5 % to 90% over 66 min, at 5 mL min^{-1}). The fraction containing the desired product were pooled, lyophilized and then dissolved in 0.1 M phosphate buffer, pH 7. The concentration was checked by UV-vis (Figure 6.6) and it was 0.16 mM, tne reaction yield was 57.4%.

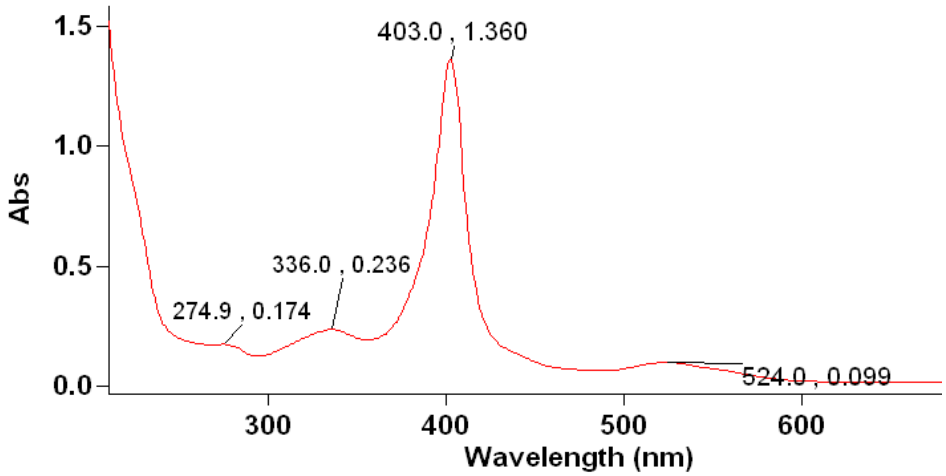

Figure 6.6: *UV-Vis spectrum of the complex Fe(III)-Mimochrome IV Lys^3-HA_epitope in 0.1 M phosphate buffer, pH 7.*

6.3 Voltammetric analysis

All cyclic and square wave voltammetry experiments were performed with a Potentiostat/Galvanostat µAUTOLAB Type III (Ecochemie) using a three-electrode cell for small volume samples (0.5-1 ml) purchased from BASi, under argon. Temperature controlled measurements were conducted using a thermo-cryostat R2 (Grant).

For all the measurement on Fe(III)-Mimochrome IV Lys^3, a 3 mm-diameter glassy carbon and a 1.6 mm-diameter polycrystalline gold electrode were used as working electrode, for the freely diffusing and the immobilized species, respectively. A Pt wire and a Ag | AgCl | NaCl 3 M as counter and reference electrode, respectively. A Vycor (PAR) set ensured the electric contact between the Ag/AgCl electrode and the working solution.

For all the measurement on Fe(III)-Mimochrome VI, a 1 mm-diameter polycrystalline gold electrode was used as working electrode, and a Pt sheet and a saturated calomel electrode (SCE) as counter and reference electrode, respectively. A Vycor (PAR) set ensured the electric contact between the SCE and the working solution.

Materials and Methods

6.3.1 Materials

Alumina was from BASi. 11-mercaptoundecanoic acid, 1-decanthiol, di-sodium hydrogen phosphate dihydrate, sodium dihydrogen phosphate monohydrate and sodium chloride were purchased from Sigma-Aldrich. Sodium perchloride, potassium hexacyanoferrate, N-hydroxysuccinimide (NHS) and N-(3-dimethylaminopropyl)-N'-ethylcarbodiimide (EDAC) were from Fluka. All solvents (H2O, ethanol, methanol, nitric acid) were obtained from Romil. All solutions and buffers were prepared with ultra pure water.

For all voltammetric analysis, argon gas was purged through the solution for at least 20 minutes to remove any dissolved oxygen before every experiment. An argon atmosphere was maintained over the solution during the measurements.

6.3.2 Cleaning of the electrodes

Glassy carbon electrodes were polished mechanically with an abrasive alumina powder. An alumina water-suspension (0.3 µm particle size) was dropped on a texmet pad. The electrodes were moved in a figure-of-eight motion for three minutes during polishing, to ensure uniform polishing. The electrode surface was then rinsed with deionized water, and the polishing procedure was repeated using a smaller particle size alumina (0.05 µm). Once polishing was completed, the electrode surface was rinsed thoroughly with deionized water, then sonicated first in distilled water and then in methanol for 5 minutes to ensure complete removal of all traces of the polishing material.

Gold electrodes were treated with HNO_3 3 M, by dropping 5 µl of the acid on the surface of the electrode. After 15 minutes, electrodes were rinsed thoroughly with deionized water, then the same polishing procedure described above for GCE was applied.

The degree of polishing of gold electrodes was evaluated by looking at the difference in the peak potential for the redox couple of Ferri/Ferrocyanide, which is expected to be close to 60 mV (Ranganathan et al., 1999). A 10 mM ferricianide solution in ethanol/0.1 M $NaClO_4$ 50/50 (v/v) was used to register a cyclic voltammogram at a scan rate of 0.05 V/s.

6.3.3 Voltammetric analysis of the freely diffusing species

6.3.3.1 Freely diffusing Fe(III)-Mimochrome IV Lys^3

Square-wave and cyclic voltammetry experiments on freely diffusing Fe(III)-Mimochrome Lys^3 were performed using a glassy carbon electrode as working electrode, at 25 C°. A 0,1 M Fe(III)-Mimochrome IV Lys^3 solution in 10 mM phosphate buffer and 100 mM $NaClO_4$ at pH 7 was used. The sample volume in the electrochemical cell was 1.0 ml. SW voltammograms were recorded at the scan rates 3.7, 4.8 and 37.5 mV/s, while for CV the measurements were performed at 0.025, 0.5 and 5 V/s.

6.3.3.2 Freely diffusing Fe(III)-Mimochrome VI

Cyclic voltammetry experiments on freely diffusing Fe(III)-Mimochrome VI were carried out using a polycrystalline gold disk coated with 4-mercapto-pyridine as

working electrode, at 20 C°. Modification of the electrode surface was performed by dipping the polished electrode into a 1.0 mM solution of 4-mercaptopyridine in water for 30 s, then rinsing it with ultrapure water. A 1.0 µM solutions of Fe(III)-Mimochrome VI, in 5.0 mM phosphate buffer and 20 mM $NaClO_4$ at pH 7 was used. The sample volume in the electrochemical cell was 0.5 ml.

6.3.4 Immobilization of Mimochromes on gold

6.3.4.1 Covalent binding of Fe(III)-Mimochrome IV Lys^3 and Fe(III)-Mimochrome IV Lys^3-HA_ep

Electrode coating with the 11-MUA SAM was done by dipping the cleaned electrode into a 1.0 mM 11-MUA solution in ethanol, for 18 h at room temperature. Then the electrode was thoroughly rinsed with ethanol and ultrapure water, and then SAM formation was checked by studying the electron-transfer reaction of a the $K_3Fe(CN)_6$ solution (10 mM ferricianide solution in ethanol/0.1 M $NaClO_4$ 50/50 v/v), previously used for the control of the cleaning procedure of the electrode surface. When the SAM formation was complete, the SAM carboxyl groups were activated by immersing the electrode in a solution of EDC 75 mM / NHS 15 mM in water, for 1.5 hours at room temperature. After this, the electrode was removed from the activating solution and thoroughly rinsed with deionized water. The activated electrode surface was immediately immersed in a 0.1 mM Fe(III)-Mimochrome IV Lys^3 solution (or Fe(III)-Mimochrome IV Lys^3-HA_epitope) in 0.1 M phosphate buffer, pH 7, for 1 hour at room temperature. After this step, the surface was rinsed with deionized water to remove unreacted protein molecules. Finally, a 1.0 M solution of Tris buffer, pH 8, was used to quench the activated carboxyl groups of 11-MUA that didn't reacted with the molecule, by immersing the electrode for 15 minutes; the electrode was then rinsed with deionized water. Functionalized electrodes were stored into phosphate buffer solution before starting measurements.

6.3.4.2 Adsorption of Fe(III)-Mimochrome VI

Electrode coating with the decane-1-thiol (DT) SAM was done by dipping the cleaned electrode into a 1.0 mM ethanolic DT solution for 12 h at 4 °C and then

rinsing the electrode with ethanol and MILLIQ water. The formation of the SAM was followed with the same method described above for Mimochrome IV Lys^3.

Adsorption of Fe-Mimochrome VI was achieved by dipping the functionalized electrode into a freshly prepared 1.0 µM Fe-Mimochrome VI solution (checked spectrophotometrically) made up in 5.0 mM phosphate buffer at pH 7, for 4 h at 4 °C.

6.3.5 Voltammetric analysis of the immobilized species

6.3.5.1 Fe(III)-Mimochrome IV Lys^3 and Fe(III)-Mimochrome IV Lys^3-HA_ep

SWV and CV experiments on the peptide (or conjugate)-coated electrodes were performed in 1.0 ml 10 mM phosphate buffer at pH 7, at 25 °C. All voltammograms were collected between -700 and +100 mV, at potential scan rate of 37.5 mV/s for SWV and between 0.5-10 V/s for CV. CV measurement at different scan rate were used to verify the effective bonding of the molecules to the surface.

The formal redox potential (E°') was calculated from the average of the cathodic and anodic peak potentials. Experiments were repeated at least two times, and the E°' values were found to be reproducible within ± 5 mV.

Antibody detection was performed by adding 2.0 µg of monoclonal antibody anti-HA_ep to the measurement buffer in the electrochemical cell, using an antibody stock solution (1.0 µg/µl). The solution was stirred for 10 minutes, then stirring was stopped and the cell was allowed to equilibrate for 60 seconds before recording SW voltammograms.

6.3.5.2 Fe(III)-Mimochrome VI

CV experiments on the peptide-coated electrodes were performed in 5 mM phosphate buffer at pH 7, at different scan rates (0.02-10 V/s). The reduction potentials (E°') of Fe-Mimochrome VI, taken as the average of the anodic and cathodic peak potentials, were invariably found to be reproducible within ±2 mV. To estimate the % surface coverage of the peptide-coated electrode, the area of the immersed portion of the gold wire was calculated after each cyclic voltammetry (CV) session by applying the Randles-Sevcik relationship to the CV signal

obtained for a solution of ferricinium tetrafluoborate (an electrochemical standard) using the bare electrode dipped into the standard solution at exactly the same depth of the peptide-coated electrode. The electron-transfer rate constants, k_s, for the adsorbed peptide, were determined with the method of Laviron, that is measuring the cathodic and anodic peak potentials at varying scan rate. The k_s values were averaged over five measurements and found to be reproducible within 10%, which was taken as the associate error.

The reaction thermodynamics of Fe(III) to Fe(II) reduction for Mimochrome VI can be determined from variable-temperature E°’ measurements carried out using a “non-isothermal” electrochemical cell, in which the reference electrode is kept at constant temperature (21 ± 0.1 °C) whereas the half-cell containing the working electrode and the Vycor junction is under thermostatic control. For this experimental configuration $\Delta S°'_{rc}$ was determined from the slope of the E°' versus T profile which is linear when assuming that $\Delta S°'_{rc}$ is constant over the limited temperature range investigated (from 5 to 35 °C). Using the same assumption, the enthalpy change ($\Delta H°'_{rc}$) can be obtained from the Gibbs-Helmholtz equation, namely as the negative slope of the plot of E°'/T versus 1/T. The non-isothermal behavior of the cell was carefully checked by determining the $\Delta H°'_{rc}$ and $\Delta S°'_{rc}$ values of the ferricyanide/ferrocyanide couple.

The electrocatalytic reduction of dioxygen by the immobilized Fe-Mimochrome VI was investigated by gradually adding air to the initially O_2-free cell solution at normal atmospheric pressure, at 20 °C.

6.4 Circular dichroism and UV-Vis analysis

6.4.1 CD analysis of Mimochrome VI

CD spectra were obtained at 25°C on a Jasco J-715 dichrograph. Data were collected from 470 to 360 nm at 0.2 nm intervals with a 20 nm min^{-1} scan speed, a 1 nm bandwidth and a 16 s response. In order to improve signal to noise ratio, spectra were averaged on 5 accumulations. Cuvette path length of 1 cm was used. Sample concentration was $2.0*10^{-5}$ M, in 5 mM sodium phosphate buffer, pH 7. The ferrous form of Mimochrome VI was obtained by adding a 2000 molar excess of dithionite to the solution of the ferric sample. CD intensities are reported

as total molar ellipticities (deg cm^2 $dmol^{-1}$). Absorption spectra have been collected as HT voltage and converted into absorbance by JASCO Spectra Manager standard software. All data are blank subtracted.

6.4.2 UV-Vis spectroscopy

UV-Vis spectra were recorded on a Cary Varian 5000 UV Spectrophotometer. All measurements were performed at room temperature. Quartz cuvettes with a path length of 1.0 cm were used for most measurements. Wavelength scans were performed at 25 °C (unless otherwise specified) from 200 nm to 800 nm, with a 300 nm min-1 scan speed. Wavelength scans were performed at 25 °C from 200 nm to 800 nm, with a 300 nm min-1 scan speed.

REFERENCES

Absolom D.R., Van Oss C.J., *CRC Critical Reviews in Immunology* (1986) 6, 1-46.

Anderson J.L., Coury L.A., Leddy J., *Anal. Chem*., (2000) 72, 4497.

Anzenbacher P., Anzenbacherová E., *Cell. Mol. Life Sci*., (2001) 58, 737–747.

Anzenbacher P., Dawson J. H., Kitagawa T., *J. Mol. Struct.* (1989) 214, 149–155.

Armstrong F.A., *Acc. Chem. Res*., (1988) 21, 407-413.

Armstrong F.A., Cox P.A., *Journal of Electroanalytical Chem.,* (1987) 217, 331-366.

Armstrong F.A., Hill H.A.O., Walton N.J., *Q. Rev. Biophys.,* (1986) 18, 261-322.

Armstrong F.A., Probing metalloproteins by voltammetry, Struct. Bonding 72, Springer-Verlag, Berlin, (1990), pp. 137-230.

Arnesano F., Banci L., Bertini I., Ciofi-Baffoni S., Woodyear T.D., Johnson C.M., Barker P.D., *Biochemistry* (2000) 39, 1499.

Arnold P.A., Shelton W.R., Benson D.R., *J. Am. Chem. Soc*. (1997) 119, 3181–3182

Balasubramanian S., Revzin A., Simonian A., *Electroanalysis*, (2006) 18, 1885-1892.

Banci L., Bertini I., Rosato A., Varani G., *J. Biol. Inorg. Chem.,* (1999) 4, 824–837.

Banci L., Rosato A., Turano P.J., *Biol. Inorg. Chem.* (1996) 1, 364-367.

Banci L.J., *Biotechnol.* (1997) 53, 253.

Barke, P.D., Ferguson S.J., *Structure* (1999) 7, R281.

Barker P.D., Nerou E.P., Cheesman M.R., Thomson A.J., deOliveira P., Hill H.A.O., *Biochemistry* (1996) 35, 13618.

Bartlett P.N., Bradford V.Q., Whitaker R.G., *Talanta*, (1991) 38, 57-63.

Battistuzzi G., Borsari M., Bortolotti C.A., Di Rocco G., Ranieri A., Sola M., *J. Phys. Chem. B* (2007) 111, 10281-10287.

Battistuzzi G., Borsari M., Cowan J.A., Eicken C., Loschi L., Sola M., *Biochemistry*, (1999) 38, 5553-5562.

Battistuzzi G., Borsari M., Cowan J.A., Ranieri A., Sola M., *J. Am. Chem. Soc*. (2002) 124, 5315-5324.

Battistuzzi G., Borsari M., Di Rocco G., Ranieri A., Sola M., *J. Biol. Inorg. Chem*. (2004) 9, 23-26.

Battistuzzi G., Borsari M., Francia F., Sola M., *Biochemistry*, (1997) 36, 16247-16258.

Battistuzzi G., Borsari M., Sola M., *Antiox. Redox Signaling* (2001) 3, 279-291.

Battistuzzi G., Borsari M., Sola M., *Chemtracts – Inorganic Chemistry* (2005) 18, 73-86.

Benson D.R., Hart B.R., Zhu X., Doughty M.B., *J. Am. Chem. Soc*. (1995) 117, 8502–8510.

Bertini I., Luchinat C., *Curr. Opin. Chem. Biol.* (1999) 3, 145.

Betso S.R., Klapper M.H., Anderson L.B., *J. Amer. Chem. Soc*., (1972) 94, 8197-8204.

Bistolas N., Wollenberger U., Jung C., Sheller F.W., *Biosensors and Bioelectronics* (2005) 20, 2408–2423.

Bortolotti C.A., Battistuzzi G., Borsari A., Ranieri A., Facci P., Sola M., *JACS* , (2006) 128, 5444-5451

Bourdillon C., Majda M., *J. Amer. Chem. Soc.,* (1990) 112, 1795-1799.

Boutelle M.G., *Neurosci. Lett.*, (1986) 72, 283-288.

Bowden E.F., Hawkridge F.M., Blount H.N., in *Comprehensive Treatise of Electrochemistry* (Edited by S. Srinivasan. Y. A. Chizmadzhev. J. O'M. Bockris. B. E. Conway 'and E. Yeager), Vdl. 10, pp. 297-346. Plenum, Nkw York (1985).

Breslow E., Koehler R., Girotti A.W., *J. Biol. Chem*. (1967) 242, 4149.

Breslow E., Koehler R.J., *Biol. Chem.* (1965) 240, 2266.

Brown K.R., Allan B.A., Do P., Hegg E.L., *Biochemistry* (2002) 41, 10906.

Casalini S., Battistuzzi G., Borsari M., Bortolotti C.A., Di Rocco G., Ranieri A., Sola M., *J. Phys. Chem. B* (2010) 114, 1698-1706.

Casalini S., Battistuzzi G., Borsari M., Ranieri A., Sola M., *J. Am. Chem. Soc*. (2008) 130, 15099-15104.

Cass T., Ligler F.S., Immobilized biomolecules in analysis: a practical approach. New York: Oxford Univ. Press; 1998.

Centi C., Laschi S., Mascini M., *Bioanalysis*, (2009) 1(7), 1271-1291.

Chaki N.K., Vijayamohanan K., *Biosens. Bioelectr*. (2002) 17, 1.

Chattopadhyay K., Mazumda, S., *Bioelectrochemistry* (2000) 53, 17−24.

Chen M.E.; Chang H.X.; Nymeyer H. (2007) NOC viewer vers. 3.01 [computer software], Florida State University.

Clark L.C., Lyons C., *Annals of the New York Academy of Sciences* (1962) 102, 29-45.

Coletta M., Costa H., De Sanctis G., Neri F., Smulevich G., Turner D.L., Santos H., *J. Biol. Chem.,* (1997) 272, 24800-24804.

Collings A., Caruso F.; *Rep. Prog. Phys.,* (1997) 60, 1397-1445

Crane B.R., Siegel L.M., Getzoff E.D., *Science* (1995) 270, 59.

D'Andrea L.D., Nastri F., Lombardi A., Maglio O., Pavone V.; Miniaturized Hemoproteins: A Covalent Asymmetric Peptide- Porphyrin System. In

Peptides 98; Bajusz S., Hudecz F., Eds.; Akade´mia Kiado´: Budapest, Hungary, 1999; pp 304-305;

D'Auria G., Maglio O., Nastri F., Lombardi A., Mazzeo M., Morelli G., Paolillo L., Pedone C., Pavone V., *Chem. Eur. J.* (1997) 3, 350-362.

Daido T., Akaike T., J. Electroanal. Chem. (1993) 344, 91.

Davies C., (1994) Principles. In: The immunoassay handbook. Ed. Wild, D. Basingstoke, The Macmillan Press Ltd, 3-80.

Davis D.G., Electrochemistry of porphyrins, in: D. Dolphin(Ed.), The porphyrins, Academic Press, New York, vol. 5(c), 1978, pp. 127-152.

De Grado W.F., Summa C.M., Pavone V., Nastri F., Lombardi A., *Annu. Rev. Of Biochem*., (1999) 63, 779-819.

Del Gatto G., PhD Thesis in Chemical Sciences, XX Cycle, University of Naples "Federico II", 2007

Detaxis Du Poet P., Miyamoto S., *Anal. Chimica Acta*, (1990) 235, 255-263.

Di Costanzo L., Geremia S., Randaccio L., Nastri F., Maglio O., Lombardi A., Pavone V., *J. Biol. Inorg. Chem.* (2004) 9, 1017-1027.

Dicks J.M., Hattori S., Karube I., Turner A.P.F., Yokozawa T*., Ann. Biol. Clin*., (1989) 47, 607-619.

Disley D.M., Cullen D.C., You H.-X, Lowe C.R., *Biosens. Bioelectr*. (1998) 13, 1213.

D'Orazio P*., Clinica Chimica Acta* (2003) 334, 41-69.

Drygas M.E., Lambowitz A. M., Nargang F. E., *J. Biol. Chem.* (1989) 264, 17897.

Eddowes M.J., Hill H.A.O., *J. Chem. Soc. Chem. Comm.,* (1977), 771.

Fantuzzi A., Meharenna Y.T., Briscoe P.B., Sassone C., Borgia B., Gilardi G., *Chem. Commun.*, (2006), 1289–1291.

Finklea H.O., *Self-Assembled Monolayers on Electrodes. Encyclopedia of Analytical Chemistry*, Meyers, R. A., Ed. Wieley, New York: (2000); Vol. 11, pp 10090-10115.

Fischer H., Zeile K., *Justus Liebigs Ann. Chem.* (1929) 468, 98.

Fung Y.S., Wong C.W., *Anal. Chimica Acta,* (2002) 456, 227.

Garcìa-Raya, D., Madueño R., Sevilla J.M., Blàzquez M., Pineda T., *Electrochimica Acta*, (2008) 53, 8026-8033.

Gerard G.D., Chaubey A., Malhotra B.D., *Bios. & Bioelect*., (2002) 17, 345-359.

Ghindilis A.L., Atanasov P., Wilkins E., *Electroanalysis* (1997) 9, 661.

Gibney B.R., Dutton P.L., *Protein Sci*. (1999) 8, 1888-1898.

Gilardi G., Fantuzzi A., *TRENDS in Biotechnology*, (2001) 19 (11), 468-476

Gilardi G., Meharenna Y.T., Tsotsou G.E., Sadeghi S.J., Fairhead M., Giannini S., *Biosens. Bioelectron.* (2002) 17, 133–145.

Goodin D.B.J., Biol. *Inorg. Chem.* (1996) 1, 360-363.

Gooding J.J., Erokhin P., Losic D., Yang W., Policarpio V., Liu J., Ho F.M., Situmomorang M., Hibbert D.B., Shapter J.G., *Anal. Sci.* (2001) 17, 3.

Gooding J.J., Hibbert D.B., *Trends in Anal. Chem*., (1999) 18, 525-533.

Gray H.B., and Ellis W.R., Electron transfer. In: *Bioinorganic Chemistry*, edited by Bertini I., Gray H.B., Lippard S.J., and Valentine J.S., Mill Valley, CA: University Science Books, 1994, pp. 315–363.

Gray H.B., Winkler J.R., *Annu. Rev. Biochem.* (1996) 65, 537.

Gross Z.J., *Biol. Inorg. Chem*. (1996) 1, 368-371.

Gui Y., Kuwana T., *J. Electroanal. Chem.* (1987) 226, 199.

Gunner M.R., Alexov E., Torres E., Lipovaca S., *J. Biol. Inorg. Chem*. (1997) 2, 126.

Guo L.H., Hill H.A.O., *Adv. Inorg. Chem*., (1991) 36, 341-375.

Hagen W.R., *Eur. J. Biochemistry*, (1989) 182, 523-530.

Hanrahan K.-L., MacDonald S.M., Roscoe S.G., *Electrochim. Acta*, (1996) 41, 2469-2479.

Harbury H.A., *J. Biol. Chem*., (1957) 255, 1009.

Hargrove M.S., Barrick D., Olson J.S., *Biochemistry* (1996) 35, 11293.

Hargrove M.S., Olson J.S., *Biochemistry* (1996) 35, 11310.

Hargrove M.S., Wilkinson A.J., Olson J.S., *Biochemistry* 1996, 35, 11300.

Hegner M., Wagner P., Semenza G., *FEBS. Lett.* (1993) 336, 452.

Heller A., *Acc. Chem. Res.,* (1990) 23, 128-134.

Hildebrandt P., Murgida D.H., *Bioelectrochem*. (2002) 55, 139-143.

Hock B., *Anal. Chim. Acta* (1997) 347, 177-186.

Hodak J., Etchenique R., Calvo E.J., Singhal K., Bartlett P.N., *Langmuir* , (1997) 13, 2708.

Hu N., *Pure Appl. Chem*., (2001) 73, 1979-1991.

Humphrey W., Dalke A., Schulten K.J., *Molec. Graphics*, (1996) 14, 33-38.

Hyung K.H., Jun K.Y, Hong H.G., Kim H.S., Shin W., *Bull. Kor. Chem. Soc.* (1997) 18, 564.

Igarashi N., Moriyama H., Fujiwara T., Fukumori Y., Tanaka N., *Nat. Struct. Biol.* (1997) 4, 276.

Ivnitski D., Abdel-Hamid I., Atanasov P., Wilkins E., *Bios. & Bioelect*., (1999) 14, 599-624.

Jelinek B., Antal J., Venekei I., Gràf L., *Protein Eng. Des. Cell*., (2004) 17(2), 127-131.

Jiang L., Glidle A., McNeil C.J., Cooper J.M., *Biosens. & Biolectr.*, (1997) 12, 1143-1155.

Kaplan L.A., Pesce A.J., Kazmierczak S.C., (2003), Clinical chemistry: theory, analysis, correlation. 4th ed. St. Louis, Elsevier.

Kassner R.J., *J. Am. Chem. Soc.* (1973) 95, 2674– 2677.

Kassner R.J., *Proc. Nat. Acad. Sci.. U.S.A*. (1972). 69, 2263-2267.

Kolodziej P.A., Young R.A., Methods Enzymol., (1991) 194, 508-519.

Koncki R., Radomska A., Glab S., *Talanta* (2000) 52, 13-17.

Kounaves S.P., "Voltammetric Techniques" in *Handbook of Instrumental Techniques for Analytical Chemistry*, (1997) F.A.Settle (Ed.) Prentice Hall PTR, Upper Saddle River,.

Lambrianou A., Demin S., Hall E.A., *Adv Biochem Eng Biotechnol*. (2008) 109, 65-96.

Lanzilotta W.N., Schuller D.J., Thorsteinsson M.V., Kerby R.L., Roberts G.P., Poulos T.L., *Nat. Struct. Biol.* (2000) 7,876-880.

Laviron E., J*. Electroanal. Chem*. (1979) 101, 19-28.

Lederer F., *Biochimie* (1994) 76, 674.

Lemberg R., Falk J.E., *Biochem. J.,* (1951) 49, 674.

Li H., Poulos T.L., *Structure* (1994) 2, 461.

Li J., Yan J., Deng Q., Cheng G., Dong S., *Electrochim. Acta*, (1997) 42, 961.

Liu G., Gooding J.J., *Electrochemistry Comm*. (2009) 11, 1982-1985.

Liu G., Paddon-Row M.N., Gooding J.J., *Chem. Comm*., (2008), 3870-3872.

Liu Y., Offenhausser A., Mayer D., *Bioelectrochemistry* (2010) 77, 89–93.

Loew G.H., Harris D.L., *Chem. Rev.* (2000) 100, 407.

Lombardi A, Nastri F., Marasco D., Maglio O., De Sanctis G., Sinibaldi F., Santucci R., Coletta M., Pavone V., *Chem. Eur. J.* (2003) 9, 5643-5654.

Lombardi A., Marasco D., Maglio O., Di Costanzo L., Nastri F., Pavone V., *Proc. Natl. Acad. Sci.* (2000) 97, 11922. (b)

Lombardi A., Nastri F., Pavone V., *Chem. Rev*. (2001) 101, 3165 – 3189.

Lombardi A., Nastri F., Sanseverino M., Maglio O., Pedone C., Pavone V., *Inorg. Chim. Acta* (1998) 301, 275-276.

Lombardi A., Summa C., Geremia S., Randaccio L., Pavone V., DeGrado W.F., *Proc. Natl. Acad. Sci.* (2000) 97, 6298. (a)

Love J.C., Estroff L.A., Kriebel J.K., Nuzzo R.G., Whitesides G. M., *Chem. Rev.* (2005) 105 (4), 1103-1169.

Luong J.H.T., Male K.B., Glennon J.D., *Biotech. Adv*., (2008) 26, 492-500.

Luppa P.B., Sokoll L.J., Chan D.W., *Clin. Chim. Acta* (2001) 314, 1-26.

Luzi E., Minnunni M., Tombelli S., Mascini M., *Trends Anal. Chem.*, (2003) 22, 810-818.

Mallat E., Barcelo D., Barze C., Gauglitz G., Abuknesha R., *Trac-Trends Anal. Chem.* (2001) 20, 124-132.

Mandler D., Turyan I., *Electroanalysis*, (1995) 8, 207-213.

Marcus R.A., Sutin N., *Biochim. Biophys. Acta*, (1985) 811, 265-322.

Martinez S.E., Huang D., Ponomarev M., Cramer W.A., Smith J.L., *Protein Sci.* (1996) 5, 1081.

Martinez S.E., Huang D., Szczepaniak A., Cramer W.A., Smith J.L., *Structure* (1994) 2, 95-105.

Matthews D.R., Bown E., Watson A., Holman R.R., Steemson J., Hughes S., Scott D., *Lancet* (1987) 1, 778-779.

Mattson G., Conklin E., Desai S., Nielander G., Savage M.D., Morgensen S., *Molecular Biology Reports*, (1993) 17, 167-183.

Mauk A.G., Moore G.R., *J. Biol. Inorg. Chem.* (1997) 2, 119.

Mello L.D., Kubota L.T., *Food Chem*. (2002) 77, 237-256.

Meric B., Kerman K., Ozkan D., Kara P., Erensoy S., et al., *Talanta*, (2002) 56, 837-846.

Michel H., Behr J., Harrenga A., Kannt A., *Annu. Rev. Biophys.Biomol. Struct.* (1998) 27, 329.

Mirsky V.M., Riepl M., Wofbeis O.S., *Biosens. Bioelectr*. (1997) 12, 977.

Moffet D.A., Hecht M.H., *Chem. Rev*. (2001) 101, 3191-3203.

Mogi T., Saiki K., Anraku Y., *Mol. Microbiol.* (1994) 14, 391.

Monari S., Battistuzzi G., Borsari M., Millo D., Gooijer C., van der Zwan G., Ranieri A., Sola M., *J. Appl. Electrochem.,* (2008) 38, 885-891.

Moore A.N.J., Katz E., Willner I., *J. Elect. chem.*, (1996) 417, 189-192.

Moore G.R., Pettigrew G. W., Cytochromes c: Evolutionary, Structural and Physiochemical Aspects; Springer-Verlag: New York, 1990.

Moore G.R., Pettigrew G.W., Cytochrome c: Evolutionary, Structural and Physiological Aspects; Eds.; Springer-Verlag: Berlin, 1990.

Morgan C.L., Newman D.L., Price C.P., *Clin. Chem*., (1996) 42, 193–209.

Murgida D.H.; Hildebrandt P., *Journal of the American Chemical Society* (2001) 123, 4062-4068.

Murphy, L.; *Curr. Op. Chem. Biol*., (2006) 10, 177-184.

Myer Y.P., *Methods Enzymol*., (1978) 54, 249-284.

Myer Y.P., Pande A., *The Porphyrins*, Vol. 4, (D. Dolphin ed.), Academic Press., New York, 1978 pp. 271-321.

Nahir T.M.,. Clark R.A, Bowden E.F., *Anal. Chem*., (1994) 66, 2595-2598.

Naray-Szabo' G.J., *Biol. Inorg. Chem.* (1997) 2, 135.

Nastri F., Lista L., Ringhieri P., Vitale R., Faiella M., Andreozzi C., Travascio P., Maglio O., Lombardi A., Pavone V., *Chemistry, submitted*

Nastri F., Lombardi A., D'Andrea L.D., Sanseverino M., Maglio O., Pavone V., *Biopolymers* (1998) 47, 5.

Nastri F., Lombardi A., Morelli G., Maglio O., D'Auria G., Pedone C., Pavone V., *Chem. Eur. J.* (1997) 3, 340-349.

Nastri F., Lombardi A., Morelli G., Pedone C., Pavone V., Chottard G., Battioni P., Mansuy D. J., *Biol. Inorg. Chem*. (1998) 3, 671-681.

Nelson D.R., Koymans L., Kamataki T., Stegeman J.J., Feyreisen R., Waxman D.J. et al. *Pharmacogenetics* (1996) 6, 1–42.

North J.R., *Trends Biotechnol.,* (1985) 3, 180–185.

Nuzzo R.G., Allara D.L., *J. Am. Chem. Soc.* (1983) 105 (13), 4481-4483.

O'Brian M. R., Thony-Meyer L., *Adv. Microb. Physiol.* (2002) 46, 257.

O'Sullivan C.K., Anal. *Bioanal. Chem.*, (2002) 372, 44-48.

Palaniappan V.,. Bocian D. F, *Biochemistry,* (1994) 33, 14264-14274.

Palecek E., *Talanta*, (2002) 56, 809-819.

Paoli M., Marles-Wright J., Smith A., *DNA and Cell Biology*, (2002) 21 (4), 271-280.

Patel N., Davies M.C., Hartshorne M., Heaton R.J., Roberts C.J., Tendler S.J.B., Williams P.M., *Langmuir* (1997) 13(24), 6485-6490.

Peng T., Cheng Q., Cheng Q., *Electroanalysis*, (2002) 14, 455-458.

Perutz M.F., Hasnain S.S., Duke P.J., Sessler, 660–663. J. L. & Hahn, J. E. *Nature* (1982) 295, 535–538.

Perutz M.F., Wilkinson A.J., Paoli M., Dodson G.G., *Annu. Rev. Biophys. Biomol. Struct.* (1998) 27, 1.

Peterson J.A., Graham S.E., *Structure* (1998) 6, 1079.

Pettigrew G.W., Moore G.R., *Cytochromes c: BiologicalAspects*. Berlin: Springer-Verlag, 1987.

Pishko M.V., Katakis I., *Angew. Chem. Int. Ed. Engl.,* (1990) 29, 82-84.

Pishko M.V., Michael A.C., Heller A*., Anal. Chem*., (1991) 63, 2268-2272.

Poulos T. L., Li H., Raman C.S., *Curr. Opin. Chem. Biol.* (1999) 3, 131.

Quan D., Shin W., *Mater. Sci. Eng. C* (2004) 24, 113.

Ramanathan K., Danielsson B., *Bios. & Bioelect*., (2001) 16, 417.

Ranganathan S., Kuo T-C., McCreery R.L., *Anal. Chem*., (1999) 71, 3574-3580.

Ranieri A, Battistuzzi G., Borsari M.,Casalini S., Fontanesi C., Monari S., Siwek M.J., Sola M., *J. of Electroan. Chem.,*(2009) 626, 123-129.

Ranieri A., Monari S., Sola M., Borsari M., Battistuzzi G., Ringhieri P., Nastri F., Pavone V., Lombardi A., *Langmuir*, (2010) 26(23), 17831-17835.

Rau H.K., DeJonge N.,. Haehnel W, *Angew. Chem*. (2000) 112, 256 - 259; Angew. Chem. Int. Ed. (2000) 39, 250–253;

Rau H.K., DeJonge N.,. Haehnel W, *Proc. Natl. Acad. Sci. USA* (1998) 95, 11526-11531.

Rau H.K., Haehnel W., *J. Am. Chem. Soc*. (1998) 120, 468-476.

Reedy C.J. and Gibney B.R., *Chemical Reviews,* (2004) 104(2), 617-649.

Reipa V., Yeh S.-M.L., Monbouquette H.G., Vilker V.L., *Langmuir* (1999) 15, 8126-8132.

Renneberg R. and Lisdat F., (2007) Biosensing for the 21st Century, Springer-Verlag (Berlin), Vol. 109, pp.1-2.

Robertson D.E., Farid R.S., Moser C.C., Urbauer J.L., Mulholland S.E., Pidikiti R., Lear J.D., Wand A.J., DeGrado W.F., Dutton P.L., *Nature* (1994) 368, 425-432.

Rogers K.R., *Molecular Biotechnology*, (2000) 14, 109-129.

Roitt I., Brostoff J., Male D., (1985), Immunologia. Florence, USES Edizioni Scientifiche.

Rosenblatt M.M, Huffman D.L, Wang X., Remmer H.A., Suslick K.S., *J. Am. Chem. Soc.* (2002) 124, 12 394 -12 395.

Ruzgas T., Gaigalas A., Gorton L.J., *Electroanal. Chem*. (1999) 469, 123-131.

Sacchi S., Rosini E., Molla G., Pilone M.S., Pollegioni L., *Protein Eng. Des. Cell*., (2004) 17(6), 517-525.

Sakamoto S., Obataya I., Ueno A., Mihara H., *J. Chem. Soc. Perkin Trans. 2* (1999), 2059-2069.

Sakamoto S., Ueno A., Mihara H., *J.Chem. Soc. Perkin Trans 2*. (1998), 2395-2404.

Sano S., Tanaka K., *J. Biol. Chem.* (1964) 1964, 3109.

Scheller F.W., Renneberg R., Strnad G., Pommerening K., Mohr P., *Bioelectrochem. Bioenerg*., (1977) 4, 500.

Schreiber F., *Journal of Physics-Condensed Matter* (2004) 16(28), R881-R900.

Scott R.A., Mauk A.G., Cytochrome c: A Multidisciplinary Approach; University Science Books: Sausalito, CA, 1996.

Sellers V.M., Wu C.K., Dailey T.A., Dailey H.A., *Biochemistry* (2001) 40, 9821.

Senillou A., Jaffrezic N., Martelet C., Cosnier S., *Anal. Chim. Acta.* (1999) 401(1-2), 117-

Shifman J.M., Gibney B.R., Sharp R.E., Dutton P.L., *Biochemistry* (2000) 39, 14813-14821.

Shifman J.M., Moser C.C., Kalsbeck W.A., Bocian D.F., Dutton P.L., *Biochemistry* (1998) 37, 16815-16827.

Smith A. T., Veitch N. C., *Curr. Opin. Chem. Biol.* (1998) 2, 269.

Sono M., Roach M.P., Coulter E.D., Dawson J H., *Chem. Rev*. (1996) 96, 2841.

Suri C.R., Raje M., Varshney G.C., *Crit. Rev. Biotechnol*. (2002) 22, 15-32.

Tainer J. A., Roberts V.A., Getzoff E.D., *Curr. Opin. Biotechnol.,* (1992) 3, 378-387.

Tarasevich M.R., *Bioelectrochem. Bioenerg*., (1979) 6, 587.

Tarasevich M.R., in *Comprehensive Treatise of Electrochemistry*, (Edited by S. Srinivasan, Y. A. Chizmadzhev, J. O'M. Bockris, B. E. Conway and E. Yeager), Vol. 10, pp. 231-295. Plenum, New York (1985).

Tarlov M.J., Bowden E.F., *J. Am. Chem. Soc*. (1991) 113, 1847-1849.

Tezcan F.A., Winkler J.R., Gray H.B.J., *Am. Chem. Soc.* (1998) 120, 13383.

Thévenot D., Toth K., Durst R., Wilson G.; *Bios. & Bioelect.,* (2001) 16, 121-131.

Tombelli S., Minnunni M., Mascini M., *Biomol. Eng.* (2007) 24, 191-200.

Tomlinson E.J., Ferguson S., *J. Proc. Natl. Acad. Sci. U.S.A.* (2000) 97, 5156.

Turano P., Lu Y., In Handbaook on Metalloproteins; Bertini, I., Sigel, H., Sigel, A., Eds.; Marcel Dekker: New York, 2001; pp 269-356.

Turner A.P.F., Karube I., Wilson G.S., *Biosensors: Fundamental and Applications*, Oxford Univ. Press, NY (1989).

Ulman A., *Chem. Rev.*, (1996) 96 (4), 1533-1554.

Ulmann G.M.; Kostic N.M., *J. Am. Chem. Soc*. (1995) 117, 4766-4774.

Vainshtein B.K., Melikadamyan W.R., Barynin V.V., Vagin A.A., Grebenko A.I., Borisov V.V., Bartels K.S., Fita I., Rossmann M.G., *J. Mol. Biol.* (1986) 188, 49.

Van den Heuvel D.J., Kooyman R.P.H., Drijfhout J.W., Welling G.W., *Analytical Biochemistry*, (1993) 215, 223-230.

Varfolomeev S.D., Berezin I.V., *J. Mol. Catal.,* (1978) 4, 387.

Wade H., Scanlan S., *Annu. Rev. Biophys. Biomol. Struct*., (1997) 26, 461-493.

Wang J. , *Analytical Electrochemistry*; Wiley-VCH: New York, 1994

Wang J., Li M., Shi Z., Li N., Gu Z., *Anal. Chem*. (2002) 74, 1993-1997.

Wang M., Kennedy M. L., Hart B.R., Benson D.R., Chem. Commun. (1997), 883–884.

Weiss R., Mandon D., Wolter T., Trautwein A.X., Muther M., Bill E., Gold A., Jayaraj K., Terner J.J., *Biol. Inorg. Chem.* (1996) 1, 377-383.

Williams P.A., Fulop V., Garman E.F., Saunders N.F.W., Ferguson S.J., Hajdu J., *Nature* (1997) 389, 406.

Willner, I., Katz, E., *Angew. Chem. Int. Ed.,* (2000) 39, 1180-1218.

Willner, I., Katz, E., Willner, B.; *Electroanalysis,* (1997) 9, 965-977.

Wilson G.S., Hu Y., Chem. Rev., (2000) 100, 2693.

Wilson M.T., Ranson R.J., Masiakowski P., Czarnecka E., Brunori M., Eur. J. Biochem. (1977) 77, 193 –199.

Wong E.L.S., Erohkin P., Gooding J.J., *Electrochem. Commun*., (2004) 6, 648-654.

Wong L.L., *Curr. Opin. Chem. Biol.* (1998) 2, 263.

Wu C.K., Dailey H.A., Rose J.P., Burden A., Sellers V.M., Wang B.C., *Nat. Struct. Biol.* (2001) 8, 156.

Wuttke D.S., Gray H.B., *Curr. Opin. Struct. Biol.* (1993) 3, 555.

Yan J., Tender L.M., Hampton P.D., López G.P., *J. Phys. Chem. B*, (2001) 105, 8905-8910.

Yaropolov A.I., Kharybin A.N., Ermn´eus J., Varga G.M., Gorton L., *Bioelectrochem. Bioenerget.* (1996) 40, 49.

Yaropolov A.I., Malovik V., Varfolomeev S.D., Berezin I.V., *Dokl. Akad. Nauk. SSSR,* (1979) 249, 1399.

Yee E.L.; Weaver M., *J. Inorg. Chem*. (1980) 19, 1977-1079.

Yeh P., Kuwana T., *Chem. Lett.* (1977), 1145.

Yokohama K., Tamiya E., Karube I., *Anal. Let.,* (1989) 22, 2949-2959.

Yuan J., Tan I., Nie L., Yao S., *Anal. Chimica Acta,* (2002) 454, 65.

Zhang W., Li G., *Analytical Sciences*, (2004) 20(4), 603.

Zhou Y., Liu S., Jiang H.-J., Yang H., Chen H.-Y., *Electroanalysis,* (2010) 22, 1323-1328.

Zull J.E., Reed-Mundell J., Lee Y.W., Vezenov D., Ziats N.P., Anderson J.M., Sukenik C.N., *J. Ind. Microbiol.,* (1994) 13, 137.

List of publications

- Flavia Nastri, Liliana Lista, **Paola Ringhieri**, Rosa Vitale, Marina Faiella, Concetta Andreozzi, Paola Travascio, Ornella Maglio, Angela Lombardi and Vincenzo Pavone*, "A heme-peptide metalloenzyme mimetic with natural peroxidase-like activity",submitted to Chemistry*

  Abstract: Mimicking enzymes with alternative molecules represents an important objective in synthetic biology, aimed to obtain new chemical entities for specific applications. This objective is hampered by the large size and complexity of enzymes. The manipulation of their structures often leads to a reduction of enzyme activity. Here, we describe the spectroscopic and functional characterization of FeIII-Mimochrome VI, a 3.5 kDa synthetic heme-protein model, which displays a peroxidase-like catalytic activity. By the use of hydrogen peroxide, it efficiently catalyzes the oxidation of several substrates, with a typical Michaelis-Menten mechanism and with several multiple turnovers. The catalytic efficiency of FeIII-Mimochrome VI in the oxidation of ABTS and guaiacol (kcat/Km = 4417 and 870 mM-1 s-1, respectively) is comparable to that of native HRP (kcat/Km = 5125 and 500 mM-1 s-1, respectively). These results demonstrate that small synthetic peptide can impart high enzyme activities to metal cofactors, and anticipate the possibility of constructing new biocatalysts, tailored to specific functions.

- Antonio Ranieri, Stefano Monari, Marco Sola, Marco Borsari, Gianantonio Battistuzzi, **Paola Ringhieri**, Flavia Nastri, Vincenzo Pavone, and Angelina Lombardi, "*Redox and Electrocatalytic Properties of Mimochrome VI, a Synthetic Heme Peptide Adsorbed on Gold*", Langmuir (**2010**) 26(23), 17831–17835.

  Abstract: Mimochrome VI (MC-VI) is a synthetic heme peptide containing a helix-heme-helix sandwich motif designed to reproduce the catalytic activity of heme oxidases. The thermodynamics of Fe(III) to Fe(II) reduction and the kinetics of the electron-transfer process for MC-VI immobilized through hydrophobic interactions on a gold electrode coated with a nonpolar SAM of

decane-1-thiol have been determined through cyclic voltammetry. Immobilization slightly affects the reduction potential of MC-VI, which under these conditions electrocatalytically turns over molecular oxygen. This work sets the premise for the exploitation of totally synthetic mimochrome modified electrode surfaces for clinical and pharmaceutical biosensing.

- Andrea Scirè, Anna Marabotti, Vincenzo Aurilia, Maria Staiano, **Paola Ringhieri**, Luisa Iozzino, Roberta Crescenzo, Fabio Tanfani, Sabato D'Auria, *"Molecular strategies for protein stabilization: the case of a trehalose/maltose-binding protein from Thermus thermophilus.",* PROTEINS-STRUCTURE FUNCTION AND BIOINFORMATICS (2008) 73, 839-850.

  Abstract: The trehalose/maltose-binding protein (MalE1) is one component of trehalose and maltose uptake system in the thermophilic organism Thermus thermophilus. MalE1 is a monomeric 48 kDa protein predominantly organized in alpha-helix conformation with a minor content of beta-structure. In this work, we used Fourier-infrared spectroscopy and in silico methodologies for investigating the structural stability properties of MalE1. The protein was studied in the absence and in the presence of maltose as well as in the absence and in the presence of SDS at different p(2)H values (neutral p(2)H and at p(2)H 9.8). In the absence of SDS, the results pointed out a high thermostability of the MalE1 alpha-helices, maintained also at basic p(2)H values. However, the obtained data also showed that at high temperatures the MalE1 beta-sheets underwent to structural rearrangements that were totally reversible when the temperature was lowered. At room temperature, the addition of SDS to the protein solution slightly modified the MalE1 secondary structure content by decreasing the protein thermostability. The infrared data, corroborated by molecular dynamics simulation experiments performed on the structure of MalE1, indicated that the protein hydrophobic interactions have an important role in the MalE1 high thermostability. Finally, the results obtained on MalE1 are also discussed in comparison with the data on similar thermostable proteins already studied in our laboratories.

ACKNOWLEDGEMENTS

First of all, I wish to express my gratitude to my research advisors, Prof. Angela Lombardi and Prof. Vincenzo Pavone, for giving me the opportunity to do this PhD within the Bioinorganic chemistry group, and the chance to participate in this interesting and challenging research project.

I would also like to extend my grateful thanks to Dr. Ornella Maglio, for her support and suggestion during these three years, and especially to Prof. Flavia Nastri. To her goes my deepest gratitude for her invaluable help and guidance, a great part of this project would not have been done without her.

I wish to thank Prof. Marco Sola and Prof. Marco Borsari, and all the group of Bioinorganic chemistry of the University of Modena and Reggio Emilia for the help in the experiments and the results discussion on Mimochrome VI.

Special thanks go to the "Lab Girls" Rosita Vitale, Tina Andreozzi, Liliana Lista and Marina Faiella, for being friends more than colleagues, and for making the lab a beautiful place to live!
Thanks also to all the students that spent some time in the laboratory, especially Claudia Vicari and Fabio De Majo, it was a pleasure to know you and work with you.

Last but not least, thanks to some special people, who have supported me a lot during my PhD years: my parents and my sister and all my family.
A big thank-you to my best friends Luisa and MariaFrancesca, and to William, to supporting and "sopporting" me during this difficult period.